UNIVERSITÀ
POLITECNICA
DELLE MARCHE

Facoltà di Ingegneria

Corso di dottorato in Ingegneria Civile, Ambientale, Edile ed Architettura

XXXIV° ciclo

"An innovative framework for Vibration Based Structural Health Monitoring of buildings through Artificial Intelligence approaches"

Dottorando:
Dott. Ing. Davide Arezzo

Tutor accademico:
Prof. Ing. Fabrizio Gara

***Co Tutor accademico**:*
Prof. Ing. Graziano Leoni

Coordinatore del corso di dottorato:
Prof. Ing. Francesco Fatone

Ad Aloisa,
la mia forza.

1. Introduction

Structural health monitoring consists of identifying all those processes aimed at assessing the safety of a structure. These processes found their first application in the field of aerospace and mechanical engineering in order to assess the performance and occurrence of damage in mechanical components of vehicles and rotating industrial machinery. Over time, the need to assess the health status of structures has also led to the use of these techniques in the field of civil engineering, in particular vibration-based monitoring through the application of Operational Modal Analysis (OMA) techniques. These techniques are well established, based on solid theoretical foundations, and implemented in numerous frameworks for structural health monitoring. However, the definition and implementation of an effective dynamic monitoring capable to detect damage requires a high degree of multi-disciplinary and the contribution of specialists from different fields, i.e., measurement engineering, computer science, electronic engineering, dynamic identification, structural engineering, data science.

During the PhD activities an effort have been made for the development of a framework for Vibration-Based Structural Health Monitoring system (VB-SHM) in all its part, attempting to achieve replicability of the system and its effectiveness in correctly tracking the health conditions of the structure over time. Replicability is crucial to promote the widest possible spread of this kind of monitoring. However, in the implementation and data management of a dynamic monitoring system, there are well-known problems that need to be addressed and solved. Some of these, which I'm going to discuss in detail, have been faced with the help of artificial intelligence algorithms.

In chapter 2, an extensive literature review on VB-SHM is reported, presenting the frameworks that have been proposed in several scientific papers and identifying the critical issues that arise when dealing with this type of monitoring. In the second section of this chapter, the rising role of artificial intelligence in supporting the development of structural health monitoring systems is highlighted.

In chapter 3, practical aspects concerning the implementation of a dynamic monitoring system are addressed. An introduction to hardware and software tools is given, together with a look to technological progress in distributed sensor networks. In this chapter, the wireless sensor node developed in collaboration with the Department of Information Engineering of the Università Politecnica delle Marche is also presented.

Chapter 4 presents the proposed VB-SHM framework, discussing in detail each part of it, from the initial dynamic identification to the management of the monitoring data. In this chapter an attempt is made to solve the main problems related to the implementation of dynamic monitoring, in particular: how to define the optimal placements of sensors, how to automatically process the data, and how to deal with the effects of environmental and operational conditions on modal parameters.

At this point, the following chapters deal with the application of the framework presented in chapter 4 to three real case studies monitored during the PhD activities, with particular emphasis on individual steps of the framework. In chapter 5 the case study of the Santa Maria in Via Church in Camerino is presented, dealing with the problem of dynamic identification, model updating and optimal sensor placement. Due to the complexity of the finite element model, model updating has been carried out with the aid of Particle Swarm Optimization algorithm.

Chapter 6 reports the monitoring results of the r.c. school building in Camerino that was monitored during the 2016 seismic sequence. Throughout the monitoring period, the response of the building to several low to medium intensity earthquakes was recorded. The building, despite the absence of damage, showed a time-varying dynamic behaviour making it difficult to track the frequencies

during the seismic response. By applying a linearisation procedure, frequencies are tracked even during strong motions.

Finally, in chapter 7, the monitoring results of the Engineering Tower of the Università Politecnica delle Marche are reported. The tower has been monitored since 2017 and, although with some interruptions, allowed the observation of a marked dependence of its vibration frequencies on environmental parameters, especially temperature and wind. These effects have been effectively cleansed through the implementation of an artificial neural network.

2. Literature review and state of the art

2.1. From EMA to OMA

The use of experimental tests to gain further understanding of the dynamic response of structures is a well-established practice in the world of civil engineering. The first experimental tests for the identification of modal parameters can be traced back to the middle of the twentieth century. These tests are based on solid theoretical foundations and, in particular, the assumption is made that the dynamic behavior of the structure can be expressed as a combination of modes, each characterized by a set of parameters, i.e., natural frequency, damping ratio, mode shape, whose values depend on the geometry, material properties and boundary conditions. Experimental modal analysis (EMA) identifies these parameters by the simultaneous measurement of the force applied to the dynamic system and its response. [1]

In recent times, experimental dynamic testing has seen increasing attention. Experimental identification of modal properties supports engineers in gaining a better physical understanding of the dynamic behavior of the structure and provide fundamental support for the validation of numerical models. Furthermore, as vibration modes are related to intrinsic properties of the structure (mass, stiffness, and damping ratio), monitoring these parameters has proved to be an excellent tool for the developing of structural health monitoring system.

The first documented modal test methods date back to the 1940s, relating to vibration tests on aircraft structures and measuring the same kind of frequency response functions that we use today [2]. Regarding the first applications in the field of civil engineering, during the 1970s and 1980s the oil industry made considerable efforts to develop vibration-based damage detection methods for offshore platforms [3].

The application of controlled and measurable excitation is often too costly for the typical size of civil structures. For this reason, the civil engineering community has focused on the opportunities provided by Operational Modal Analysis (OMA). OMA is a dynamic identification procedure that allows the experimental estimation of the modal parameters of the structure from vibration response measurements only. What was formerly a measurable input is now replaced by the natural excitation of environmental forces and operational loads (wind, anthropogenic activities, micro-quakes, etc.). Operational modal analysis is the stochastic counterpart of experimental modal analysis [1] and over the years, OMA has evolved as an autonomous discipline.

In the field of civil engineering, OMA is very attractive because the tests are cost-effective and fast, and do not interfere with the normal use of the structure. In recent years there has been exponential growth in the application of OMA within frameworks for monitoring the structural health of structures based on ambient vibration measurement.

2.1.1. Vibration-based structural health monitoring frameworks

As mentioned above, research on structural health monitoring from vibration measurement was started in the late 1970s, starting in the offshore aerospace and oil industries, and rapidly expanding to the civil engineering industries [4]. The basic idea of this technology is that the modal parameters depend on the physical properties of the structure (mass, damping and stiffness) and therefore, changes or damage in the physical properties will cause detectable changes in the modal properties [5]. In general, damage can be defined as a change introduced in a dynamic system that negatively affects current or future performance [4]. The definition implies that a comparison between two different states of the system is necessary.

Damage identification requires a multidisciplinary approach, and the development and application of successful frameworks requires the cooperation of a plurality of specialists. In particular, the disciplines that contribute to damage identification are structural health monitoring (SHM), condition monitoring, non-destructive evaluation (NDE), statistical process control (SPC) and damage prognosis [5].

The main objective of damage identification is to identify structural damage at a very early stage and to predict the remaining useful life of structures for decision making [5]. As defined in the work of Rytter et al. [6], based on the amount of information provided on the state of the damage, the identification of the damage to the structure can be classified into four levels: determination of the occurrence of the damage (level 1), determination of the geometric position of the damage (level 2), quantification of the severity of the damage (level 3), and prediction of the remaining useful life and decision-making (level 4). The most sophisticated level (Level 4) can predict the remaining life of the structure and make autonomous decisions from the results of damage diagnosis. This level requires the combination of global structural models with local damage models to predict damage evolution, or probabilistic failure models based on previously failed or damaged components [7].

There have been many review publications on this topic. In the work of Doebling et al. [8] a review of vibration-based damage identification methods up to 1997 is presented. Sohn et al. [9] published an updated version containing new technical developments up to 2001. Carden and Fanning [4] propose a review on structural engineering applications. Yan et al [10] present the development of modern vibration-based methods using modern signal processing techniques and artificial intelligence. Wang and Chan [11] focused on bridges, reviewing the recent development of statistical damage detection and condition assessment techniques for bridge structures. Moughty and Casas [12] presented developments with a focus on the use of advanced computational methods. Recently, Kong et al [13], proposed an interesting state of the art review on the vibration-based structural damage identification framework for decision making. The literature reviews just mentioned focus mainly on levels 1 to 3 of damage identification, i.e. the determination of damage occurrence, location and severity.

Noteworthy applications of VB-SHM systems have also been made on the Italian territory with particular emphasis on culturally heritage buildings [14, 15] and bridges [16].

2.1.2. Optimal sensors placement

The key part of a VB-SHM system is the sensors, as all analyses for the extractions of damage-sensitive features are conducted on data acquired from them. The cost associated with a dynamic monitoring system is largely influenced by the number of sensors to be installed, as well as the on-line data processing and the costs required for the initial installation of the system. Therefore, optimization of the number of sensors and their position is crucial in the design and implementation of an effective VB-SHM system [17]. Due to the existence of a large volume of redundant information, it is not necessary to monitor all degrees of freedom (DOF) of a structure. Optimal Sensor Placement (OSP) deals with how many and which DOF of a structure to monitor. OSP procedure has the task of eliminating as many unnecessary DOFs as possible, while still providing enough information to describe the dynamic behavior of the structure with sufficient accuracy [18].

One of the first applications of OSP for the design of a monitoring system was presented by Kammer in 1991 [19]. In this work, the position of the sensors for an orbiting space station is optimized using the Effective Independence (EI) method.

In the following years, OSP has received considerable attention and has become the subject of several recent studies in the SHM area, and several applications can be found in the literature. Heo

et al [20] presented a kinetic energy optimization technique to obtain a higher signal-to-noise ratio for better identification of modal shapes. In the work of Guo et al [21], a performance index of OSP based on a genetic algorithm is presented. Flynn et al [22] proposed a Bayesian approach to minimize the type I and II error in measurements. Worden [23] and Li [17] presented review papers on OSP search in SHM comparing many different algorithms.

In any case, EI has proven to be a robust and simple method to apply. Moreover, unlike other methods, such as genetic algorithms, EI method does not rely on computationally intensive search techniques. In the work of Jiang et al. [24] a very useful numerical example is provided for the implementation of the algorithm.

2.1.3. Effects of environmental parameters on modal properties

VB-SHM systems may not be effective when modal properties have significant variance under environmental effects, especially severe temperature changes [25]. Some studies have found that changes in structural vibration properties because of temperature variations could be more significant than those caused by a medium degree of structural damage or under normal operational loads [26].

A lack of understanding of the effects of temperature can lead to a false identification of structural conditions. By now, many experimental and field studies have observed the importance of temperature variations on modal parameters. Different conclusions have been drawn for different structures. Probably, an increase of the structural temperature leads to a decrease of the material modulus and thus to a decrease of the vibration frequencies. This is an observation that can only partially explain these effects as temperature influences structures in a rather complicated way. In particular, it can lead to movements of the supports or changes in the boundary conditions and, consequently, influence the modal parameters.

Another aspect that complicates this problem is the non-uniform temperature distribution of a structure due to different solar irradiations at different times of the day. Consequently, using temperatures measured at different points in the structure can lead to qualitatively and quantitatively different conclusions. In addition to temperature, wind conditions also influence the thermal absorbability of structural surfaces [26].

Thermal effects on structural dynamic properties have been studied since the 1970s and many researchers have made contributions to this field. Jung et al [27] developed a dynamic monitoring system for the Gwang-An Bridge in South Korea, which was built in 2002. The bridge measurement system monitors and analyses the state of the bridge by receiving signals from sensors that were installed in some parts of the bridge in real time. With the passage of time from January to June 2013, the temperature increased from -2.8°C to 26°C and the natural frequency at the center span seems to be on a decreasing trend.

Xia et al [26] studied the effect of temperature on the vibration properties of the Tsing Ma suspension bridge (Hong Kong). The SHM system of the bridge has been in operation since 1997. The first four bending frequencies of the overall structure in the vertical direction in different seasons were studied and the percentage of variation of the frequencies, compared to the actual temperature.

Cross et al. [28] analyzed the dynamic response of the Tamar bridge (Plymouth, UK) to its environmental and operational conditions. shows that each of the first five natural frequencies of the deck tends to decrease with increasing temperature and increasing traffic load. For the frequency that appears to be most sensitive to temperature (the second, which corresponds to the

first laterally symmetrical mode), the frequency decreases by approximately 4.5% over a temperature variation of 20°C.

Another work on bridge health monitoring considering temperature change is presented by Kim et al [29]. In this paper, the results obtained from monitoring the Seohea Grand bridge (cable stayed bridge in South Korea) with a focus on the effects of temperature are shown.

Cornwell et al. [30] found that the first three natural frequencies of the Alamosa Canyon Bridge varied to about 4.7%, 6.6%, and 5.0%, respectively, over a 24 hour period as temperature of the bridge deck changed by approximately 22° C. In his PhD dissertation, Zolghadri [31] studied the effect of temperature on the vibrational characteristics of three continuously monitored bridges. Other very interesting results can be found in the PhD dissertations of Li [32].

With reference to bridges, experimental tests on the Z24 bridge are certainly among the most impactful in this topic. Interesting results can be found in the work of Peeters et al. [33].

For buildings it is more difficult to find monitoring report in which dependencies between dynamic properties and temperature have been observed.

One of the first works to address the effects of environmental conditions on buildings is the study by Clinton et al [34]. In this work, the results of monitoring of a Caltech Campus building, the Millikan Library, are presented. This is a very interesting case study in which the effects of many environmental parameters including temperature, wind, rain, level of anthropic activities and earthquakes are analyzed. A very interesting aspect that has been observed concerns the torsional mode, which is more sensitive to temperature than the translational modes. In general, frequency increases during the day seem to be associated with thermal expansion of the concrete, but since the amplitudes of ambient motion also increase by an order of magnitude during the day, this is not consistent with the general observation that natural frequencies decrease with increasing amplitude.

It is worth also mentioning the work of Mikael et al. [35] who analyzed the wandering of long-term frequency and damping values of three reinforced concrete buildings. In this case it is very interesting to observe the behaviors of the buildings for temperature values below freezing point. While in general the correlation of frequencies with temperature seems to be positive when the temperature drops below zero the trend reverses and the buildings become stiffer (as observed for the Z24 bridge [33]). Regarding the effects of temperature on the modal parameters of buildings, other results can be found in Regni et al. [36].

Numerous studies have also been conducted on historical masonry buildings. Saisi et al. [14] present the main results of a recent post-earthquake evaluation of a masonry tower in Mantua (Italy) observing that the natural frequency of global modes tends to increase with increasing temperature.

This behavior, also observed in other long-term studies of masonry towers [15, 37] has been explained through the closure of surface cracks, minor masonry discontinuities or mortar voids induced by the thermal expansion of the materials. Thus, the temporary "compaction" of the materials induces a temporary increase in stiffness and thus in modal frequencies.

In the work of Rainieri et al [38], strategies are proposed to eliminate the effects of environmental conditions on the characteristics of damage-sensitive structures. One of the critical issues in this task is to determine which environmental influences should be measured and where the corresponding sensors should be placed. When measurements of the parameters influencing the estimates are not available, statistical methods must be adopted to eliminate the effects of

environmental and operational factors in the absence of exploitable information on them. Rainieri et al explore the potential of Blind Source Separation Techniques (BSS) methods.

It should be noted that changes in environmental conditions are much slower than the lowest fundamental period of the monitored structure. When monitored for a short period of time (seconds, minutes), the hypothesis of considering the structure as a time-invariant dynamic system is realistic. As the observation period increases (hours, days, months, years) these changes often become non-linear, as they are due to non-linear temperature-rigidity relationships in the structural materials or in the boundary conditions of the structure [39]. For this reason, simple linear regression models are often not sufficient. To overcome this problem Reynders et al [39] propose the application of the kernel PCA technique. Recently, researchers facing this problem have increasingly relied on machine learning techniques [40].

2.2. The rising role of artificial intelligence in structural health monitoring

In recent years, there has been an increasing use of Artificial Intelligence end in particular, Machine Learning (ML) techniques in civil engineering for SHM.

Artificial intelligence (AI) techniques involve several tools that can be implemented for optimization and logical regression along with statistics and probability learning methods as well as classification. As illustrated in the work of Ibrahim et al [42] it is useful to categorize AI models into 4 main categories indicating supervised and unsupervised machine learning. Figure 2-1 shows an explanatory graphical classification of methods just as shown in the work of Ibrahim et al [42].

A critical discussion of the effectiveness and performance of individual methods and a comparison of them is beyond the scope of this thesis work. In this chapter some of the works found in the scientific literature are reported, highlighting how, given the large amount of data typical of VB-SHM problems, the use of Machine Learning is very often useful if not indispensable. However, most of the work focuses on individual issues of VB-SHM and an overview of the overall topic, addressing the problem in its full complexity, still lack.

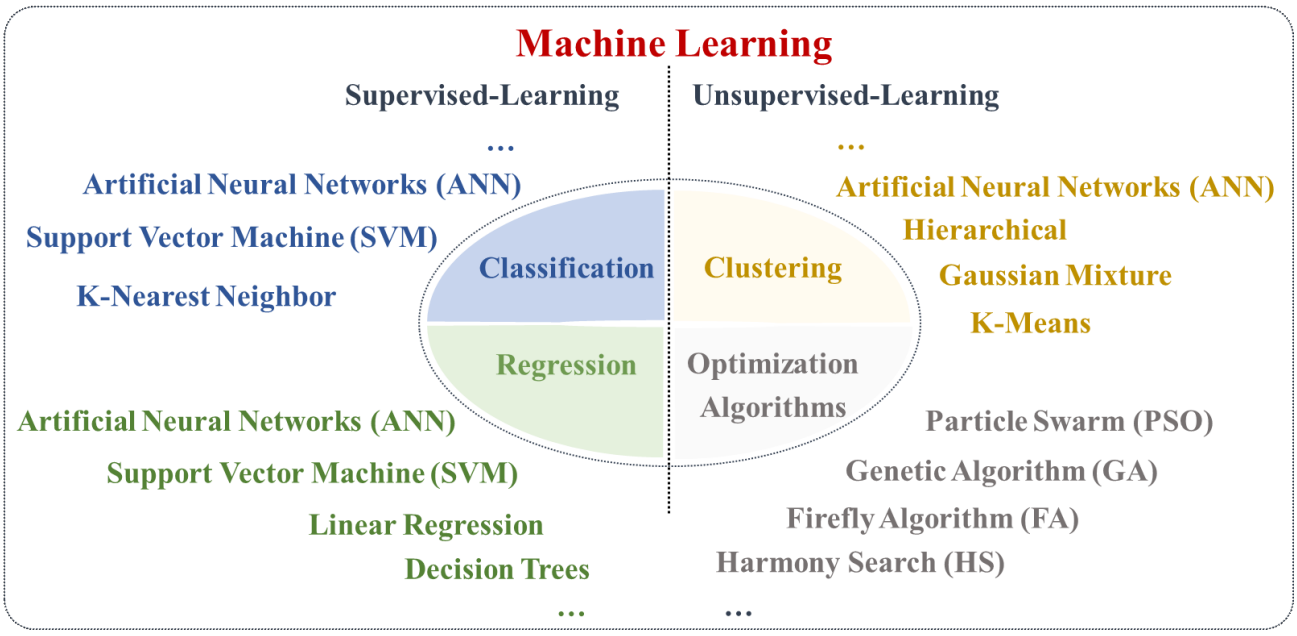

Figure 2-1: Machine Learning and Optimization Algorithms. Figure inspired from the works of Ibrahim et al [42].

One of the most recent and interesting ones is the work of Mishra [41] which focuses on SHM of culturally heritage buildings. Xu et al. [43] present applications of computer vision-based methods to monitor displacements in civil engineering structures and compare the results with those obtained from traditional approaches. In the work of Salehi et al. [44] an interesting general overview of ML techniques in structural engineering applications is provided. In the work of Mishra et al. [45], a review of studies on structural damage detection by applying different meta-heuristic techniques is presented. Das et al. [46] focused on vibration-based techniques in civil engineering for damage detection in engineering systems. Barontini et al. [47] have applied nature-inspired optimization algorithms in order to solve an inverse problem from changes in the elastic mechanical properties of a building.

Another important review work can be found in Falcone et al. [48] where the applications of fuzzy computing, evolutionary computing, swarm intelligence and artificial neural networks in solving problems related to structural and earthquake engineering are summarized.

Due to the increasing number and type of sensors deployed in today's monitoring systems, data fusion becomes a common issue. Wu and Jahanshahi [49] summarized the data fusion approaches used for SHM and their applications for civil engineering structures.

The large number of works in the literature refer to applications in many different fields, such as structure modal property identification, structural model updating and damage detection. In this work, an attempt has been made to explore the possibilities provided by this emerging field of machine learning in order to address especially the problems related to the large amount of data acquired by a dynamic monitoring system and to the automatic updating of complex finite element models.

2.2.1. Automatic extraction of dynamic features from data

VB-SHM is basically based on measuring acceleration time histories of the monitored structure with very high sampling frequencies. The minimum sampling frequency for dynamic monitoring of civil structures is around 50 Hz. Very often it is interesting to monitor local vibration modes with much higher frequency values and, considering the Nyquist frequency, it is not uncommon to reach sampling frequencies of the order of 1000 Hz. Furthermore, OMA techniques require measurements of durations on the order of 1000 - 2000 times the first fundamental period of the structure. This leads to an accumulation of billions of observations repeated several times a day, which would be impossible to process individually by human operators. Automating the processing of accelerometer signals using OMA techniques is critical for an effective VB-SHM system. In recent years, researchers working in this field have addressed this issue and the literature is now extensive. Among the first to address this problem were certainly Rainieri and Fabbrocino [1, 50, 51] presenting approaches for the automatic identification and tracking of modal parameters. The algorithm used has been integrated into a fully automated SHM system and is based on a well-established operational modal analysis technique, Frequency Domain Decomposition.

Another widely used approach is based on the analysis of the solutions obtained through the use of parametric identification techniques (e.g. stochastic subspace identification). In this case, a widely used solution is to adopt hierarchical clustering algorithms. The work of Hasan et al. [52] reviews exactly the use of this technique in automatic dynamic identification for structural health monitoring purposes.

Hierarchical clustering algorithms are built from a hierarchy of a tree structure. In theory, at the beginning of the analysis, each object is considered as a cluster. Then, the two closest clusters are joined together to become a new aggregated cluster that can reduce the number of clusters by one

at each step until the distance between all remaining clusters is greater than a user-defined threshold value. Finally, all individuals are grouped into one large cluster [53]. The difference in the application of hierarchical algorithms lies in the type of linkage which can be single, complete, or average or the Ward's method, and the centroid method can be used [54].

As mentioned above, when using a parametric identification algorithm, hierarchical clustering analysis is possible. Verboven et al. [55] used hierarchical clustering solutions obtained by applying the LSCF (Least Squares Complex Frequency Domain) method. In this work, mode shapes are neglected and only applied in a second step to assess the quality of the formed groups. Meanwhile, Pappa et al [56] were perhaps the first to use the eigenfrequency difference and MAC value as distance measures in order to automate the Eigensystem Realization Algorithm (ERA) for an experimental modal analysis (EMA) of the Space Shuttle tail rudder. Goethals et al [57] introduced another way of measuring distance by considering also the damping ratio.

A very effective application of hierarchical clustering was presented in the work of Magalhães et al. [58], in which more than 2500 high-quality datasets collected on a 280 m long concrete arch bridge are analyzed. The use of hierarchical clustering has the great advantage of requiring only two user-defined parameters, i.e. the upper limit for the distance between any point and its nearest point in the same cluster and the number of expected modes, and thus does not require the prior construction of a stabilization diagram except for the purpose of mere graphical representation of the solutions. In addition to this, hierarchical algorithms have the advantage of being deterministic and allowing a good selection of the final number of clusters, based on the previously constructed hierarchical tree. The major disadvantage of this approach is that it is computationally demanding in the presence of an increasing number of solutions [51].

2.2.2. Model updating, genetic algorithms and particle swarms

Model updating (MU) technologies are well established in the fields of mechanical and aerospace engineering, and in recent years there have been several attempts to transfer this technology to the field of civil structural engineering. The availability of calibrated numerical models from experimental tests results can be a powerful support for the design of structural retrofit works or for the proof testing of new structures.

In any case, model updating is certainly crucial in a VB-SHM system, on the one hand to correctly interpret the results of the dynamic identification, and on the other hand to physically interpret any variations in the modal parameters of the monitored structures.

Although this is more difficult to implement in civil engineering, several successful examples can be found in the literature for different types of structures such as bridges (Zhang et al. [59]), buildings (Gara et al. [60]), historical buildings (Saisi et al. [14], Bayraktar et al. [61]), high-rise structures (Wu et al. [62]) as well as applications to footbridges (Bayraktar et al. [63]).

One of the main difficulties in the application of MU in the field of civil engineering is undoubtedly found in facing historical structures, which are characterized by an enormous complexity in terms of geometry, material properties, loads and boundary conditions, resulting in complex Finite Element Models (FEM) that are difficult to validate. An interesting review of classical and advanced approaches for the structural analysis of historical masonry buildings can be found in Roca et al. [64]. Castellazzi et al. [65] present an innovative strategy for the numerical modelling of historical masonry buildings introducing an interesting review on the use of finite element computation for the analysis of culturally relevant structures. For the MU of FEM models of historic buildings there are several significant applications in the literature. Ramos et al. [66] presents the results of the experimental tests with output-only techniques and FE model updating analysis of the San Torcato

Church (Guimarães, Portugal); Torres et al. [67] carry out operational modal analysis and update of the FE model of the Metropolitan Cathedral Cathedral of Santiago, Chile; in the work of Sabbatini et al. [68] a characterization of the structural behavior of the historical masonry church of San Filippo Neri in Macerata (severely damaged after the Central Italy Earthquake) are presented.

MU of FEM models is essentially based on the minimization of an error function that summarizes the distance between the dynamic behavior of the model and that of the real structure. Also in this area, the role of artificial intelligence algorithms has begun to emerge in recent years, although in a smaller degree than in the areas previously discussed. In particular, a family of artificial intelligence algorithms, namely Swarm Intelligence, seems to be very promising.

Swarm Intelligence (SI) is a family of population-based meta-heuristic algorithms inspired by the collective behaviors of insects, such as ants, termites, bees, wasps and other animals capable of performing certain intrinsic social actions [69], although the term 'Swarm Intelligence' was introduced by Gerardo Beni and Jing Wang in 1989, in the context of cellular robotic systems [70]. A review of the literature on soft computing techniques in structural and earthquake engineering can be found in the work of Falcone et al. [71]. SI simulates a population of simple individuals called 'particles', which evolve by interacting with each other and the external environment. The population of particles flies across the search space. In detail, each particle moves in the direction of the position of the best particle and thus finds a new, more promising possible region of the search space. The position is evaluated with a fitness function that reflects the nature of the problem. The algorithms included in the SI domain are: Particle Swarm Optimization (PSO) [72], Artificial Bee Colony (ABC) [73], Firefly Algorithm (FA) [74,75], Harmony Search (HS) [76] and Ant Colony Optimization (ACO) [77]. Among these, PSO is the most common algorithm and it is possible to find some applications in the MU of FEM models also in the field of civil engineering [78, 79].

3. Tools for dynamic monitoring

3.1. Hardware and software tools

The main components for carrying out an Operational Modal Analysis of a structure are the transducers, which can be installed at different points of the structure and also at different times (if an adequate number of reference sensors are kept), an acquisition device, and a control system to process and store the acquired data.

The fundamental step to achieve a successful dynamic identification is to obtain quality measurements with an adequate signal-to-noise ratio. The type of sensors and their characteristics must be selected on a case-by-case approach according to the type of structure to test and the excitation level expected for the experimental tests.

3.1.1. Transducers

The function of a transducer is to convert a physical quantity into an electrical one, typically a voltage, which is then transferred to hardware for conversion from an analogue to a digital signal. Sensors can, therefore, be interpreted as sources of voltage signals. The physical quantities measured can be of a different nature; for example, motion transducers convert displacement, velocity, or acceleration into an electrical quantity (typically, voltage) that is proportional to the magnitude of the physical quantity being measured. In this work, the most employed sensors were accelerometers, in particular piezoelectric and MEMS, although there are several types of sensors commercially available that are equally suitable for performing environmental vibration tests, such as electromagnetic sensors (e.g., seismograph, geophone).

Piezoelectric sensors exploit the piezoelectric property of certain natural materials (e.g., quartz) in order to convert a mechanical quantity into an electrical one.

Piezoelectricity is the property of a material to accumulate negative and positive ions on opposite surfaces of the crystal when a force is applied to it. The amount of charge accumulated is directly proportional to the force applied. In piezoelectric accelerometers, a mass is coupled to the crystal and, when subjected to an acceleration at the base of the accelerometer, the inertia force associated with the mass causes the crystal to deform. The crystal then generates an electrical charge proportional to its deformation. Piezoelectric sensors differ in the way electrical charge can be induced on piezoelectric crystals, either by compression, shear or bending. The Compression design (or compression mode) offers the advantage of few parts and high stiffness leading to a high frequency range. This design tends to be more susceptible to base strain and thermal transient effects since the crystal is in intimate contact with the base of the housing. The Shear design offers the best overall performance trade-off for an accelerometer; the accelerometer has a rigid structure, providing a high frequency range, and because the crystal is not in direct contact with the base, the effects of deformation and thermal transients are minimized. Flexural designs allow exceptionally high output signals to be generated as the crystal is subjected to high levels of stress. Flexural-mode accelerometers are also less rigid than compression or shear mode accelerometers, which allows a limited frequency range to be investigated. For OMA applications on civil structures, they are certainly among the most widely used and some models, with the right signal transmission and the right digitization, even achieve geophone performances. However, since the crystal is subjected to high levels of stress, they are more easily damaged than other types if exposed to excessive shock or vibration. In Figure 3-1 is shown a diagram of piezoelectric sensor designs and examples of commercial products with their relevant features.

It is interesting to note that from a mechanical point of view, a piezoelectric accelerometer is equivalent to a dynamic SDOF system excited by a force with a frequency far below its resonance. The sensor therefore has quasi-static response to the acceleration to which it is subjected. It is therefore necessary to verify that its resonance is sufficiently far from the dynamic characteristics of the structure under test but, in civil structures, this rarely happens, and it is more important to verify that the sensor is able to pick up very low frequency accelerations.

The other increasingly popular technology is MEMS sensors. MEMS stands for micro electro-mechanical system and covers any sensor manufactured using microelectronic fabrication techniques. These techniques create microscopic mechanical sensing structures, typically on silicon. When coupled with microelectronic circuits, MEMS sensors can be employed to measure physical parameters such as acceleration. MEMS sensors are capable of measuring frequencies down to 0 Hz (static or DC acceleration).

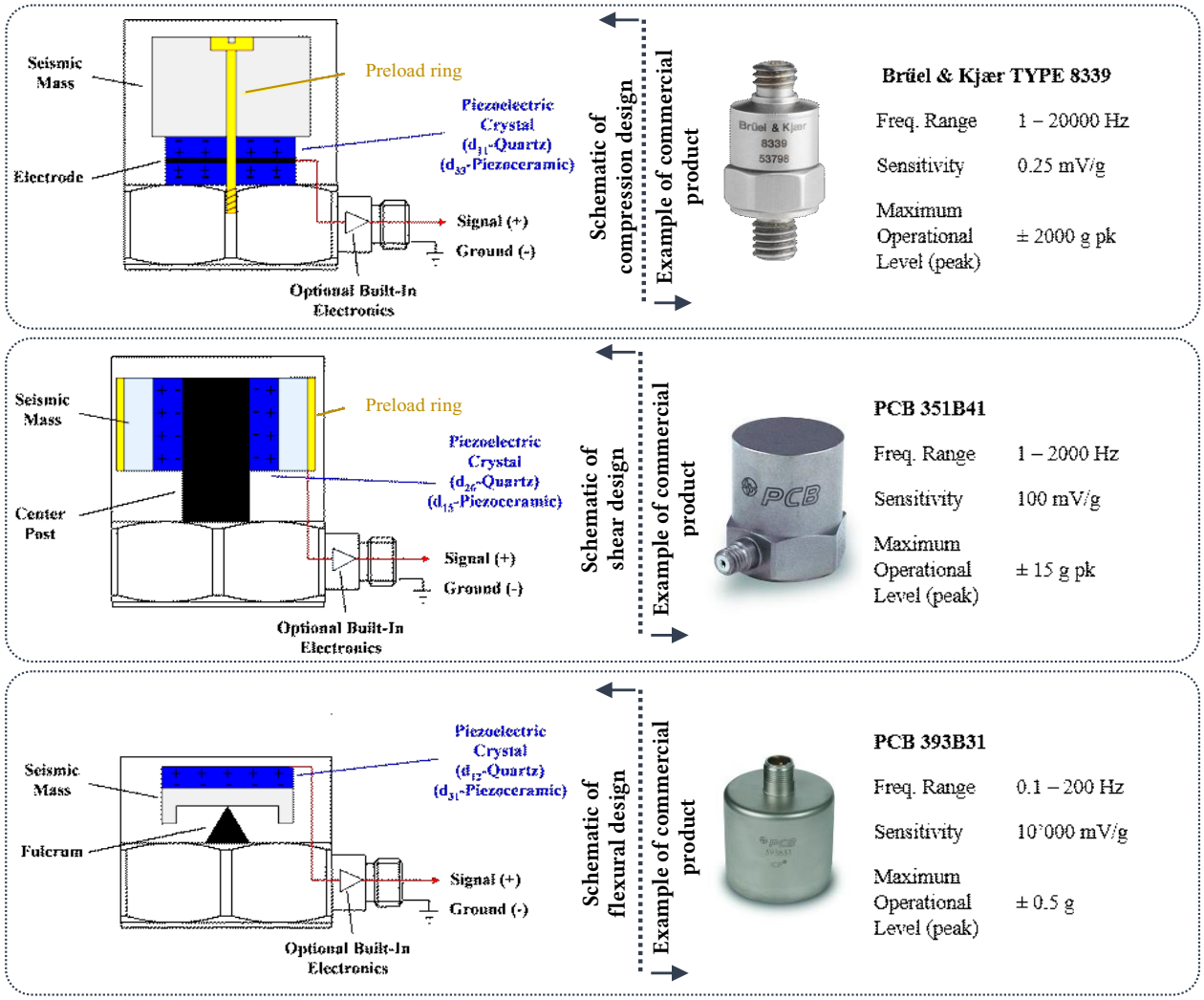

Figure 3-1: Schematization of crystal geometry (shear, compression, flexure construction) and relative example of commercial product with relevant performance. Schematization from the article "Accelerometer Internal Structure" https://www.modalshop.com/calibration.asp?ID=176.

Regardless the technology with which they are made, the main properties of accelerometric sensors are:

- sensitivity: describes the relationship between the physical quantity to be measured and the electrical quantity acquired (usually Volt) and it is commonly expressed as V/PQ (PQ: Physical Quantity).
- frequency range: the operating range of the instrument; the lower value is limited by the instrument electronics, while the upper value is a function of the physical and mechanical characteristics of the sensor.
- peak value: the maximum value of acceleration that the sensor is able to appreciate; it is a function of both the instrument and the acquisition system.
- minimum resolution: the minimum value of acceleration that the sensor is able to capture depends on the electronic background noise.

3.1.2. Signal digitization

The voltage output from the sensor must be digitized by a suitable data acquisition system. The term used for signal digitization is 'quantization' and the instruments that carry out this task are analog-to-digital converters (ADCs). Quantization is the process where the Least Significant Bit (LSB) is determined if the input analog voltage lies in the lowest sub-range of the input voltage range. This section does not go into detail on how ADC devices work, but simply provides some general characteristics needed to select the right hardware among many on the market. Below some of the key features of these instruments are discussed.

The resolution of an ADC is specified in bits (n) and determines how many distinct output codes (2^n) the converter is capable of producing. In other words, a resolution is the smallest voltage increment corresponding to a 1 LSB (Least Significant Bit) change. It's an important ADC specification because it determines the smallest analog input signal an ADC can resolve. The transition between low and high resolution typically occurs at the 16-bit level; a device with less than 16 bits is considered with low resolution, while the one with more than 16 bits is considered to own high resolution.

The noise level depends on the number of bits occupied by noise when the input is zero. In good quality 24-bit digitizer only the last two bits are typically corrupted by noise.

Dynamic range is defined as the ratio between the highest and lowest value that the ADC can acquire without considerable distortion and is expressed in dB on the datasheets of ADC devices. Considering that lowest bits often contain only noise, it is possible to define the dynamic range as the ratio between the maximum input voltage and the noise level of the digitizer. As an example, the digitizers used in this work, which are suitable for most of AVTs on civil structures, have a dynamic range of 102 dB.

The sampling rate is defined as the number of samples acquired every second. It is a parameter that defines the largest frequency range that can be investigated. For AVTs on civil structures, a maximum sampling rate of 100 Hz may be sufficient. It is also important to know the minimum sampling rate because, in the case of structures with very high fundamental periods (e.g., isolated structures), can be crucial for successful measurements. When it is necessary to measure very low frequencies, devices with a frequency range starting from DC can be considered.

The analysis of datasheets in the selection of the most appropriate device for a test must be carried out carefully. The characteristics listed in these documents are the main ones, but for further information, the reader should refer to specialist texts [80]. A good overview of the measurement hardware required for dynamic measurements can be found in Rainieri and Fabbrocino [1]. Figure 3-2a shown a digital to analogue Conversion schematization while in Figure 3-2b a commercial ADC module from National Instruments with its relevant characteristics is reported.

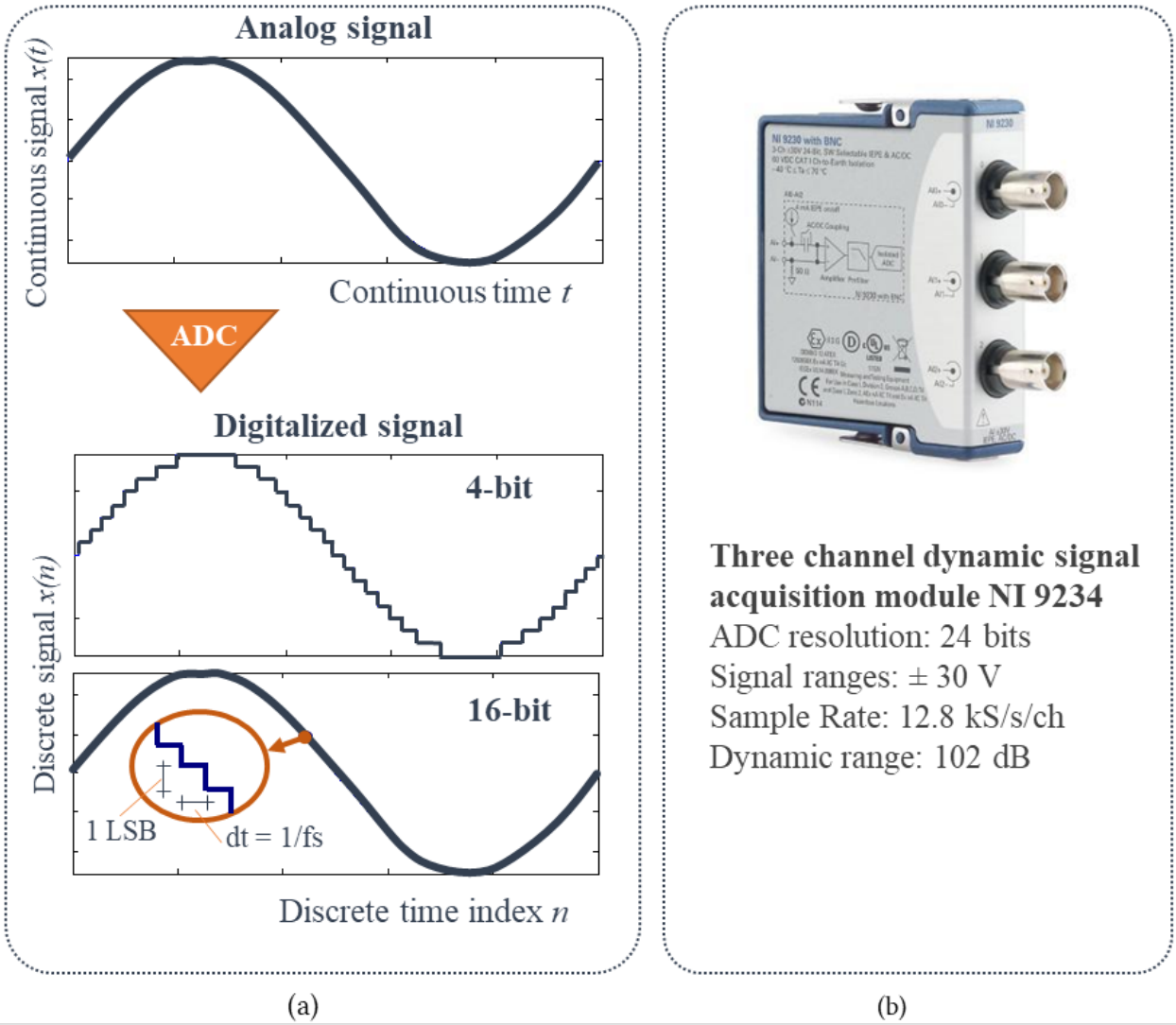

Figure 3-2: (a) Digital to Analogue Conversion schematization; (b) commercial ADC module from National Instruments.

3.1.3. Real-time software and determinism

In the development of dynamic monitoring systems, the concept of real-time monitoring is of great importance, especially when early warning systems for seismic monitoring frameworks need to be developed.

A real-time computing system must be able to execute programs with very specific time requirements in a very reliable process. The key to a real-time system is a real-time operating system (RTOS). Real-time computing systems provide precise timing and can be set to run reliably for days, months or years without stopping. This is critical not only for engineering building systems that need to run 24//7, but also for any application where downtime is costly. In addition, the hardware used in a real-time system is often very robust to survive in tough conditions for long periods. Even where precise timing and long-term reliability are not absolute requirements, developing a real-time system can provide higher guarantee that the software will continue to run without interrupting the measurement or the control process.

Real-time operating systems typically run only one program at a time, and most real-time systems do not have a user interface, in which case a separate computer must be used to provide graphics or user controls. Some projects require hardware determinism where the logic is implemented on an FPGA (Field Programmable Gate Arrays). An operating system, in order to be considered 'real-time', must have a known maximum time for each of the critical operations it performs (or at least must guarantee that maximum for most of the time). Operating systems that can absolutely guarantee a maximum time for these operations are commonly referred to as "hard real-time", while operating systems that can only guarantee a maximum for most of the time are referred to as "soft real-time". These rigid categories are of limited use as each RTOS solution demonstrates unique performance characteristics and the task of carefully investigating these characteristics remains with the system designer.

Thus, if programmed correctly, an RTOS can ensure that a program runs with very consistent timing, as well as providing a high degree of control over how prioritized tasks are executed.

In contrast to ROTS, the most popular operating systems for personal computer use (such as Windows) are called general-purpose operating systems and are designed to maintain user responsiveness with many programs and services running.

When talking about real-time monitoring systems, some of the most important terminologies and concepts are:

- Determinism: an application running on a hard ROTS is said to be deterministic if its time can be guaranteed within a certain margin of error.
- Soft vs Hard Real-Time: an operating system that can absolutely guarantee a maximum time for the operations it performs is called hard real-time. Conversely, an operating system that can usually execute operations in a certain time is called soft real-time.
- Jitter: the amount of error in the timing of an operation in subsequent iterations of a program or cycle is called jitter. ROTS are optimized to provide a low amount of jitter when programmed correctly; task execution will always take the same amount of time.

The measurement setup at the base of a VB-SHM system of a structure should have the aforementioned characteristics in order to correctly measure and evaluate the structural response in case of seismic events or extreme events in general. For this reason, monitoring systems treated in this work have been developed by using National Instruments CompactRIO controllers that with a NI Linux Real-Time processor, a programmable FPGA and modular I/O. Despite these systems require a higher level of software programming skills than PC-based measurement systems, they own higher reliability and flexibility in managing a large and diversified sensor array. Figure 3-3 shows a schematic representation of the so called jitter and some examples of commercial controllers with real time features provided by National Instruments.

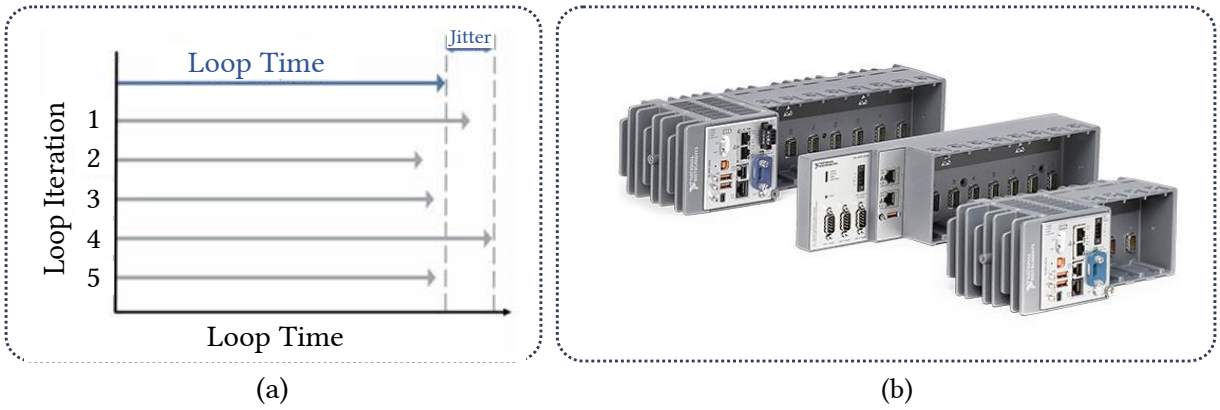

Figure 3-3: (a) Schematic representation of the so called jitter: "Jitter is a measure of how much the execution time of a task differs over subsequent iterations. Real-time operating systems are optimized to minimize jitter." From https://www.ni.com/it-it/innovations/white-papers/07/what-is-a-real-time-operating-system--rtos--.html; (b) Examples of commercial controllers (CompactRIO).

3.2. Distributed sensors network

Progress in sensor and computer network technology has allowed distributed sensor networks (DSNs) to evolve from tiny groups of large sensors to large swarms of microsensors, from fixed to mobile sensor nodes, from wired to wireless communications, from static to dynamically changing network topology. DSNs have recently emerged as an important area of research. The research carried out during this PhD work has not focused on this area but, given the multi disciplinarity required to address dynamic monitoring, the advances made in the DSN field must necessarily be taken into account.

3.2.1. Distributed Ethernet-Based Measurement Systems

Regarding wired networks, one of the technologies used during the PhD activities is the one provided by National Instruments. Time Sensitive Networking (TSN) is an update to the IEEE Ethernet standard intended to address the needs of control systems with standard Ethernet technology. TSN provide new features to standard Ethernet. This includes standard time synchronization and deterministic network communication over standard Ethernet, allowing operations networks to leverage the advantages of traditional Ethernet while meeting the timing and control needs of control and measurement applications. The measurements synchronization for dynamic identification tests is crucial and the most reliable method of communication is to carry the analogue signal to the DAQ (Data Acquisition) system via copper cables.

Typical civil engineering structures are large and the possibility of having DAQ systems distributed throughout the structure allows a significant reduction in cables usage. Figure 3-4 shows the Raffaello Marche Region building that has been dynamically identified by the ICEA Department of the Università Politecnica delle Marche. Using a system composed of one CompactRIO, three TSN-enabled CompactDAQs, and 20 piezoelectric accelerometers, it has been possible to perform the dynamic identification on 80 DOFs of the structure within a single day and using a limited amount of cables.

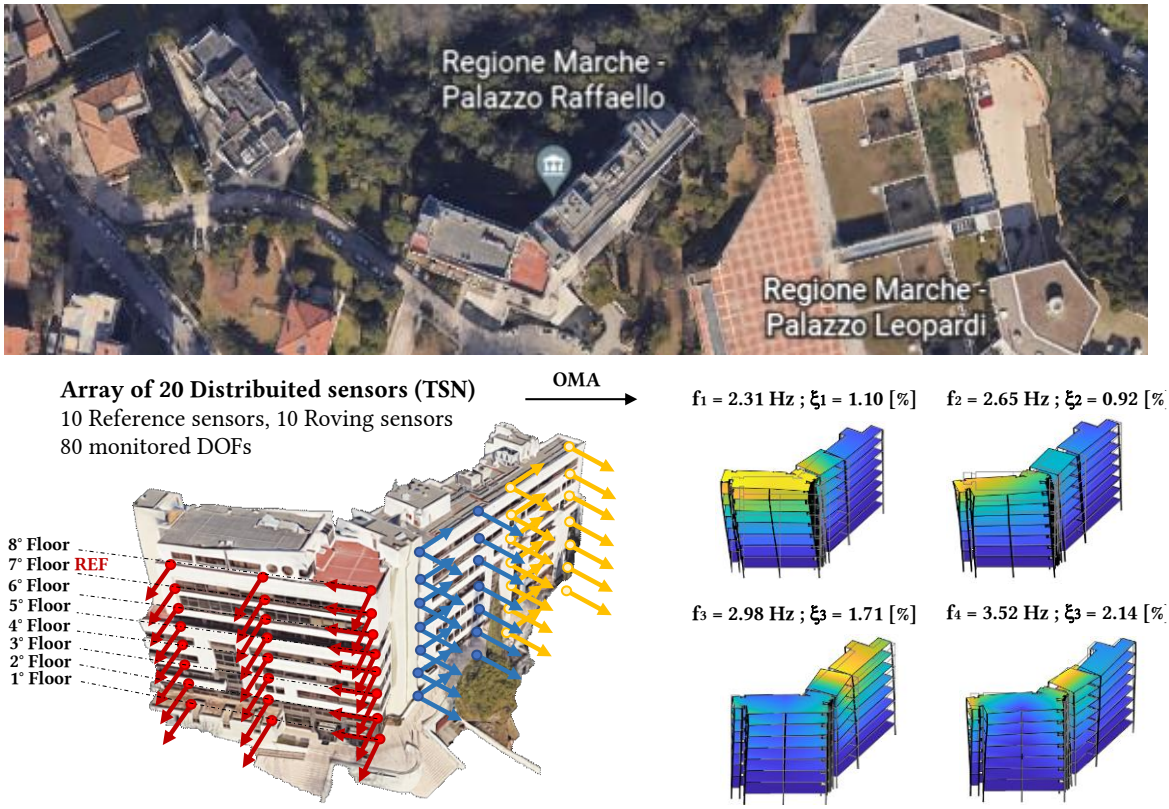

Figure 3-4: Dynamic identification of the Raffaello Palace, headquarters of the Marche Region.

3.2.2. Wireless sensors network

The chance to completely remove cables during dynamic testing would certainly make this type of measurement faster and less expensive. In recent years there has been a high research interest in wireless sensor networks (WSN). Thanks to the collaboration with the Information Engineering Department of the Università Politecnica delle Marche, a wireless sensor node for dynamic monitoring activities has been developed.

The work carried out in the realization of the sensor node involved an initial selection among various sensing units and MicroController Unit (MCU) boards proposed in the literature. The aim was to obtain the best compromise in balancing the performance/cost ratio for the project objectives. Therefore, four hardware components were used: a development board equipped with a low-power and high-performance MCU chip with the possibility of data transmission via Wi-Fi, a 3-axis MEMS accelerometer sensor and a micro-SD module for data storage.

The microcontroller used in this project is the Esp32 System on Chip (SoC) (Figure 3-5). Esp32 is a single combined Wi-Fi and Bluetooth 2.4 GHz chip designed with TSMC's 40 nm and ultra-low power technology. It is designed to achieve the best (radio frequency) power and performance, showing robustness, versatility and reliability in a wide variety of application scenarios. Esp32 is

designed for mobile devices, wearable electronic devices and IoT applications, presenting all the cutting-edge features of low-power chips, multiple power modes and dynamic power scalability. For example, in an application scenario with a low-power IoT sensor hub, Esp32 is activated periodically and only when a specific condition is detected. This module comes with many GPIOs and support for a variety of protocols such as SPI, I2C, I2S and UART. It also features a Wi-Fi module and Bluetooth. The processor core, named LX6 by Espressif, is based on the Xtensa® dual-core 32-bit LX6 processor controller and operates at a frequency range of 80-240 MHz. It has a 448kB boot ROM and 520kB of on-chip SRAM; in addition, it has 4MB of external flash memory that can be accessed via the SPI interface.

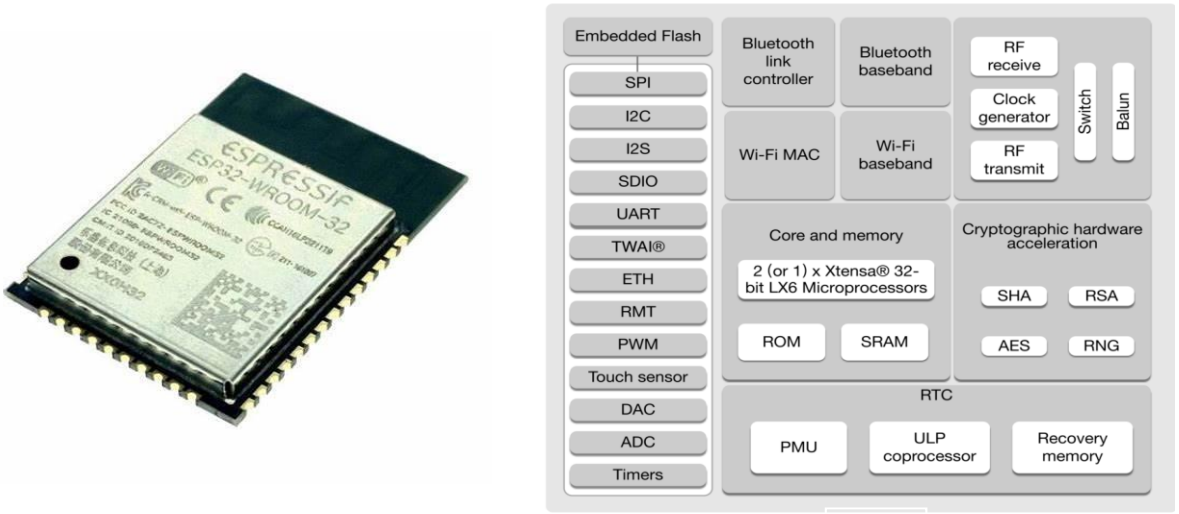

(a) (b)

Figure 3-5: (a) pictures of the ESP32 board and (b) overview of its features.

Regarding the accelerometer, ADXL355, from Analog Devices, is a MEMS sensing unit ideal for integration into a wireless device for low-power IoT (Internet of Things) applications (Figure 3-6). The ADXL355 digital 3-axial accelerometers perform high-resolution vibration measurement with very low noise to also enable early detection of structural defects via wireless sensor networks. The low power consumption of the ADXL355 accelerometers extends battery life and enables extended product use, extending the time between battery changes. The ADXL355 also features low offset drift at 0 g, low power, with selectable measurement intervals. It also offers industry-leading noise, supporting ranges of ±2.048 g, ±4.096 g, and ±8.192 g, minimal thermal offset drift and long-term stability to enable precision applications with minimal calibration and very low power consumption.

The Internet of Things allows more than one protocol to be used for each individual need. This clearly shows that the IoT world is based on different messaging protocols in order to manage all possible applications of the IoT. One of the goals of the IoT is to have intelligent devices that measure, process and transmit information in real time, improving efficiency and the timeliness of corrective actions to be taken.

Among the different synchronization protocols available in the literature implemented in the WSN framework for structural monitoring, the need to balance both the cost containment and performance in terms of accuracy in the synchronization between sensors led to opt for the choice of the NTP1 protocol widely used in SHM applications. NTP was developed by David L. Mills, a

professor at the University of Delaware. The first official description of the protocol, which is part of the Internet protocol family, was published in September 1985 in the RFC 958 document. Here, NTP is described as a protocol for the synchronization of multiple network clocks via a distributed set of clients and servers.

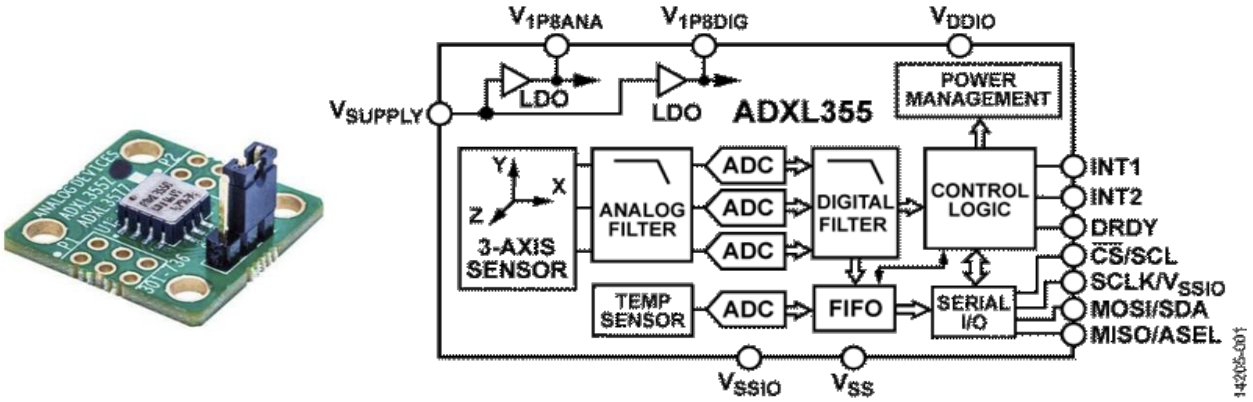

(a) (b)

Figure 3-6: (a) pictures of the ADXL355 accelerometers and (b) its functional block diagram.

On the one hand, NTP owns some practical advantages, such as not adding additional hardware, owing an external RTC clock or GPS, and obtaining a high synchronization rate, up to 1 ms, generally more than satisfactory for node synchronization in wireless network applications for SHM, hence for the applications studied in this thesis work. Finally, the implementation of the NTP protocol in hardware is not particularly onerous both at a computational level and in terms of resources required for the power supply, therefore suitable to be used in devices where low energy consumption is required. The main disadvantage is that it requires Internet access for each new global time request.

For data communication, the choice fell on the FTP3 protocol, which allows large files to be sent efficiently. FTP is the protocol used for data transfer based on a client-server system that allows files to be uploaded, moved and downloaded within directories. This makes it possible to upload files and data to the hosting space quickly and easily and to transfer them securely. In order for the transfer system to work properly, it is necessary to use an FTP client, which allows files to be uploaded or downloaded locally and also remotely via drag & drop, making hosting management simple and straightforward. FTP uses the Transmission Control Protocol (TCP) for data transfer and requires authentication of the client by means of username and password.

This sensor node has been successfully installed within the monitoring system of the Church of Santa Maria in Via in Camerino (Italy). This case study is going to be presented in chapter 5, but data of the developed sensor are not shown as they are still at a very preliminary stage.

4. Outline of the proposed framework

4.1. Preliminary operations

During PhD activities, a framework for the VB-SHM of buildings has been developed. In this chapter, the framework is introduced, and the various steps are discussed in detail.

A preliminary phase for the design of a monitoring system can be defined, in which all necessary tests and analyses are carried out in order to understand the structure to be monitored. The main purpose of a VB-SHM monitoring system is to monitor the dynamics of the structure over time. It is therefore necessary, before undertaking the monitoring, to define an initial step in which efforts are made to gain a comprehensive understanding of the structural dynamics. To do this, the well-established OMA techniques are the best that can be adopted.

Finite element modelling and model updating is often useful, and in most cases necessary, to understand the dynamics identified by preliminary tests. The second step, then, is to model the structure and update the material parameters and boundary conditions. As already mentioned in the second chapter, artificial intelligence now makes various tools available for the automatic updating of models. At this stage, it is important to note that what is being investigated is the dynamics of the structure under operational conditions. Unless destructive tests or forced dynamic tests are performed, there is still no information available on the constitutive law of materials and on the non-linear behavior of the structure, except information available from the design documents and results of the proof tests. Figure 4.1 shows the flow chart of this preliminary phase which already anticipates some numerical techniques used to complete the first three steps.

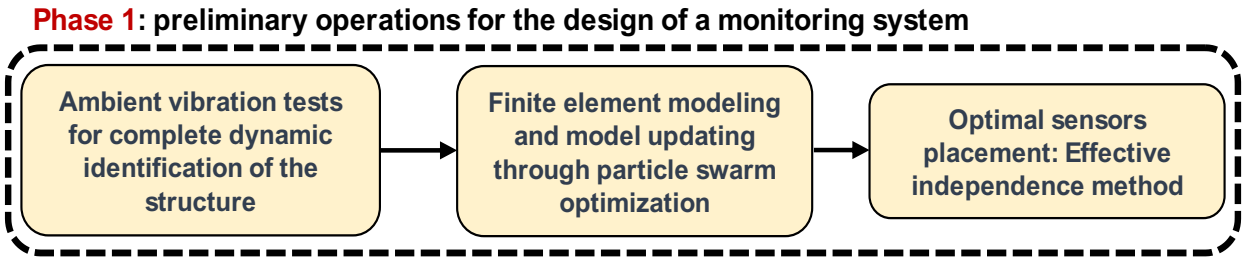

Figure 4-1: Flow chart of the phase one.

4.1.1. Dynamic identification from AVTs

Systems identification can be defined as the science of creating mathematical models of dynamical systems from a set of experimental data. System identification acts as an interface between the physics of dynamic systems and their idealization by means of mathematical models. Early applications of OMA were mainly based on frequency domain analysis of the measured signal.

However, over time new effective output-only modal identification techniques that work in the time domain, such as Stochastic Subspace Identification (SSI) methods, have become available, overcoming the limitations of previous techniques that require a lot of experience in identifying a system by treating the signal in the frequency domain.

Nowadays, it is well established that subspace identification methods are among the most robust and valid in OMA applications. In the author's experience, they often prove to be much more effective than methods operating in the frequency domain, especially in cases where slight non-linearities are present in the structure or when there are modes with very close resonant

frequencies. Also, they are much more versatile and easier to automate for continuous monitoring purposes.

This chapter deals with stochastic system identification methods. Estimation of modal parameters with stochastic identification means that the structure is excited by an unmeasurable input force and that only output measurements (e.g., accelerations) are available. In these methods deterministic knowledge of the input is replaced by the assumption that the input is a stochastic input (white noise). SSI, by solving the dynamic problem in terms of state matrices, leads to a direct estimation the latter and thus, allows the vibration modes to be traced analytically. The breakthrough of the SSI algorithms occurred in 1996 with the publication of the book by van Overschee and De Moor [81]. It is possible to find a short summary developed in the work of Brinker and Andersen [82] and also in PhD dissertation of Peeters [83]. The procedure is based on the extraction and identification of a system matrix A defined in discrete time in the state space represented by the equation of motion. Considering the second-order differential equation of motion of a system with n2 degrees of freedom (MDOF) expressed as:

$$\boldsymbol{M}\ddot{q}(t) + \boldsymbol{C_2}\dot{q}(t) + \boldsymbol{K}q(t) = \boldsymbol{B_2}u(t) \tag{4.1}$$

Where M, C_2 and K are the $n2$ x $n2$ mass, damping and stiffness matrices with $n2$ degrees of freedom, the B_2 matrix (n2 x m) specifies the input position, $u(t)$ is the vector describing the m inputs in time and $q(t)$ is the displacement vector at time t.

The equation (4.1) can be rewritten in the form:

$$\boldsymbol{M}\ddot{q}(t) + \boldsymbol{C_2}\dot{q}(t) + \boldsymbol{K}q(t) + \boldsymbol{M}\dot{q}(t) - \boldsymbol{M}\dot{q}(t) = \boldsymbol{B_2}u(t) \tag{4.2}$$

We now introduce the state vector formulation:

$$x(t) = \begin{pmatrix} q(t) \\ \dot{q}(t) \end{pmatrix} \tag{4.3}$$

we write equation (4.2) in the form:

$$\begin{pmatrix} \boldsymbol{C_2} & \boldsymbol{M} \\ \boldsymbol{M} & \boldsymbol{0} \end{pmatrix} \begin{pmatrix} \dot{q}(t) \\ \ddot{q}(t) \end{pmatrix} + \begin{pmatrix} \boldsymbol{K} & \boldsymbol{0} \\ \boldsymbol{0} & -\boldsymbol{M} \end{pmatrix} \begin{pmatrix} q(t) \\ \dot{q}(t) \end{pmatrix} = \begin{pmatrix} \boldsymbol{B_2} \\ \boldsymbol{0} \end{pmatrix} u(t) \tag{4.4}$$

Substituting (4.3) into (4.4) we obtain:

$$\boldsymbol{P}\dot{x}(t) + \boldsymbol{Q}x(t) = \begin{pmatrix} \boldsymbol{B_2} \\ 0 \end{pmatrix} u(t) \tag{4.5}$$

which represents the differential equation of motion transformed to the first order using the state vector. If at this point, we normalize the (4.5) multiplying it by P^{-1} obtaining the state equation of the system:

$$\dot{x}(t) = \boldsymbol{A_c}x(t) + \boldsymbol{B_c}u(t) \tag{4.6}$$

where c stands for continuous as this is a model described in the continuous and:

$$\boldsymbol{A}_c = \begin{pmatrix} \boldsymbol{0} & \boldsymbol{I} \\ -\boldsymbol{M^{-1}K} & -\boldsymbol{M^{-1}C_2} \end{pmatrix} \quad \boldsymbol{B}_c = \begin{pmatrix} \boldsymbol{0} \\ \boldsymbol{M^{-1}B_2} \end{pmatrix} \tag{4.7}$$

A_c is defined as the state matrix of the system in the form of continuous time.

Considering that in vibrational tests not all the degrees of freedom of the structure are measured but only a subset of them, we can assume that the measurements are made at position l by defining the observation equation as follows:

$$y(t) = \boldsymbol{C_a}\ddot{q}(t) + \boldsymbol{C_v}\dot{q}(t) + \boldsymbol{C_d}q(t) \tag{4.8}$$

where $y(t)$ is the output and C_a, C_v, C_d are the matrices of the positions of the outputs for accelerations, velocities, and displacements, i.e., they represent the matrices that select the measured degrees of freedom among all the degrees of freedom of the structure. By deriving $\ddot{q}(t)$ from (4.1) and substituting it to (4.8) we obtain the observability equation in the continuum written in its final form:

$$y(t) = \boldsymbol{C_c}x(t) + \boldsymbol{D_c}u(t) \tag{4.9}$$

where:

$$\boldsymbol{C_c} = (\boldsymbol{C_d} - \boldsymbol{C_a}\boldsymbol{M^{-1}}\boldsymbol{K} \quad \boldsymbol{C_v} - \boldsymbol{C_a}\boldsymbol{M^{-1}}\boldsymbol{C_2}) \tag{4.10a}$$

$$\boldsymbol{D_c} = \boldsymbol{C_a}\boldsymbol{M^{-1}}\boldsymbol{B_2} \tag{4.10b}$$

Then, putting together the equation of state and the observability equation, one obtains the equation of motion written in the space of state that can be used to calculate the response $y(t)$ of the system to a given input $u(t)$:

$$\dot{x}(t) = \boldsymbol{A_c}x(t) + \boldsymbol{B_c}u(t) \tag{4.11a}$$

$$y(t) = \boldsymbol{C_c}x(t) + \boldsymbol{D_c}u(t) \tag{4.11b}$$

where A is the state matrix, B is the input matrix, C is the output matrix and D is the direct transmission matrix. In order to fit the models to the measurements they have to be converted to discrete time because the measurements are made in discrete time instants. After choosing a period ΔT the equations are discretized and solved at all times.

$t = k\,\Delta T$ with k being a natural number, obtaining:

$$x_{k+1} = \boldsymbol{A}x_k + \boldsymbol{B}u_k \tag{4.12a}$$

$$y_k = \boldsymbol{C}x_k + \boldsymbol{D}u_k \tag{4.12b}$$

where:

$$\boldsymbol{A} = e^{\boldsymbol{A_c}\Delta t} \tag{4.13}$$

$$\boldsymbol{B} = \int_0^{\Delta t} e^{A_c \Delta t}\delta\tau\,\boldsymbol{B_c} = (\boldsymbol{A} - I)\boldsymbol{A_c^{-1}}\boldsymbol{B_c} \quad \text{(only valid if Ac is invertible)} \tag{4.14}$$

$$\boldsymbol{C} = \boldsymbol{C_c} \tag{4.15}$$

$$\boldsymbol{D} = \boldsymbol{D_c} \tag{4.16}$$

What an SSI algorithm does is to derive the state matrix of the system, being the unknown of the problem in the case of vibration measurements, knowing only the measured response of the system.

In a civil engineering context, the only vibration information is the response of a structure excited by some unmeasurable input. Due to the lack of input information, it is not possible (from the point of view of system identification) to distinguish between the terms in u and the input due to noise. So, in discrete time the stochastic state space is written:

$$x_{k+1} = \boldsymbol{A}x_k + \boldsymbol{B}u_k + w_k \tag{4.17a}$$

$$y_k = \boldsymbol{C}x_k + \boldsymbol{D}u_k + v_k \tag{4.17b}$$

where w_k and v_k are both unmeasurable vectors assumed to be zero mean signals (white noise). The input is now modelled implicitly by the noise terms. The consequence is that if this white noise assumption is violated, for example if the input contains, in addition to white noise, some dominant frequency components, these frequency components cannot be separated from the system's own frequencies and will appear as (spurious) poles of the state matrix $\boldsymbol{A}$.

The advantage of formulating the problem in state space is that the general solution is directly derivable:

$$x_k = \boldsymbol{A}^k x_0 \tag{4.18}$$

$$y_k = \boldsymbol{C}\boldsymbol{A}^k x_0 \tag{4.19}$$

where x_0 is the initial state.

In the discrete state, the response of the system is represented by the data matrix

$$\boldsymbol{Y} = [y_1 \quad y_2 \quad \cdots \quad y_N] \tag{4.20}$$

where N is the number of data elements. The Hankel Block Matrix $\mathbf{Y}h$ defined in the ISS is simply a collection of a family of data matrices:

$$\boldsymbol{Y}_h = \begin{bmatrix} \boldsymbol{Y}_{(1:N-2s)} \\ \boldsymbol{Y}_{(2:N-2s+1)} \\ \vdots \\ \boldsymbol{Y}_{(s:N)} \end{bmatrix} = \begin{bmatrix} \boldsymbol{Y}_{hp} \\ \boldsymbol{Y}_{hf} \end{bmatrix} \tag{4.21}$$

The upper half of this matrix is called "past" and is denoted by $\mathbf{Y}_{hp}$ and the lower half of the matrix is called "future" and is denoted by $\mathbf{Y}_{hf}$. The total data shift is $2s$ and indicates "the number of rows" (of the top or bottom half of the Block Hankel matrix). The number of rows of the Block Hankel matrix is $2sM$, the number of columns is N - $2s$.

In the work of van Overschee and De Moor, projection is introduced as a geometric tool. Specifically, in the ISS it is defined as the projection of the future into the past.:

$$\boldsymbol{O} = E(\boldsymbol{Y}_{hf} \,|\, \boldsymbol{Y}_{hp}) \tag{4.22}$$

Since data matrices also define covariances, it is not surprising that the projection can be calculated directly as also defined by van Overschee and De Moor:

$$\boldsymbol{O} = \boldsymbol{Y}_{hf}\boldsymbol{Y}_{hp}^T(\boldsymbol{Y}_{hp}\boldsymbol{Y}_{hp}^T)^{-1}\boldsymbol{Y}_{hp} \tag{4.23}$$

The last matrix in this product defines the conditions, the first four product matrices introduce the covariance between the channels at different times. Using equation (1.18) and (1.19) each column of $\mathbf{O}$ can be expressed as:

$$o_{col} = \boldsymbol{\Gamma}_s x_0 \tag{4.24}$$

$$\boldsymbol{\Gamma}_s = \begin{bmatrix} \boldsymbol{C} \\ \boldsymbol{C}\boldsymbol{A} \\ \boldsymbol{C}\boldsymbol{A}^2 \\ \vdots \\ \boldsymbol{C}\boldsymbol{A}^{s-1} \end{bmatrix} \tag{4.25}$$

Since we do not know the initial state, we cannot calculate the observability matrix $\boldsymbol{\Gamma}$, the expedient is to use SVD (Singular Value Decomposition) on the matrix $\mathbf{O}$

$$\boldsymbol{O} = \boldsymbol{USV}^T \tag{4.26}$$

It is nothing more than a matrix factorization that allows the information contained within it to be synthesized.

And so calculate the matrix $\boldsymbol{\Gamma}_s$ the initial state matrix $\widehat{\boldsymbol{X}}_0$ (constituted by the initial conditions for all columns of the projection matrix) from:

$$\widehat{\boldsymbol{\Gamma}} = \boldsymbol{US}^{\frac{1}{2}} \tag{4.27}$$

$$\widehat{\boldsymbol{X}}_0 = \boldsymbol{S}^{\frac{1}{2}}\boldsymbol{V}^T \tag{4.28}$$

There are other methods for calculating the observability matrix, the one described here is the SSI-PC (Stochastic Subspace Identification- Principal Component) method, which determines the state matrix from the singular values and left singular vectors of the projection matrix.

The state matrix $\mathbf{A}$ can be found from the matrix $\boldsymbol{\Gamma}$ by removing one block from the top and one block from the bottom:

$$\widehat{\boldsymbol{\Gamma}}_{(2:s)}\boldsymbol{A} = \widehat{\boldsymbol{\Gamma}}_{(1:s-1)} \tag{4.29}$$

By doing so, the matrix $\mathbf{A}$ can be found by regression. The output matrix $\mathbf{C}$ can be found simply by taking the first block of the observability matrix:

$$\boldsymbol{C} = \boldsymbol{\Gamma}_{(1:1)} \tag{4.30}$$

Finally, to obtain the modal parameters, we perform a spectral decomposition of the system matrix:

$$\boldsymbol{A} = \boldsymbol{\psi}[\mu_i]\boldsymbol{\psi}^{-1} \tag{4.31}$$

where μ_i are the eigenvalues, $\boldsymbol{\psi}$ are the eigenvectors and i is the number of vibration modes. One can calculate the eigenvalues of the system matrix in continuous time from those calculated in discrete time with the relation:

$$\lambda_i = \frac{ln(\mu_i)}{dt} \tag{4.32}$$

where dt is the discrete sampling period calculated as the inverse of the sampling frequency. At this point the modal parameters of the system can be easily determined from the following formulas:

$$\omega_i = |\lambda_i| \tag{4.33}$$

$$f_i = \frac{\omega_i}{2\pi} \tag{4.34}$$

$$\xi_i = \frac{Re(\lambda_i)}{|\lambda_i|} \tag{4.35}$$

$$\boldsymbol{\phi} = \boldsymbol{C\psi} \tag{4.36}$$

Where ω_i are the pulsations, f_i are the frequencies, ξ_i are the damping ratios and $\boldsymbol{\phi}$ is the modal form matrix. The number s defines the size of the Block Hankel matrix, and therefore also the size

of the projection matrix $\mathbf{O}$. The number sM defines the number of eigenvalues in our model, i.e., sM defines the order of the model.

Parametric identification methods, such as the SSI presented here, suffer a substantial problem: the a priori choice of the order of the dynamic system, i.e., the number of degrees of freedom. The most common practice to overcome this drawback is to repeat the identification for different orders of the dynamic system, included in a priori established interval. In this way, many values of the modal parameters are obtained for each vibration mode, resulting in what is called a stabilization diagram. This inevitably leads to the occurrence of non-physical modes, called spurious modes, which will have to be isolated from the real modes, and discarded from results. In practice, the size of the Block Hankel matrix defines the maximum order of the model, and the order of the real model is varied by varying the number of singular values taken into account when performing the singular decomposition of the projection matrix. The maximum number of eigenvalues sM must be appropriate for the system which must be identified.

4.1.2. Automatic modal updating

The aim of Model Updating (MU) of FEM is to numerically reproduce the dynamic behavior of the structure experimentally identified through OMA procedures. Basically, the aim is to bring the analytical modal parameters as close as possible to the experimental ones.

In order to determine which model is closest to the experimental measurement and therefore to reality, in addition to comparing frequencies of the first three vibration modes, the Modal Assurance Criterion (MAC) between numerical and experimental mode shapes was also calculated.

$$MAC_{ij} = \frac{\left|\psi_i^T \psi_j\right|^2}{\left(\psi_i^T \psi_i\right)\left(\psi_j^T \psi_j\right)} \tag{4.36}$$

MACij is an index that varies between 0 and 1 and determines how two mode shapes match to each other; when MAC is equal to 1 there is a perfect match between the modes.

In order to speed up the analysis, instead of manually varying parameters for each analysis, an algorithm has been developed in MATLAB, which allows the calibration of the elastic modulus values for the various materials, the execution of the modal analysis and the return of frequency values of the structure and the modal displacements of the nodes relative to DOFs monitored during the preliminary dynamic test. Then, this algorithm was incorporated into an artificial intelligence algorithm for automatic calibration, called particle swarm optimization algorithm.

As already mentioned in the literature review of Chapter 2, Particle Swarm Optimization is a stochastic optimization technique inspired by the social behavior of a population of birds and applied in many research areas. It is a method aimed at optimizing non-linear functions using a stochastic-based algorithm that requires only the use of simple mathematical operators and, therefore, it is computationally cheap.

In PSO, a number of particles are placed in the search domain of some objective function, and, for each position assumed by the particles, this function is calculated. Each particle then determines its movement through the search domain by combining some aspect of its own position and the best-fit position found with those of one or more members of the swarm. The aim of this algorithm is to find the global minimum of the chosen objective function. Each individual in the particle swarm is composed of three D-dimensional vectors, where D is the dimension of the search space. They are the current position, the best position found up to that iteration and the velocity. The current position can be considered as a set of coordinates describing a point in space. At each iteration of

the algorithm, the current position is evaluated as the solution to the problem. If this position is better than any found so far, then the coordinates are stored in the second vector. The value of the best result of the function so far is stored in a variable for comparison in subsequent iterations.[14] The goal, of course, is to continue to find better positions and update the value of the objective function. To begin with, the particles are distributed randomly in the search space and a random velocity vector is defined, which is why PSO is called a stochastic algorithm. During the iterations the velocity of each particle is accelerated towards its previously found best position and towards the best solution found by the particle group. Therefore, this velocity is governed by the two best values found so far (personal and group) and by the inertia the particle is subjected to.

$$P_i^{t+1} = P_i^t + V_i^{t+1} \tag{4.37}$$

$$V_i^{t+1} = wV_i^t + c_1 r_1 (P_{best(i)}^t - P_i^t) + c_2 r_2 (P_{bestglobal}^t - P_i^t) \tag{4.38}$$

where P is the position and V the velocity at time. The three vectors that allow to evaluate the velocity at each iteration are calibrated and weighted through three coefficients w, c1, c2 that are defined as hyperparameters, moreover the contribution of the position of the single particle and the position of the group of particles are weighted through two coefficients r1 and r2. The hyperparameter w is used to define the ability of the swarm to change its direction. The particles have an inertia proportional to this coefficient w. The lower the coefficient w, the faster the convergence. In other words, a low w coefficient facilitates the exploitation of the best solutions found so far, while a high w coefficient facilitates exploration around these solutions. The inertia weight w then makes a balance between exploration and exploitation of the best solutions found so far. The hyperparameter c1 allows to define the ability of the group to be influenced by the best personal solutions found during the iterations. The hyperparameter c2 allows us to define the group's ability to be influenced by the best global solution found during the iterations. In the literature there are many indications on the values to assign to these hyperparameters derived from various experimental evidence. After having tried different combinations of values of the hyperparameters, it was decided to adopt w varying between 0 and 0.8, c1 equal to 1 and c2 equal to 2 because these are the ones that lead to a faster decrease of the objective function for the problem under examination. Another parameter to be set for the analysis is the population size. This is set empirically based on the size of the problem and the difficulty of the solution; in this case a population size of 10 times the number of parameters to be varied was adopted.

To deploy PSO, the domain in which the particles search for the solution must be defined, i.e., the range of variation of each parameter. Any objective function representing the distance between the experimental and theoretical dynamics can be used. One of the simplest functions to implement that considers both frequency and modal shapes is given in eq. 4.39.

$$err = \left| \frac{f_{num} - f_{exp}}{f_{exp}} \right| + \left(1 - MAC_{num,exp.}\right) \tag{4.39}$$

4.1.3. Optimal Sensor Placement

Optimal Sensor Placement (OSP) is one of the issues to be addressed in the design of a proper SHM System. As described in Chapter 2, several methods and algorithms have been developed over time to address and solve OSP.

The Effective Independence method was at first proposed by D.C. Kammer in 1991 [19]. The method was presented for the selection of a set of sensor positions from a larger set of possible positions in

order to identify the vibration modes of an orbiting structure. The positioning of the sensors on an orbiting structure was a key problem because of the weight and cost of each sensor; the aim was to position as few sensors as possible.

Kammer's aim was to validate a FEM of the orbiting structure using measurements obtained from sensors. The sensors must then be positioned to collect data such as vibration modes and eigenfrequencies during dynamic tests in space, and these data are then compared to the FEM in order to bring it closer to the dynamic behavior of the real structure.

Unlike other methods, such as genetic algorithms, the Effective Independence method does not rely on computationally intensive search techniques. The method is based on the choice of what are called 'target modes' that are used for dynamic identification. A set of possible sensor positions is then chosen and ranked according to how much they contribute to the linear independence of the various vibration modes. Positions that do not contribute are discarded. The method proposed by Kammer is an iterative method: the set of candidate positions is quickly reduced to the number of available sensors.

In the following, the theoretical formulation of Kammer's Effective Independence Method is presented. Initially, a set of candidate positions must be selected, which must be large enough to include all the target modes one wishes to identify. In the case study Kammer selected the set of candidate positions based on the modal kinetic energy distribution which gives a measure of the dynamic contribution of each degree of freedom of the FEM to each mode of vibration. The energy distribution is calculated as:

$$KE_{in} = \Phi_{in} \sum_{j} M_{ij} \, \Phi_{jn} \tag{4.40}$$

Where KE_{in} is the kinetic energy associated with the i-th degree of freedom of the n-th mode, Φ_{in} is the i-th coefficient of the n-th mode of vibration, M_{ij} is the term in the i-th row and j-th column of the FEM mass matrix, φjn is the j-th coefficient of the n-th mode of vibration. The candidate positions must have a sufficient value of kinetic energy for each target mode, e.g., 40-50%.

The spatial independence between modal shapes implies that at each instant, if the sensor output is given by:

$$u_s = \boldsymbol{\Phi}_s q \tag{4.41}$$

Then the sensor can be sampled and an estimate for the target states can be calculated using:

$$\hat{q} = [\boldsymbol{\Phi}_s^T \boldsymbol{\Phi}_s]^{-1} \boldsymbol{\Phi}_s^T u_s \tag{4.42}$$

Where us is the output of the sensors, $\boldsymbol{\Phi}_s$ is the modal matrix of the FEM partitioned with the candidate positions, q is the vector of modal coordinates.

If the set of candidate sensors contains s positions, but the available resources limit the number of sensors to m < s, the problem is to place m sensors within the s positions while retaining as much information as possible. The best estimate implies that the covariance matrix of the estimated error is minimal.

Following a development proposed by Udwadia and Garba [84] the output of the sensors is written as:

$$u_s = \boldsymbol{H}(q) + N = \boldsymbol{\Phi}_s q + N \tag{4.43}$$

Where H represents the measurement process and N represents the noise. For efficient estimation without error, the covariance matrix of the estimated error is given by:

$$\boldsymbol{P} = E[(q - \hat{q})(q - \hat{q})^T] = \left[\left(\frac{\partial \boldsymbol{H}}{\partial q}\right)^T [\boldsymbol{\Psi}_0^2]^{-1} \left(\frac{\partial \boldsymbol{H}}{\partial q}\right)\right]^{-1} \tag{4.44}$$

Where E is the expected value. Furthermore, given:

$$\boldsymbol{H}(q) = \boldsymbol{\Phi}_s q \tag{4.45}$$

The covariance matrix becomes:

$$\boldsymbol{P} = [\boldsymbol{\Phi}_s^T (\boldsymbol{\Psi}_0^2)^{-1} \boldsymbol{\Phi}_s]^{-1} = \boldsymbol{Q}^{-1} \tag{4.46}$$

Where $\boldsymbol{Q}$ is the Fisher information matrix. Maximising $\boldsymbol{Q}$ leads to minimising the covariance matrix and thus to a better estimate of $\hat{q}$. To simplify the analysis, we assume that the noise measurement is uncorrelated and has identical statistical properties for each sensor. The Fisher Information Matrix can be expressed as:

$$\boldsymbol{Q} = \frac{1}{\boldsymbol{\Psi}_0^2} \boldsymbol{\Phi}_s^T \boldsymbol{\Phi}_s = \frac{1}{\boldsymbol{\Psi}_0} \boldsymbol{A}_0 \tag{4.47}$$

In terms of the contribution of each degree of freedom, $\boldsymbol{A}_0$ can be written as:

$$\boldsymbol{A}_0 = \sum_{i=1}^{s} \boldsymbol{\Phi}_s^{iT} \boldsymbol{\Phi}_s^i = \sum_{i=1}^{s} \boldsymbol{A}^i \tag{4.48}$$

Where $\boldsymbol{\Phi}_s^i$ the i-th row of the partitioned modal matrix $\boldsymbol{\Phi}_s$ corresponding to the i-th position of a sensor. The equation shows how adding or subtracting a degree of freedom from the set of candidate sensor positions removes or adds information to the Fisher matrix. From the set of candidate positions all positions that do not contribute significantly to the independence of the information about the target modes can be removed.

The analysis starts by solving the problem at the eigenvalues:

$$[\boldsymbol{A}_0 - \lambda \boldsymbol{I}]\boldsymbol{\Psi} = \boldsymbol{0} \tag{4.49}$$

The k columns of $\boldsymbol{\Phi}_s$ corresponding to the target modes are assumed to be linearly independent for the initial set of candidate sensor positions. This means that $\boldsymbol{A}_0$ is a k x k matrix, defined as positive and symmetric. The eigenvalues of $\boldsymbol{A}_0$ are therefore real and positive and the eigenvectors $\boldsymbol{\Psi}$ are orthonormal, obtained from the relations:

$$\boldsymbol{\Psi}^T \boldsymbol{A}_0 \boldsymbol{\Psi} = \lambda \tag{4.50}$$

$$\boldsymbol{\Psi}^T \boldsymbol{\Psi} = \mathrm{I} \tag{4.51}$$

Since the vectors $\boldsymbol{\Psi}$ are orthogonal, they represent k directions in a space of dimension k, which is called absolute identification space. By making the product:

$$\boldsymbol{G} = [\boldsymbol{\Phi}_s \boldsymbol{\Psi}] \otimes [\boldsymbol{\Phi}_s \boldsymbol{\Psi}] \tag{4.52}$$

where the symbol $\otimes$ represents the term-by-term multiplication between matrices, the result being the matrix $\boldsymbol{G}$ that in each row contains the square of the components of each row of φs in terms of the coordinate system defined by the columns of $\boldsymbol{\Psi}$. Each column of $\boldsymbol{G}$ sums the corresponding eigenvalues of $\boldsymbol{A}_0$. Thus, the i-th term within a column represents the contribution of the sensor at

the i-th position to the associated eigenvalue. If $\boldsymbol{G}$ is post-multiplied by the inverse of the eigenvalue matrix λ:

$$\boldsymbol{F}_E = [\boldsymbol{\Phi}_s \boldsymbol{\Psi}] \otimes [\boldsymbol{\Phi}_s \boldsymbol{\Psi}] \lambda^{-1} \tag{4.53}$$

Each direction of the absolute identification space now has the same importance. The i-th term in the j-th column of the F_E matrix (s x k) represents the contribution of the i-th sensor to the j-th eigenvalue. Adding up the terms in each row of F_E we obtain:

$$E_D = \left[\sum_{j=1}^{k} \boldsymbol{F}_{E1j} : \sum_{j=1}^{k} \boldsymbol{F}_{E2j} : \cdots : \sum_{j=1}^{k} \boldsymbol{F}_{Esj} \right]^T \tag{4.54}$$

Where F_{Eij} represents the j-th term of the i-th row of the F_E matrix. The vector ED represents the distribution of "Effective Independence" of a set of candidate positions, the i-th term of E_D represents the contribution of the sensor at the i-th position to the linear independence of the modes.

For example, a vector of "Effective Independence" described as:

$$E_D = \begin{bmatrix} 1.0 \\ 0.5 \\ 0.5 \end{bmatrix} \tag{4.55}$$

It indicates that the sensor positioned at 1 is vital for linear independence and identification of vibration modes, while the sensors at 2 and 3 are of equal importance and one of the two can be eliminated without affecting mode independence. The E_D vector thus offers an evaluation of the various positions according to their importance for the identification and correlation of the target modes.

$$0 \leq E_{Di} \leq 1 \tag{4.56}$$

If E_{Di} is equal to 0, the sensor at that position does not contribute; if E_{Di} is equal to 1, that position must be maintained in the final sensor configuration. Different sensor positions are classified iteratively and those that do not contribute are identified and eliminated. Using this approach, the final configuration of the set number of sensors is achieved. It is important to note that the "Effective Independence" value of each sensor changes each time when there is a sensor elimination and a new iteration such that the sum of the components of the E_D vector is always equal to k number of target modes. The individual position becomes more or less important as iterations go on. The best approximation of the optimal configuration is achieved by deleting one position at a time.

4.2. Deploying the monitoring system

Once the preliminary steps have been carried out, it is possible to proceed with the implementation of the dynamic monitoring system (Figure 4-2). As already mentioned in chapter 2, it is not possible to make a standard choice of the sensor typologies and, once the most interesting DOFs to monitor have been identified, the sensor optimal characteristics must be established. It is also necessary to define the communication protocols and the file format in which data are stored.

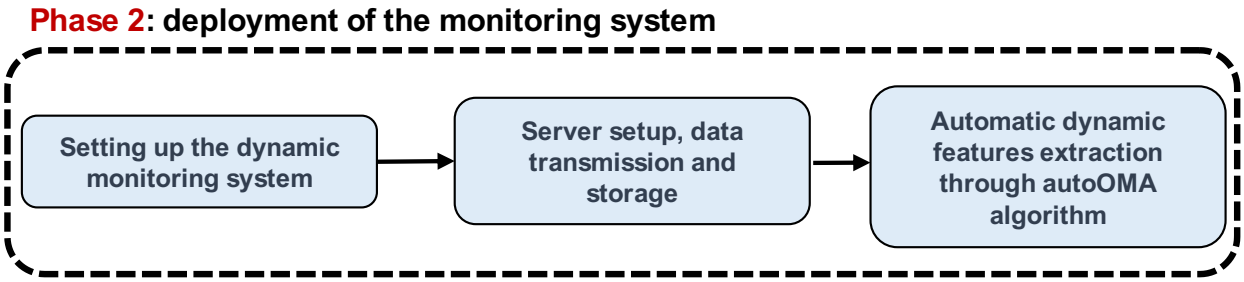

Figure 4-2: Flow chart of phase two.

Figure 4.3 gives an overview of the typical monitoring system that has been developed during the PhD work. It is a monitoring system with real-time features, with an ad-hoc developed acquisition software that is very versatile in managing different types of sensors and able to handle different sampling rates simultaneously. Over time it has proved to be robust without ever experiencing abrupt breakdowns or loss of files. Files are stored in National Instruments proprietary format, TDMS (Technical Data Management Streaming).

The TDMS file format is an easily exchangeable, inherently structured file format capable of high-speed streaming. The TDMS file format is structured using three levels of hierarchy, namely file, group and channel. The file level can contain an unlimited number of groups, and each group can contain an unlimited number of channels. At each level of the hierarchy, an unlimited number of custom scalar properties can be stored. Each level accepts an unlimited number of custom attributes to obtain well-documented, search-ready data files. The descriptive information located in the file, a key advantage of this model, provides an easy way to document data without having to design your own header structure. Regarding the communication protocol, the FTP protocol was chosen.

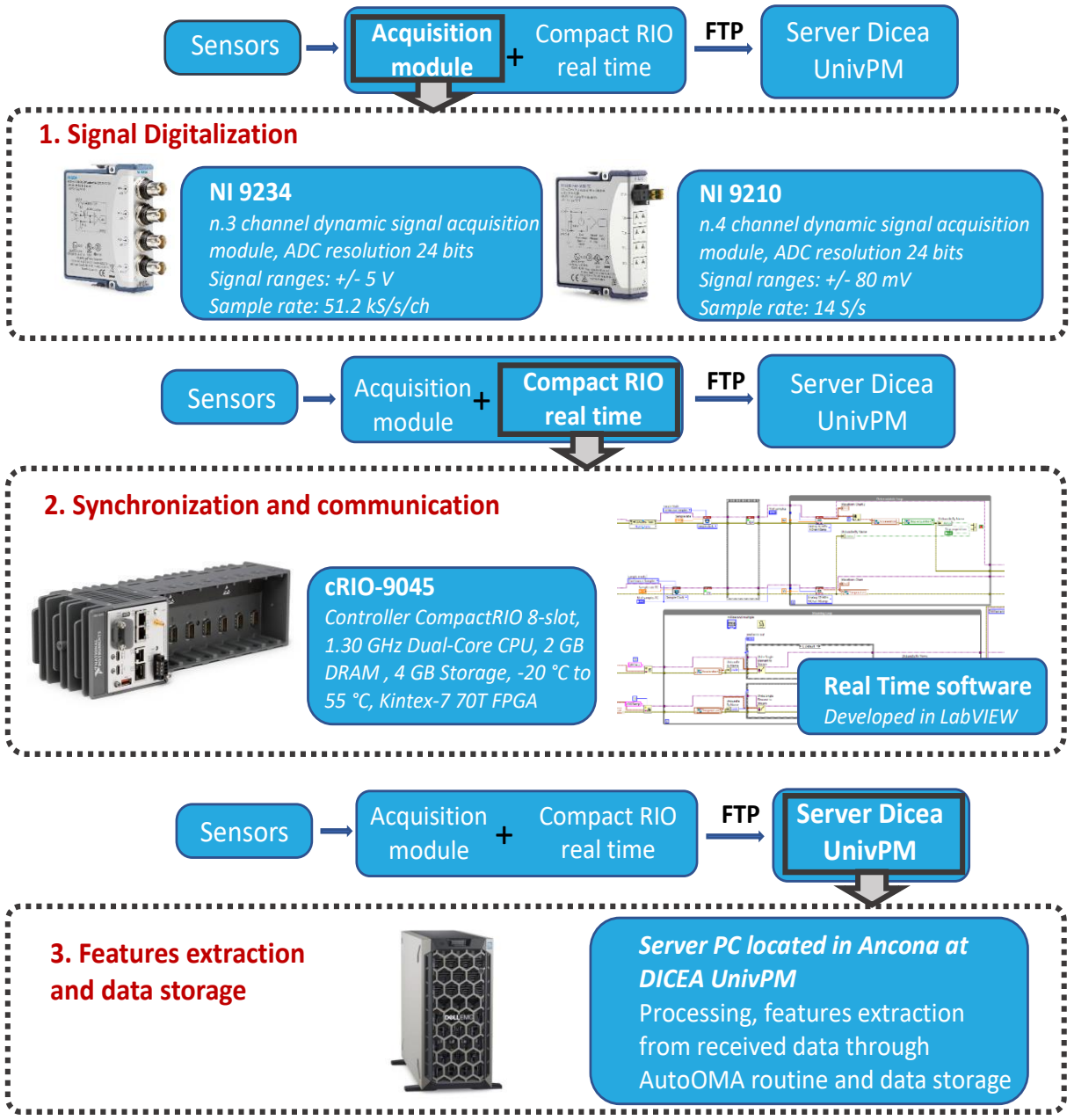

Figure 4-3: Schematization of the monitoring system representing all its components.

4.2.1. Automatic identification through hierarchical clustering

As anticipated in 4.1.1, in dynamic identification through subspace identification algorithm, one would want to vary the model order so that a stabilization diagram can be drawn. This can be done by establishing a set of Block Hankel matrices of different sizes, but it is easier, instead of varying the size of the Block Hankel matrix, to vary the number of singular values used in equation (4.26). Dynamic identification methods in the time domain, especially those based on state-space theory, need a priori choice of the order of the dynamic system, i.e., the number of degrees of freedom. The most common practice to overcome this drawback is to repeat the identification for different orders of the dynamical system, included in an a priori established interval. In this way, many values of the modal parameters are obtained for each mode of vibration, resulting in what is called a stabilization diagram. This inevitably leads to the occurrence of non-physical modes, called

spurious modes, which will have to be isolated from the real modes, and discarded from the results. Once all solutions have been collected in the stabilization diagram, the operation of distinguishing spurious modes from real modes remains to the operator. A very advantageous way to automate OMA is to use a cluster analysis on the total solutions obtained by varying the order of the model.

Cluster analysis (or group analysis) is a technique based on the grouping of elements with similar characteristics. These resulting groups are called clusters. This technique is adopted in the context of stabilization diagram interpretation with the aim of grouping together estimated modes with the same modal characteristics. The most common clustering algorithms can be divided into two main categories:

- Non-Hierarchical Clustering Algorithms.
- Hierarchical Clustering Algorithms.

Non-hierarchical clustering algorithms usually use the k-means algorithm, in which the data set is divided into an arbitrarily defined number of clusters (K). For each cluster a centroid is defined, i.e., a point at the centre of the cluster. Then the algorithm initially calculates the Euclidean distance between each dataset and each centroid. Each dataset will then be assigned to the centroid with the minimum distance. After this operation, new clusters can be formed. The algorithm proceeds iteratively until the centroids do not change, i.e., convergence is achieved and there are no more changes in the clusters. The main problem in using this type of algorithm is that the number of clusters must be defined in advance. Furthermore, this algorithm randomly chooses the distance from the centre, and this may lead to non-repeatable results. The hierarchical clustering algorithm is based on the construction of a binary fusion tree which can be done through two techniques:

- AHC Agglomerative Hierarchical Clustering.
- DHC Divisive Hierarchical Clustering.

Agglomerative hierarchical clustering AHC is based on the principle that initially each piece of data is considered a cluster. In the next step the two closest clusters are paired into a new agglomerative cluster. In succession the number of clusters tends to decrease until all elements have been clustered and consequently the aggregations become larger and larger. Divisive hierarchical clustering works in the opposite way. Specifically, it starts with the complete data set and progressively divides this set down to the individual elements. The graphical representation of a cluster analysis is called a dendrogram and an example is shown in the Figure 4-4, with an observation also on the type of hierarchical clustering.

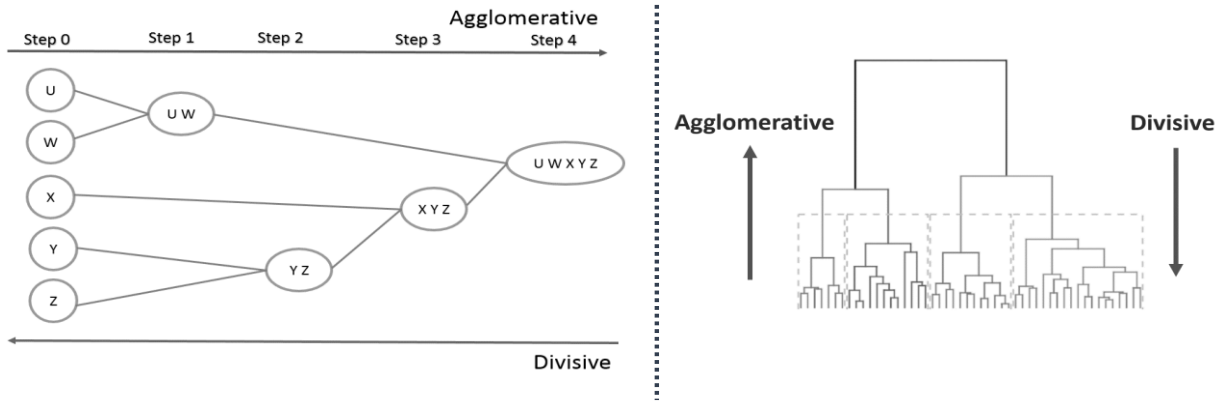

Figure 4-4: outline of the two approaches: Agglomerative Hierarchical Clustering and Divisive Hierarchical Clustering.

When creating a hierarchical agglomerative clustering algorithm, it is essential to define two quantities: distance and linkage. The calculation of the distance between the modal parameters of the stabilization diagram can be carried out using the following formulas.

The automatic identification algorithm includes a first step in which the stabilization diagram is obtained by applying the SSI-PC algorithm, after which the modal parameters are selected by an algorithm based on Agglomerative Hierarchical Clustering (AHC). Agglomerative hierarchical clustering is based on the fact that initially each data item is considered as a cluster. In the next step the two closest clusters are paired into a new aggregated cluster. In succession the number of clusters tends to decrease until all elements have been clustered. In order to develop an agglomerative hierarchical clustering algorithm, it is essential to define the distance between solutions. The distance between solutions of the stabilization diagram is calculated using following equation:

$$D_{ij}(f) = \left|\frac{f_i - f_j}{f_j}\right| + (1 - MAC_{ij}) \tag{4.57}$$

While the first term of the formula represents the error between the frequencies calculated with model order equal to n and those with model order equal to n-1. Hierarchical clustering algorithms differ depending on how the distance between two clusters is calculated. This particular distance is called linkage Δ and can be of different types (Figure 4-5):

1) Single linkage (SL) where the shortest distance between two data clusters is taken into account X_i and X_j

$$\Delta(X_i, X_j) = \min_{x_i \in X_i,\, x_j \in X_j} D(x_i,\, x_j) \tag{4.58}$$

2) Complete linkage (CL) where the longest distance between two data clusters is taken into account X_i and X_j

$$\Delta(X_i, X_j) = \max_{x_i \in X_i,\, x_j \in X_j} D(x_i,\, x_j) \tag{4.59}$$

3) Group average linkage (LAGs) where the average between each cluster element is taken into account X_i and X_j

$$\Delta(X_i, X_j) = \frac{1}{|X_i||X_j|} \sum_{x_i \in X_i} \sum_{x_j \in X_j} D(x_i,\, x_j) \tag{4.60}$$

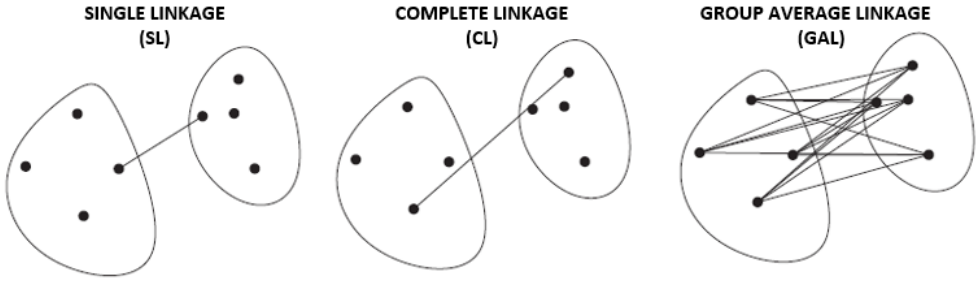

Figure 4-5: Different approaches to defining linkage.

The methodology proposed for the automatic identification of the modal parameters is based on the calculation of the distance through equation (4.57) and the linkage between the clusters of single type.

In this study, 2% has been taken as the threshold distance between one solution and another in order to group them in the same cluster. Furthermore, for the subsequent case studies, solutions with negative frequencies or damping ratios greater than 10% are discarded, and clusters with a low number of solutions are not considered (the threshold relative to the minimum number of solutions depends on the maximum model order and is defined case by case).

4.3. Management and interpretation of data

At this stage, we can assume that the monitoring system is installed on the structure subject to dynamic monitoring and that the data regularly flows to the control server. To assess changes in structural dynamics, it is necessary to consider two main phenomena. At first, during its life a structure will be exposed to events characterized by higher acceleration levels than those related to the operational conditions. Buildings rarely show time invariant dynamic behavior when exposed to a deviation from the operating conditions and this must be managed. In such cases, an intuitive and easily developable solution is that of trying to linearize the structural response, so that the evolution of the modal parameters can continue to be monitored.

Then, environmental parameters, and especially temperature, tend to have important effects on modal parameters. Both daily and seasonal phenomena can be observed when monitoring data are analyzed. The physical interpretation of these effects is not trivial; the effect of temperature on modal parameters in summer may be different from that in winter. This very often makes these types of dependencies non-linear. The solution to this issue can be approached in different ways. This non-linearity may be due to a lack of knowledge of the structure under consideration, so it could be thought to expand the hyperspace in which the phenomenon is described by increasing the number of sensors on the structure (thermocouples at different points, strain gauges, etc.) until the phenomenon becomes linear, but this is very often economically unfeasible. On the other hand, a sustainable solution is possible by applying BSS techniques already mentioned in Chapter 2. A very attractive approach is to rely on artificial neural networks, which are now well-established numerical techniques and that can easily handle non-linear dependencies between modal parameters and environmental parameters. In any case, a preliminary observation period, which in most cases can range from 12 to 18 months, is necessary.

Figure 4-6 shows the layout of this last phase that leads to data-driven structural monitoring. It is important to emphasize that this type of monitoring can lead to a detection of damage (Level 1 of VB-SHM [6]), but is not able, at this stage, to localize the damage and to quantify it. In this section, solutions are proposed to address these two problems, namely linearization of the structural non-linear response and management of the effects of environmental conditions.

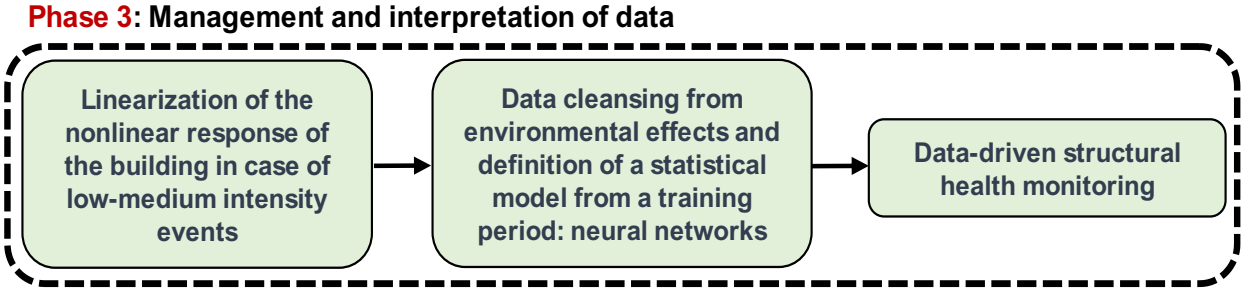

Figure 4-6: Flow chart of phase three.

4.3.1. Linearization of the non-linear structural response

Recording the dynamic response of the structures during seismic events offers significant benefits: on one hand, it provides useful information for the damage identification and the post-earthquake emergency management (especially in case of strategic buildings); on the other hand, it allows the reduction of seismic risk through the decrease of uncertainties related to both the hazard estimation (e.g. unexpected frequency contents of seismic events, unpredicted soil-structure interaction detrimental effects) and the structural vulnerability (e.g. unexpected damage or structural performance). The reduction of uncertainties about vulnerability can derive from the comparison

of the real structural response for low-medium intensity events with the expected numerical one (e.g., obtained through the design model), while the reduction of uncertainties related to the hazard presupposes the monitoring of the free-field (nearby the building) and of the soil-foundation system.

With reference to a specific structural typology, the availability of simple and direct relationships between the variation of modal parameters (with respect to the undamaged condition), and the presumed damage levels, are of the utmost importance for the practical utility of data collected by monitoring systems [85], especially in the case of medium-high seismic intensities. However, the definition of these relationships presents problems related to the intrinsic variability of the modal parameters of the structure with respect to both the intensity of the excitation and the environmental conditions. With specific regard to the frequency variation of RC buildings during strong seismic events, the work of Calvi [86] presents an interesting state of the art of the problem. More recently, the variation in modal parameters of civil structures subjected to seismic actions has been the subject of several studies, including Ditommaso et al. [87], Ghahari et al. [88], Ceravolo et al. [85], Hu and Xu [89] and O'Reilly et al. [90].

In case of seismic excitations, the characteristics of the input to the dynamic system do not satisfy the assumptions required for OMA. Therefore, it is necessary to apply input-output identification techniques. Also in this case, subspace identification methods have proven to be reliable and robust approaches for the dynamic characterization of complex multi-input multi-output (MIMO) dynamic systems with close eigen-frequencies and have been successfully used for several years also in the field of civil engineering. In particular, two of the most popular algorithms used for combined MIMO systems identification (deterministic and stochastic) are the Multivariable Output Error State Space (MOESP) [91] and the Numerical algorithm for Subspace State Space System IDentification (N4SID) [81]. Skolnik et al. [92] adopted the N4SID algorithm to identify the dynamics of a 17-story steel moment resisting frame, the UCLA Louis Factor building, during low-amplitude earthquake; Ceravolo et al. [85] used the same algorithm to investigate the dynamic response of three buildings subjected to the seismic swarm occurred in Lunigiana-Garfagnana starting from June 21st, 2013; Illescas et al. [93] used both the N4SID and the MOESP for the structural health monitoring of an elevated railroad segment of Mexico City Metro Line 12, while Boroschek et al. [94] implemented the MOESP algorithm to identify the dynamic of a building subjected to the 2010 Gigantic Chile Earthquake.

As known, the first step to use a subspace identification methodology, is to represent the structural dynamics through a state space system model, which is described by the following set of equations, including a state equation (Eq. 4.61a) and an output equation (Eq. 4.61b) (process form):

$$\boldsymbol{x}_{k+1} = \boldsymbol{A}\boldsymbol{x}_k + \boldsymbol{B}\boldsymbol{u}_k + \boldsymbol{w}_k \tag{4.61a}$$

$$\boldsymbol{y}_k = \boldsymbol{C}\boldsymbol{x}_k + \boldsymbol{D}\boldsymbol{u}_k + \boldsymbol{v}_k \tag{4.61b}$$

where $\boldsymbol{u}_k \in \mathbb{R}^m$ and $\boldsymbol{y}_k \in \mathbb{R}^l$ denotes the input and output signals, respectively, at a certain time k, while $\boldsymbol{x}_k \in \mathbb{R}^n$ is the state vector. In addition, $\boldsymbol{A} \in \mathbb{R}^{n\times n}$ is the dynamical system matrix, $\boldsymbol{B} \in \mathbb{R}^{n\times m}$ is the input matrix that describes how the deterministic inputs influence the next state, $\boldsymbol{C} \in \mathbb{R}^{l\times n}$ is the output matrix that characterizes how the internal state influence the outputs and $\boldsymbol{D} \in \mathbb{R}^{l\times m}$ is the direct transition matrix. For a linear time-invariant system above matrices are constant.

Furthermore, $\boldsymbol{w}_k \in \mathbb{R}^n$ and $\mathbf{v}_\mathrm{k} \in \mathbb{R}^\mathrm{l}$ are unmeasurable vector signals, which are assumed to be normally distributed, zero mean, white noise signals for which:

$$E\left[\begin{pmatrix}\boldsymbol{w}_p\\ \boldsymbol{v}_p\end{pmatrix}\begin{pmatrix}\boldsymbol{w}_q^T & \boldsymbol{v}_q^T\end{pmatrix}\right] = \begin{pmatrix}\boldsymbol{Q} & \boldsymbol{S}\\ \boldsymbol{S}^T & \boldsymbol{R}\end{pmatrix}\delta_{pq} \geq 0 \tag{4.62}$$

where E is the expected value operator and δ_{pq} is the Kronecker delta. Finally, $\boldsymbol{Q} \in \mathbb{R}^{n\times n}$, $\boldsymbol{S} \in \mathbb{R}^{n\times l}$ and $\boldsymbol{R} \in \mathbb{R}^{l\times l}$ are matrices of suitable dimensions. The mathematical problem, which is solved through the N4SID algorithms, is that of identifying matrices $\boldsymbol{A}$, $\boldsymbol{B}$, $\boldsymbol{C}$, $\boldsymbol{D}$, $\boldsymbol{Q}$, $\boldsymbol{R}$ and $\boldsymbol{S}$ given input and output measurements. It is well known that Eq. 61 can be also expressed as (innovation form):

$$\boldsymbol{x}_{k+1} = \boldsymbol{A}\boldsymbol{x}_k + \boldsymbol{B}\boldsymbol{u}_k + \boldsymbol{K}\boldsymbol{e}_k \tag{4.63a}$$

$$\boldsymbol{y}_k = \boldsymbol{C}\boldsymbol{x}_k + \boldsymbol{D}\boldsymbol{u}_k + \boldsymbol{e}_k \tag{4.63b}$$

where $\boldsymbol{K}$ is the steady state Kalman gain while $\mathbf{e}_k$ is a white noise, independent of past input and output data. Finally, the system can be also expressed in the predictor form:

$$\boldsymbol{x}_{k+1} = \boldsymbol{A}_k\boldsymbol{x}_k + \boldsymbol{B}_k\boldsymbol{z}_k \tag{4.64a}$$

$$\boldsymbol{y}_k = \boldsymbol{C}\boldsymbol{x}_k + \boldsymbol{D}\boldsymbol{u}_k + \boldsymbol{e}_k \tag{4.64b}$$

Where:

$$\boldsymbol{z}_k = [\boldsymbol{u}_k^T \quad \boldsymbol{y}_k^T]^T \tag{4.65}$$

$$\boldsymbol{A}_k = \boldsymbol{A} - \boldsymbol{K}\boldsymbol{C} \tag{4.66}$$

$$\boldsymbol{B}_k = [\boldsymbol{B} - \boldsymbol{K}\boldsymbol{D} \quad \boldsymbol{K}] \tag{4.67}$$

Similarly to Eq. 61, Eq. 63 and Eq. 64 are able to represent the input and output data; for instance, the MOESP algorithm uses the innovation form (Eq. 63) while other approaches use the predictor form [95].

In the case of seismic events, as already highlighted by the various scientific work mentioned above, during the strong motion, the system dynamics is clearly time-varying, and the state space system matrices change over the time k. There are several works in literature dealing with the identification of time-varying systems through subspace methods. Tamariz et al. [96] developed an iterative state-space identification algorithm for discrete time-variant systems, based on MOESP type subspace methods and called MOESP-VAR, following the basic idea that a linear operator can be described as a composition of local linear transformations. Further interesting approaches can be found in Robles et al. [97], where a version of the N4SID algorithm for the identification of multivariable linear time-variant systems, named N4SID-VAR, is developed, and in Loh and Chen [98], where several methods are used to keep track of modal parameters from structural seismic response data.

In this work, an iterative procedure is proposed, consisting in tracking the evolution of the dynamic parameters of the system starting from the identification made on signal windows within which the dynamic behavior can be assimilated to that of a linear time-invariant system. The proposed procedure aims to optimize the number of samples, and therefore the length of windows, in which the system dynamics can be described as a linear time-invariant process. The length for the first iteration is deduced from a preliminary time frequency analysis and a short window is initially selected. For the generic window length, the identification is carried out through a subspace identification methodology, and the obtained dynamic model is used to predict, starting from the recorded seismic input, the analytical response of the building which is compared with the registered one. Thereafter, the window length is adjusted until the system identified in the initial window can accurately predict the structure response to the event, namely the length of the window is adjusted until the model accurately predicts the experimental response. The steps of the

optimization procedure are summarized in the flow chart reported in Figure 4-7. At the end of the process, a set of optimal time windows are determined in which the overall signal can be divided; the response of the system in each window can be considered as time-invariant and the system can be identified through a subspace identification method. The proposed approach allows tracking the evolution of the modal parameters of the system during the shaking.

The identification within each window has been made through the "robust combined algorithm" proposed by Van Overschee and De Moor [81]. This algorithm consists in a Singular Value Decomposition (SVD) of a weighted projection matrix for the determination of the model order.

Then, the state space matrices ***A***, ***B***, ***C*** and ***D***, and the corresponding covariance matrices ***Q***, ***S*** and ***R***, are determined by solving a set of linear equation, according to the N4SID algorithm. The system inputs are two time-histories recorded at the building foundation level, while, as outputs, the time-histories recorded by all the other sensors on the structures, are adopted. Both the inputs and the outputs were detrended in order to remove any slope and mean offset and properly filtered with the aim of considering only the contribution of the building dynamics.

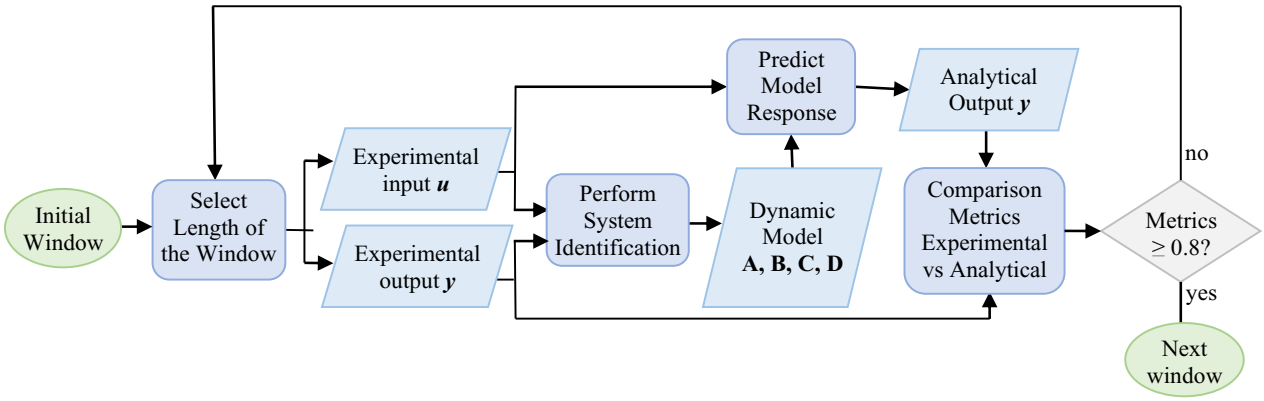

Figure 4-7: Flow chart of the proposed linearization procedure.

The accuracy of the identified model in reproducing the response of the building is assessed using the comparison metrics proposed by Kavrakov et al. [99], which consider different signal properties. In detail, metrics are constructed using the following exponential function:

$$M(u_e, u_a) = \exp\left(-\lambda |A(u_e, u_a)|\right) \tag{4.68}$$

so that results vary between 0 and 1. In Eq. 4.68, u_e and u_a are the experimental and analytical response that have to be compared, λ is the metric parameter (assumed to be equal to 1) and A is suitably constructed to account for a particular property of the signals.

In particular, the phase M_φ, the peak M_p and the root mean square M_{rms} are obtained considering the following exponents:

$$A_\varphi = \frac{t_{lag}}{T_c};\ t_{lag} = \arg max_t u_e(t) * u_a(t) \tag{4.69}$$

$$A_p = \frac{max_t|u_e(t)| - max_t|u_a(t)|}{max_t|u_e(t)|} \tag{4.70}$$

$$A_{rms} = \frac{\sqrt{\int_0^T [u_e(t)]^2 dt} - \sqrt{\int_0^T [u_a(t)]^2 dt}}{\sqrt{\int_0^T [u_e(t)]^2 dt}} \tag{4.71}$$

The phase metric accounts for the mean phase discrepancy between signals, with respect to the reference time delay T_c; the latter coefficient depends on what is considered to be a large delay between the signals; in this case, the period of the first mode has been used. The peak metric M_p accounts for the difference in the maximum peak response, while the root mean square metric M_{rms} quantify discrepancies of signals with respect to their average quantities. Furthermore, to evaluate the signal differences in the time-frequency plane, two further metrics based on the wavelet transform have been used: the wavelet metric M_w, which allows studying the overall signal discrepancies in the time-frequency plane, and the frequency normalised wavelet metric M_{wf}, which allows to understand if these discrepancies are due to the signal amplitudes or frequency content. The relevant metric exponents are obtained with the following expressions:

$$A_w = \frac{\int_0^\infty \int_0^T \left| |W_{u_e}(a,t)| - |W_{u_a}(a,t)| \right| dtda}{\int_0^\infty \int_0^T |W_{u_e}(a,t)| dtda} \tag{4.72}$$

$$A_{wf} = \int_0^T \frac{\int_0^\infty \left| \frac{|W_{u_e}(a,t)|}{max_a|W_{u_e}(a,t)|} - \frac{|W_{u_a}(a,t)|}{max_a|W_{u_a}(a,t)|} \right| da}{\int_0^\infty \frac{|W_{u_e}(a,t)|}{max_a|W_{u_e}(a,t)|} da} dt \tag{4.73}$$

where $W_{u_i}(a,t)$ for $u_i(a,t)$ is obtained as

$$W_{u_i}(a,t) = \frac{1}{\sqrt{|a|}} \int_{-\infty}^{\infty} u_i(\tau) \psi\left(\frac{t-\tau}{a}\right) d\tau \tag{4.74}$$

in which a is the scale and ψ is the Morlet wavelet. In this work, the analytical response predicted within a window has been considered "accurate" if the metric values obtained from analytical and experimental signal comparison in each superstructure measurement point, are all greater than 0.8. In this case, the optimal length has been reached with a few iterations thanks to the nature of the recorded events which did not induce extreme variations of the dynamic system. However, the method can be improved by implementing machine learning procedures (e.g., Bayesian optimization, neural networks) that could automatically identify the number and the length of time windows.

The results of the application of this method are presented in Chapter 6 for data from a reinforced concrete school monitored during the 2016 Central Italy earthquake sequence.

4.3.2. Data cleansing: Principal component analysis

In this thesis work, the technique of principal component analysis (PCA) is used to remove the influence of environmental factors on the eigenfrequencies of vibration. PCA linearly transforms the original set of autocorrelated variables into a smaller set of uncorrelated variables that can describe most of the information in the original data set. It is a technique used in many works in the literature such as in [100] and [101]. In this work PCA is used to find the main components of the dataset that depend mostly on environmental parameters and then remove them from the original data, thus obtaining a dataset cleansed of the components representing the variations due to environmental parameters.

Before showing the obtained results, a brief description of the analytical steps that lead to the definition of the purified parameters, is given. More details from a numerical point of view can be found in the work of Tharwat [102].

In order to develop a PCA it is necessary to insert all the correlated variables in a matrix m x n containing m observations obtained from n sensors. Once the matrix of X variables is constructed, the mean of each variable is calculated, and the data is centred by subtracting the mean from each sample obtaining the X matrix̂. At this point the covariance matrix can be calculated:

$$\boldsymbol{C} = \widehat{\boldsymbol{X}}\widehat{\boldsymbol{X}}^T \tag{4.75}$$

it is an n x n matrix representing the variance of variable i with variable j.

The principal components space can be defined by performing a spectral decomposition of the covariance matrix:

$$\boldsymbol{C} = \boldsymbol{A}\boldsymbol{\Lambda}\boldsymbol{A}^T \tag{4.76}$$

where the eigenvectors are the columns of the matrix $\boldsymbol{A}$, and the corresponding eigenvalues are the terms in the diagonal of the matrix $\boldsymbol{\Lambda}$. Each column of the eigenvector matrix (in MATLAB called *coeff*) represents a principal component and the columns are sorted in order of significance on the variance as a function of the eigenvalues. This process gives the principal components of the original dataset in order of significance. The rows of this matrix are the variables, so the *coeff* matrix tells us how much each variable counts within each principal component. At this point the initial variables can be geometrically projected onto the principal component space.:

$$\boldsymbol{Z} = \boldsymbol{X}\boldsymbol{A} \tag{4.77}$$

Z (called *score* in MATLAB) represents the matrix of variables projected in the principal components space. Figure 4.8 shows a schematic representation of the principal components in a two-variable space.

If all principal components present in $\boldsymbol{A}$ are used to construct $\boldsymbol{Z}$, we can reconstruct the initial data by simply inverting the matrix:

$$\boldsymbol{X} = \boldsymbol{Z}\boldsymbol{A}^T \tag{4.78}$$

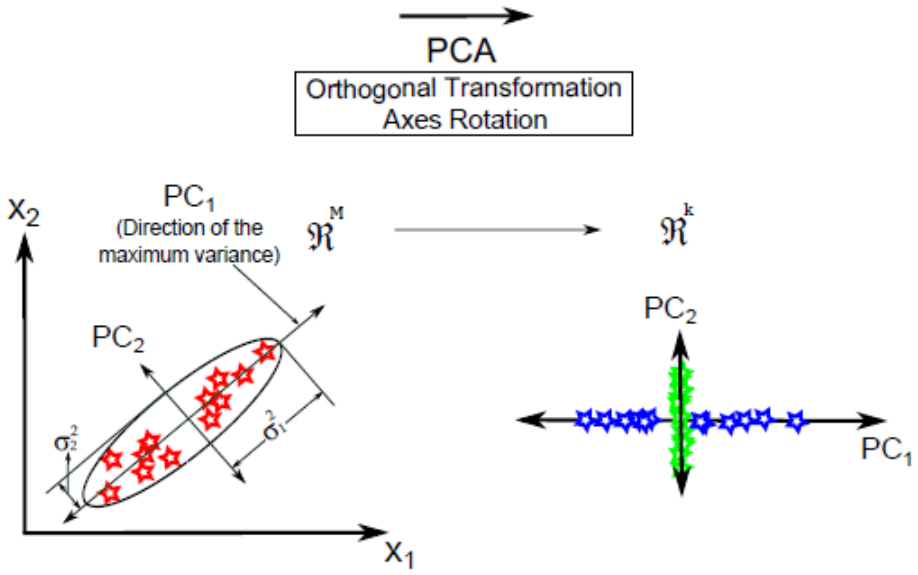

Figure 4-8: schematic representation of the principal components in a two-variable space. Figure from the work of Tharwat [101].

In the present case we are interested in projecting the initial variables along the principal components that are influenced by the environmental parameters, so all columns of $\boldsymbol{A}$ are selected except the one referring to the principal component that is mostly influenced by frequency and then the data are reconstructed considering only those principal components

$$\boldsymbol{X}_r = \boldsymbol{Z}_r \boldsymbol{A}_r^T \tag{4.79}$$

Where the matrices $\boldsymbol{A}_r$ and $\boldsymbol{Z}_r$ are the matrices $\boldsymbol{A}$ and $\boldsymbol{Z}$ in which the principal component influenced by frequency is removed. We thus obtain a matrix $\boldsymbol{X}_r$ containing the initial variables reconstructed by considering only the principal components in which environmental parameters dominate. At this point, these effects can be removed by subtracting the reconstructed variables from the initial variables:

$$\boldsymbol{X}_e = \boldsymbol{X} - \boldsymbol{X}_r \tag{4.80}$$

In $\boldsymbol{X}_e$ we find all the initial variables cleansed by the environmental variables initially inserted in the matrix $\boldsymbol{X}$, so the final result that interests us is the column of $\boldsymbol{X}_e$ relating to the frequency that will be purified by the effects of the other variables considered.

4.3.3. Data cleansing: artificial neural network

As discussed in the review of Chapter 2, traditional multivariate statistical analysis techniques cannot always efficiently cleanse the data due to the non-linearity of the phenomenology underlying these phenomena. More advanced numerical techniques such as machine learning may therefore be necessary.

Human brains tend to learn new concepts and ideas by means of examples. Rather than understanding the algorithm step by step, the human brain tends to grasp new things by analyzing and studying examples. Thanks to the invention of the computer and the enormous advancement of the digital world, many efforts have been made to replicate this human approach to learning. Many attempts have been made to create artificial neurons that work in a similar way to biological neurons. A network of such artificial neurons is called artificial neural network [103]. An interesting introduction to the method can be found in the work of Markova [103].

A technical neural network is made up of simple processing units, the neurons, and of direct, weighted connections between these neurons. A typical multiple-input neuron with R inputs is shown in Figure 4-9.

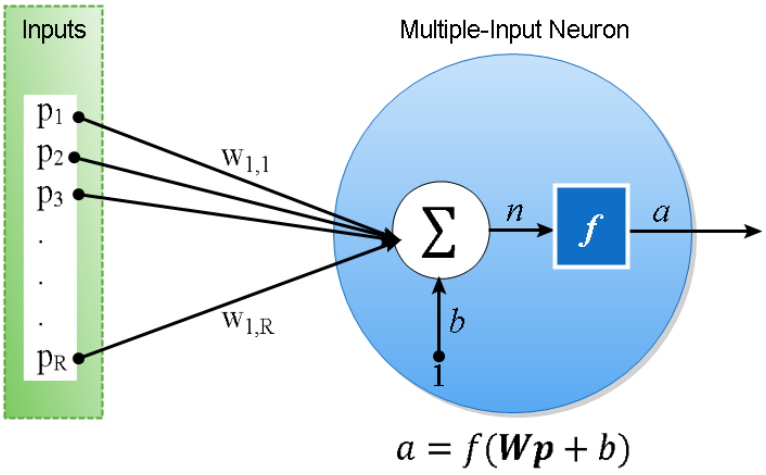

Figure 4-9: Schematization of a typical multiple-input neuron with R inputs. Figure from the work of Markova [103].

The individual inputs p_1, p_2, ..., p_R are individually weighted by the respective elements $w_{1,1}$, $w_{1,2}$, ..., $w_{1,R}$ of the weight matrix W. The neuron has a bias b, which is summed with the weighted inputs to form the net input n:

$$n = w_{1,1}p_1 + w_{1,2}p_2 + \cdots + w_{1,R}p_R \tag{4.81}$$

This expression can be written in a matrix form:

$$n = w_p + b \tag{4.82}$$

And the neuron output can be written as:

$$a = f(W_p + b) \tag{4.83}$$

The added output n, often referred here as net input, is passed into a transfer function f, which produces the output of neuron a. The transfer function in Figure 4-9 can be either a linear or non-linear function of n. A specific transfer function is chosen to satisfy some specification of the problem the neuron is attempting to solve.

Commonly one neuron, even with many inputs, may not be sufficient. We might need five or ten, operating in parallel, in what we call a “layer.” Usually, neural networks have multiple connected layers. A layer whose output is the network output is called an output layer. The other layers are called hidden layers.

There are infinite ways to build a neural network. Neurodynamic and architecture are two terms used to describe how a neural network is structured. One of the easiest parameters to select after the independent variables have been reworked is the number of input neurons since each independent variable is represented by its input neuron. The tasks of selecting the number of hidden layers, the number of neurons in the hidden layers and the number of output neurons, as well as the transfer functions, are not trivial.

Hidden layers give the network its ability to generalize. As the number of hidden layers increases, it also increases computation time and the danger of overfitting, which in turn leads to bad out-of-sample prediction performance. In the case of neural networks, the number of weights, which is related to the number of hidden layers and neurons, and the dimension of the training set determine the probability of overfitting [104]. Although it is important, there is no standard formula for choosing the optimal number of hidden neurons, so researchers resort to experimentation. Masters [105] proposed an approximation of the optimal number of hidden neurons that can be obtained with the geometric pyramid rule. According to Baily and Thompson [106], for a three-layer network with n input neurons and m output neurons, the hidden layer would have $\sqrt{n \cdot m}$ neurons. Furthermore, they suggest that the number of neurons of the hidden layer in a three-layer neural network should be 75% of the number of input neurons. In the work of Katz [107] it is suggested that the optimal number of hidden neurons is generally between half and three times the number of input neurons. In Ersoy's work [108] it is proposed to double the number of hidden neurons until the performance of the network on the test set deteriorates. Another recommendation can be found in the work of Klimasauskas [109] according to which there should be at least five times as many training facts as there are weights, which sets an upper bound on the number of inputs and neurons.

On the other hand, deciding on the number of neurons is somewhat easier, as there are convincing reasons to always use only one output neuron [103]. Neural networks having multiple outputs, especially if these outputs are widely spaced, yield inferior results compared to networks with only one output [104].

Most current neural network models use the sigmoid transfer function, but it is possible to find other proposals, such as the hyperbolic tangent, the arctangent and linear transfer functions [110]. Linear transfer functions can be useful for nonlinear mapping and classification. Transfer functions such as sigmoid are commonly used for time series data because they are nonlinear and continuously differentiable, desirable properties for network learning [103]. In this paper, the sigmoid transfer function is applied in the proposed networks.

Neural networks can be divided into dynamic and static categories. The static networks (feedforward) do not have feedback elements and do not include delays; the output is directly computed from the input via the feedforward connections. In dynamic networks, the output not only depends on the current input to the network, but also on the current or previous inputs, outputs, or states of the network. The non-linear autoregressive network with exogenous inputs [111] is a recurrent dynamic network with feedback connections enclosing different layers of the network. The NARX model is popularly used in time series modelling. The equation that defines the NARX model is:

$$y(t) = f(y(t-1), y(t-2), \dots, y(t-n_y), u(t-1), u(t-2), \dots u(t-n_a)) \qquad (4.84)$$

wherein the next value of the dependent output signal y(t) is regressed on the past values of the output signal and the past values of an independent (exogenous) input signal. A two-layer feedforward network is utilized for the approximation. The tapped delay line (TDL) is used to feed the network with the past values of the inputs. There are several applications for the NARX network. It can be employed as a predictor, to predict the next value of the input signal. It can also be used for non-linear filtering, where the target output is a noise-free version of the input signal.

The output of the NARX network could be an estimate of the output of some non-linear dynamical system that is intended to be modelled. As shown in Figure 4-10a, the output is fed back to the input of the feedforward neural network as a part of the standard NARX architecture.

Since the true output is available during network training, we could create a series-parallel architecture, where the true output is used instead of deferring the estimated output, as shown in Figure 4-10b. There are two major advantages to this: one the one hand, the input to the feedforward network is more accurate. On the other hand, the resulting network has a pure feedforward architecture, and static backpropagation can be used for training.

There is a toolbox function in MATLAB that facilitates the preparation of data for dynamic (time series) networks.

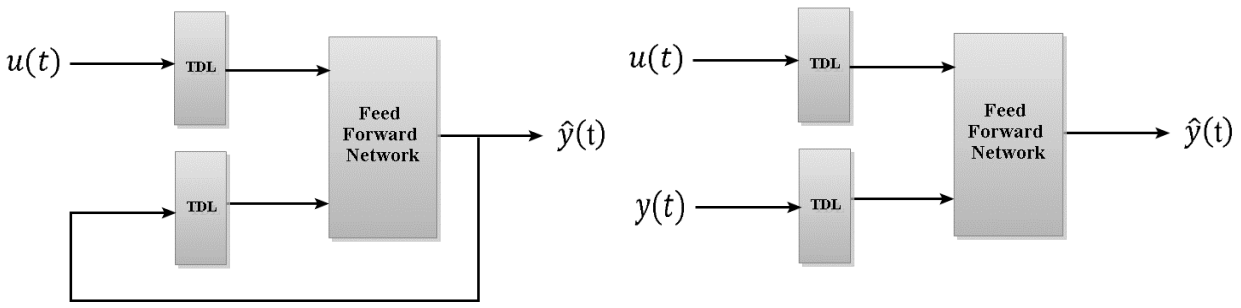

(a) Parallel Architecture

(b) Series - Parallel Architecture

Figure 4-10: different NARX architecture. Figure from the work of Markova [102].

The general practice in training multilayer networks is to first divide the data into three subsets. The first subset is the training set, which is used to compute the gradient and update the weights and biases of the network. The second subset is the validation set. The error on the validation set is monitored during the training process. The validation error usually decreases during the initial phase of training, as well as the error of the training set. Nevertheless, when the network begins to overfit the data, the error on the validation set typically begins to increase. The weights and biases of the network are saved to the minimum of the validation set error [103]. The input vectors and destination vectors are randomly split into three groups as follows:

- 70% used for training.
- 15% used to validate that the network is generalizing and to stop training before overfitting.
- 15% used as a completely independent test of network generalization.

When the weights and biases of the network are initialized, the network is then ready for training. The training process of a neural network implies adjusting the values of the weights and biases of the network to optimize the performance of the network. The default performance function for feedforward networks is the mean square error (*mse*) between network outputs and target outputs t.

$$F = mse = \frac{1}{N}\sum_{i=1}^{N}(e_i)^2 = \frac{1}{N}\sum_{i=1}^{N}(t_i - a_i)^2 \tag{4.85}$$

Training can be implemented in two different modes: incremental mode and batch mode.

In the incremental mode, the gradient is calculated, and the weights are updated after each input is applied to the network. In batch mode, all inputs in the training set are applied to the network before the weights are updated. Batch mode training was used in this work.

In order to train multilayer feedforward networks, any of the standard numerical optimization algorithms [111] can be employed to optimize the performance function, however there are a few key ones that have exhibited excellent performance for training neural networks.

In particular, the algorithm used in this work is Bayesian regularization (BR) [111]. It is a network training algorithm that updates the weight and bias values according to Levenberg-Marquardt optimization. It works by minimizing a combination of square errors and weights and then determines the correct combination to produce a network that generalizes well. This algorithm typically takes more time, but can result in good generalization for difficult, or noisy datasets.

4.4. Framework summary

At this point, all hardware and software tools for the implementation of a data-driven VB-SHM have been introduced. Figure 4-11 gives a general overview of the presented framework. In the following chapters, the results obtained from the application of the framework are reported in order to illustrate in detail the significance and potential of the single steps. In particular, in chapter 5 the results of the application of phase 1 for the design of the monitoring system of the Church of Santa Maria in Via in Camerino are reported. This is a relevant example given its complexity in terms of the geometry of the structure and the heterogeneity of the materials. The application of phase 2 is not presented explicitly as it has already been introduced in detail in the current chapter; however, all data collected in the monitoring activities presented in this thesis are derived from the application of this second phase. The first two steps of phase 3 are illustrated individually through results obtained from the dynamic monitoring of two case studies. The linearization procedure introduced in this chapter is applied to the seismic response recorded by a reinforced concrete school building in Camerino, during the 2016 seismic sequence in Central Italy. The effect of the environmental conditions on modal parameters is illustrated through the monitoring results of a 10-storey RC building, the tower of the Faculty of Engineering of the Università Politecnica delle Marche. The data of this latter case study have been processed both by means of principal component analysis and by means of an artificial neural network. The latter approach allowed to correctly identify changes in the dynamics of the structure due to some retrofit works on the seismic joints. At this point, it is possible to proceed to the last step of phase 3, Data-Driven Structural Health Monitoring. In this thesis work, due to the modest duration of the monitoring activities, this last step is addressed by simply monitoring the residuals of the identified statistical model. The definition of appropriate warning thresholds remains one of the future developments of this work.

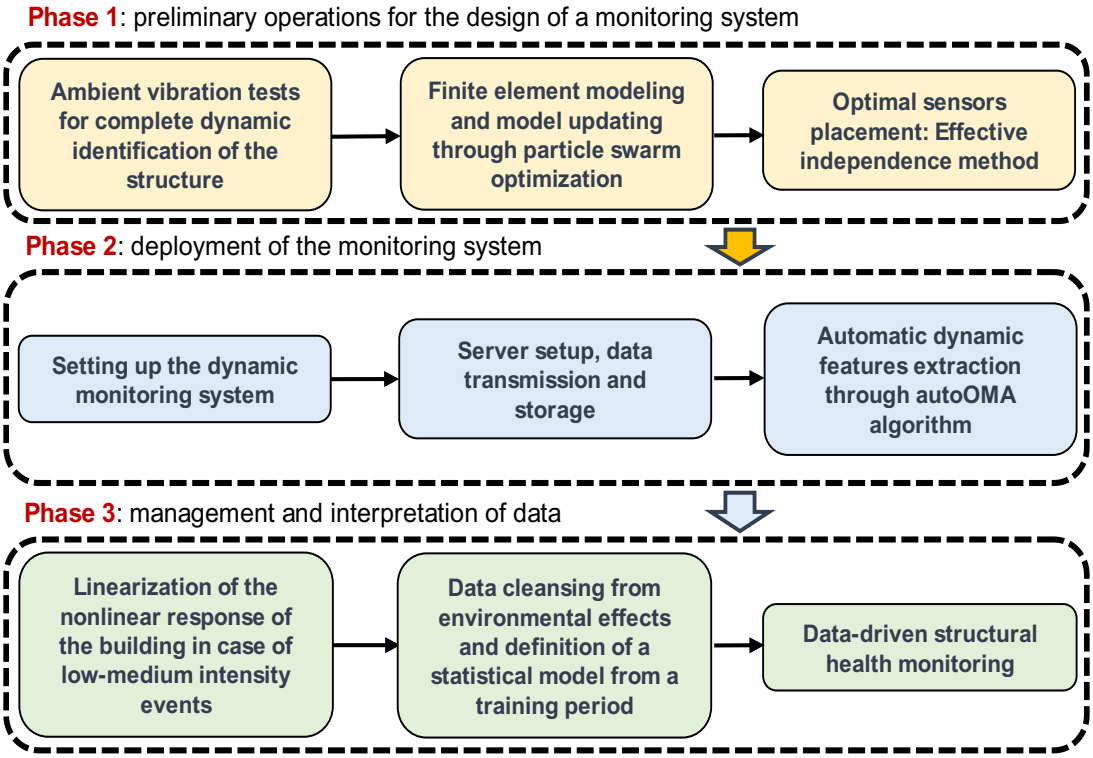

Figure 4-11: General overview of the level 1 VB-SHM framework.

5. The church of Santa Maria in via in Camerino: MU and OSP

5.1. Presentation of the case study

The Church of Santa Maria in Via is located in the center of Camerino town (MC) in Central Italy, and overlooks the historical square entitled to Umberto I. Over the years, the building undergone various architectural restoration and static consolidation works following the earthquakes of 1799 and 1997. One of these interventions concerned the original brick dome, which was replaced with a false dome in camorcanna construction technology covered by a double-pitched wooden roof.

Following the earthquake sequence that struck Central Italy in 2016 and the adverse weather conditions in early 2017 characterized by heavy snowfalls, the structure of the church was compromised. This led to the installation of a steel securing system to contain the wall box of the façade body and the portion of the tiburium closest to it. Since the system was designed to counteract further mobilization of the kinematic mechanisms activated during the seismic sequence of 24 August 2016 and the consequent collapses, a monitoring system has been installed with the aim of assessing both the evolution of the efficiency of the securing system over time and the occurrence of new kinematic mechanisms or further mobilization of those already activated.

5.1.1. Historical background

Considering the cultural relevance and the geometric complexity of the building, it is worth describing its historical evolution. The first evidence of the existence of a church of Santa Maria in Via in Camerino is found in the "Rationes Decimarum" of 1299 and in a testament of 1341; in the 16th century, the church was a poor, irregular building. Later, in the 17th century, Cardinal Angelo Giori, secretary of the Pope Urban VIII Barberini, transformed the church by purchasing the neighboring buildings and integrating them with the pre-existing rectory and oratory, in order to make it suitable for hosting those who came to venerate the sacred icon of the Madonna and Child, a portrait brought back from Smyrna by the Crusaders led by Rodolfo II da Varano.

The current building was built between 1639 and 1642 and works were supervised by Camillo Arcucci da Sigillo, a figure very close to Francesco Borromini. The actual building is characterized by an irregular trapezoidal plan that is the result of the combination of the pre-existing buildings and a wall fabric with a particularly incoherent core, while the external cladding was added to regularize the various buildings.

In the dome, shown in Figure 5-1d, which was restored following the seismic event of 1799 and currently damaged by the earthquake that hit the historical center, there is a cycle of frescoes depicting the Eternal among hosts of angels; the crowning of the Virgin in the sub-arch; the arrival of the image of Mary from Izmir at the time of the Crusaders and the crowning of the sacred image on 14 June 1864.

In its present state, the church (Figure 5-1a, b and c) consists of a single massive building body from which rise the tiburium, with an irregular octagonal plan, the bell tower and the façade body. The hall has an elliptical plan, with the major axis coinciding with the axis that connects the entrance to the main altar, located in a deep apsidal presbytery; on the minor axis, above two side entrances, there are two “coretti”. The right chapel, where Cardinal Giori's tomb was located once, houses the crucifix whereby St. Paul of the Cross blessed the people of Camerino in 1750 at the end of a mission.

The tiburium, which rises more than 8 m above the inner frame, is characterized by the presence of four large windows at the side altars. On the outside, it has buttresses at the corners. There is no information about the construction of the bell tower, which has an octagonal plan with a rather slender belfry, but its architectural aspect suggest that it was built together with the church.

The body of the façade consists of two levels; the lower level is incorporated into the main body of the church, while the upper one rises next to the tiburium, to a maximum height of approximately 23 meters above the ground. The body of the façade has an isosceles trapezoidal plan with an average length of the bases of about 16 m and a height of about 6 m. Inside, the body of the façade has three floors, the first of which, at +4.5 m from the floor of the hall, consists of barrel vaults; the others, one at the level of the first ledge and the other at the level of the clock, are made of wooden decks. In plan, the body of the façade is subdivided into three rooms, separated by two masonry walls.

Inside the façade wall, on the left side, there is a spiral staircase that allows the access to the chancel and the upper floor. This produces a significant discontinuity in the body of the façade wall. Regarding the walls of the church, the external face is entirely exposed and is made of very regular and compact brickwork and lime mortar. The body of the façade, on the other hand, is made of stone covered with very thin brick layer.

In the corner nearby the sacristy there is the bell tower with a rather slender belfry, served by a spiral staircase.

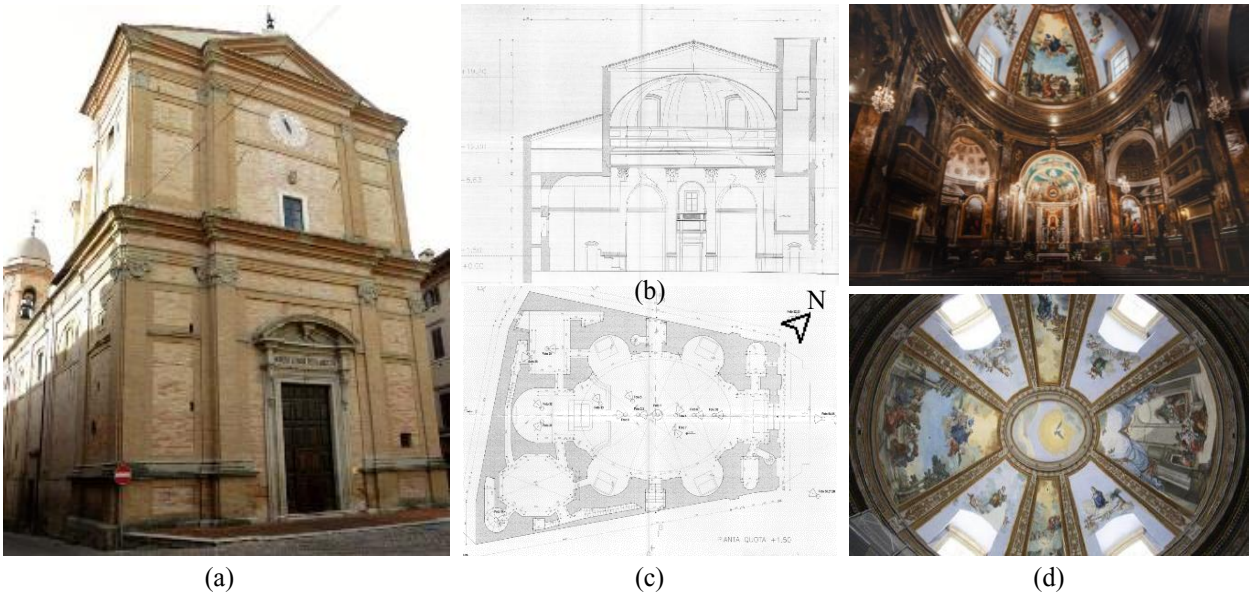

Figure 5-1: Santa Maria in Via church before the 2016 Central Italy earthquake: (a) Photo of the church façade; (b) and (c) technical drawings of the geometrical survey; (d) photos of the church interior.

5.1.2. Damage due to the 2016 Central Italy earthquake

The church is currently in a serious state of damage and, in order to provide a better understanding of the case study, a detailed report of the damage is given. Following the seismic event that struck central Italy in 2016, in conjunction with the adverse environmental conditions of the first months of 2017, the church suffered a lot of damage that affected the bell tower, with the collapse of a part of it, and both the wooden roof and the façade, with scattered cracks on both internal and external walls. In Figure 5-2, several photos of the damage suffered by the church are shown. In particular, the bell tower, collapsed as a consequence of the 26th October 2016 earthquake. The numerous collapses exhibited by the tiburium have also affected the wooden roof and parts of the camorcanna fake dome. The vertical structures of the tiburium consist mainly of stone masonry walls with rough blocks characterized by unworked stone and brick inserts. The presence of large infilled openings is evidence that the structure of the church has undergone many changes over the centuries that have probabily weakened the structural system, which is characterized by many internal discontinuities.

The greatest collapse occurred in the rear part of the tiburium, which collapsed mainly inside the nave as a consequence of the progressive damage caused by the seismic activity of 26th October 2016 and the heavy snowfall of January 2017. Both the interior and exterior walls of the nave and apse are not affected by significant collapses or cracks, except for the two side altars adjacent to the façade section, which suffered significant damage to the arches and vault. At the south-west corner, under the shaft of the bell tower, there are diagonal cracks, which are concentrated on the floor bands between openings. The interior of the body of the façade was aggravated by the seismic events of 2016 and later, affecting both the upper and lower levels. The façade of the lower level has undergone an out-of-plane rotation, while the upper block has undergone a rigid translation motion that also affects the portion of the tiburium adjacent to the façade.

Figure 5-2: (a) Aerial photos showing the collapse of the rear part of the tiburium and part of the roof; (b) collapse of the fake dome in camorcanna; (c) collapses of the main body of the façade due to activation of the overturning mechanism

5.1.3. Securing interventions

After the seismic sequence that stroke the church and produced many damages, the structure has been secured with several interventions. At first, a massive external retaining steel structure designed to prevent the front body collapse (Figure 5-3a) was built. This system has to retain a mass of about 1300 tons with an out of verticality of about 30 cm. Two lateral steel braces combined with four latticed beams were used to avoid the collapse of the body. The structure covers the front side and the two lateral sides of the anterior façade body for the whole height. The contact with masonry is realized with timber elements to adapt the steel system to the deformed masonry. To ensure the system stability in case of extreme events and to confine the base body of the church, fourteen steel strand cables connected to the steel structure and surrounding the whole church, are used. The whole steel structure is founded on a stiff RC shallow foundation. A typical buttress system was not suitable for this case, since it would require a large space in front of the church which would drastically reduce the space necessary to the vehicles mobility and for future reconstruction worksites. The holes on the wall of the lateral sides produced by the overturning mechanism, were filled with steel latticed systems to restore gravitational loading paths (Figure 5-3d). Moreover, a provisional roof was built to protect the interior of the church, and a latticed structure as well (Figure 5-3b and c), to prevent the out of plane collapse of the tiburium walls.

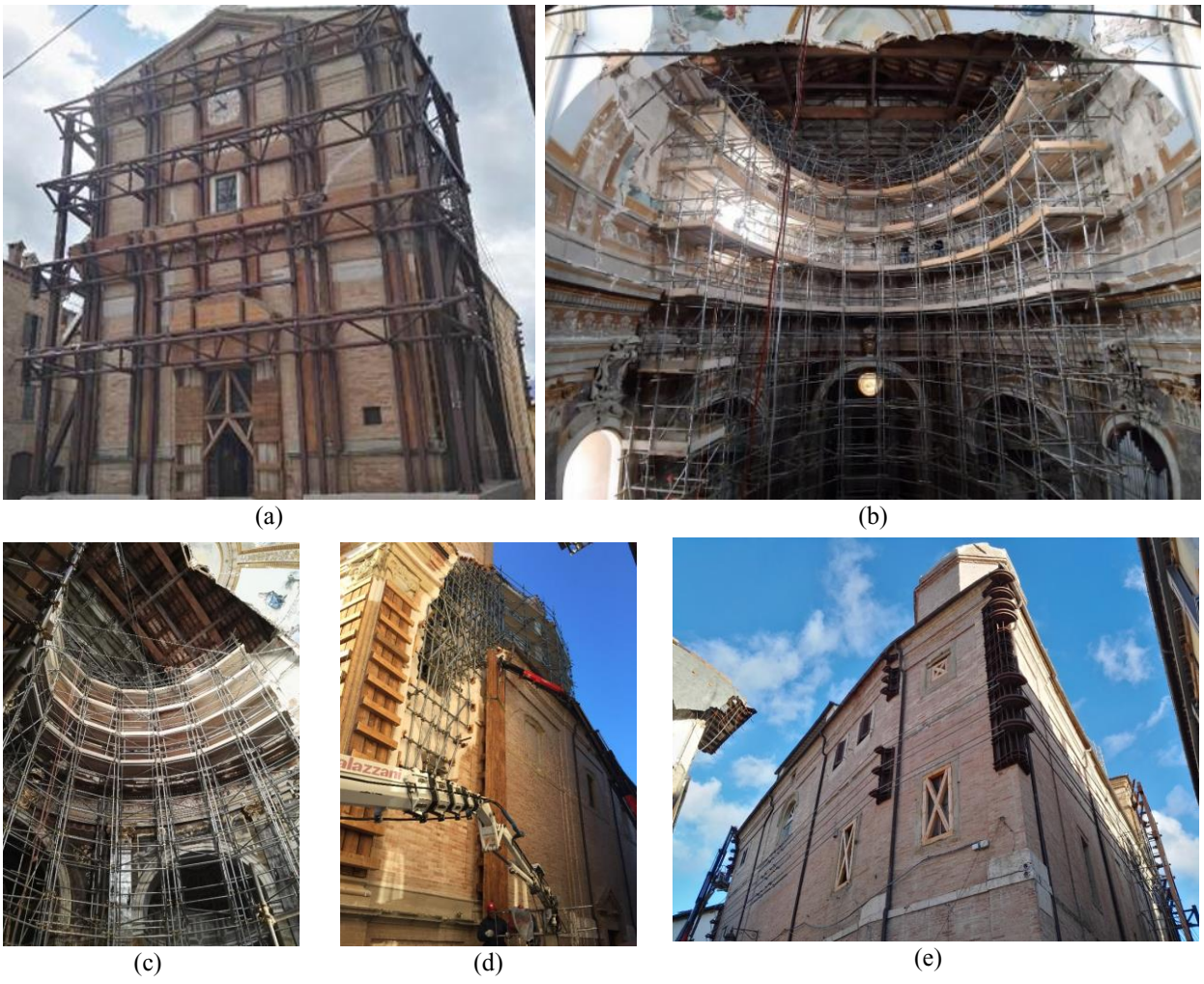

Figure 5-3: (a) External retaining steel structure; (b) and (c) latticed structure to prevent the out of plane collapse of the tiburium; (d) steel latticed systems to restore gravitational loading paths; (e) tensioning cables and guides.

5.2. Preliminary identification tests

In 2020, within the ARCH research project (European-funded research project that aims to better preserve areas of cultural heritage from hazards and risks), in collaboration with the University of Camerino, it was decided to develop a monitoring system of the church with the aim to investigate the best approach to define a SHM system for cultural heritage buildings. In particular, it was decided to combine a static monitoring system with a VB-SHM system. As already discussed, identifying the global dynamics of the building is the first step.

The identification of the global dynamics of the church has been carried out through ambient vibration tests employing 16 accelerometers and two sensor configurations shown in Figure 4a and 4b. To get information on the overall behavior of the church, it was decided to monitor 8 points located around the ellipse of the tiburium, at two different heights from the ground level. At each point (from A to H) two uniaxial accelerometers were placed with measurement directions along the main axes of the church hall (called x and y directions). In detail, in the first configuration P1, shown in Figure 5-4a, the accelerometers were positioned in 8 different points at 12 m from the ground, while in the second configuration P2, shown in Figure 5-4b, two accelerometers were left in the same position (1B) to be used as references, while the others were moved at 19.7 m from the ground; positions 2C and 2H were excluded as inaccessible. As for the instrumentation, PCB 393B31 accelerometers with a sensitivity of 10V/g, NI 9234 analog-to-digital conversion modules, a 9045 cRIO and three 9185 cDAQs, were used. A distributed sensor network has been set up by placing one cRIO for the measuring station close to the reference point 1B and three mobile cDAQs near the remaining measuring points. Synchronization has been achieved through TSN technology providing distributed time synchronization and deterministic communication using standard Ethernet networks.

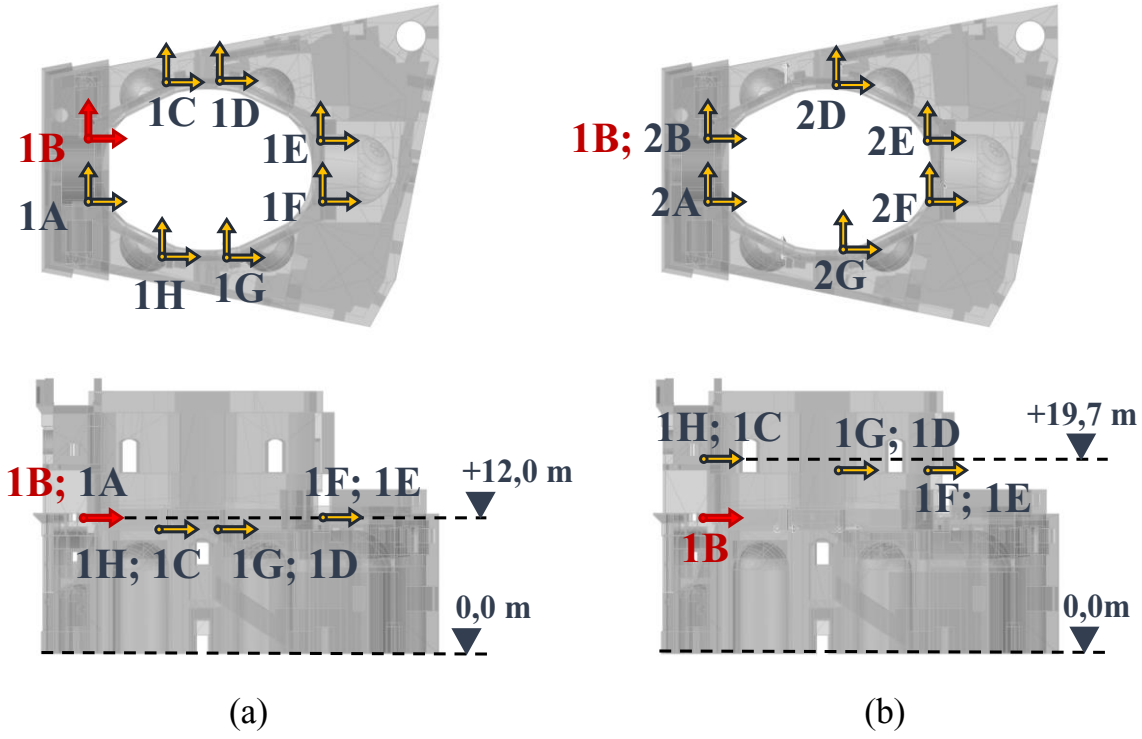

Figure 5-4: Sensor layout for test configurations: (a) P1 and (b) P2 configurations.

The identification of modal parameters has been carried out using the Principal Component - Subspace Stochastic Identification (SSI-PC) technique. Since the acquisitions relevant to the two configurations are asynchronous, in order to obtain a correct mode shape, it has been necessary to proceed with a data merging operation through scaling techniques; in this case, global results have been obtained applying the PoSER (Post Separate Estimation Re-scaling) technique.

Figure 5-5a and Figure 5-5b show the stabilization diagram obtained from the tests in Configuration P1 and Configuration P2, respectively. The global results in terms of frequencies, damping ratios and modal shapes are shown in Figure 5-6, while in Figure 5-7 the relative AutoMAC matrix is shown. The MAC value between two modes is essentially the normalized dot product of the complex modal vector at each common nodes (i.e., points) as shown in Equation 4.36, and it can be useful to validate the identified vibration modes. If a linear relationship exists (i.e., the vectors move the same way) between the two complex vectors, the MAC value will be near to one. If they are linearly independent, the MAC value will be small (near zero). As can be seen from Figure 5-7, the identified modes are all almost perfectly orthogonal to each other.

Globally, 10 vibration modes have been identified. It is interesting to note that, despite the complex crack pattern, the dynamics of the structure presents the first two translational and well decoupled modes and a third torsional mode, which could be expected for the undamaged system. As for the higher modes, these need to be further investigated, but they overall seem to involve the local dynamics of the tiburium and of the façade. For a deeper understanding of the structural dynamics, a refined FEM has been developed.

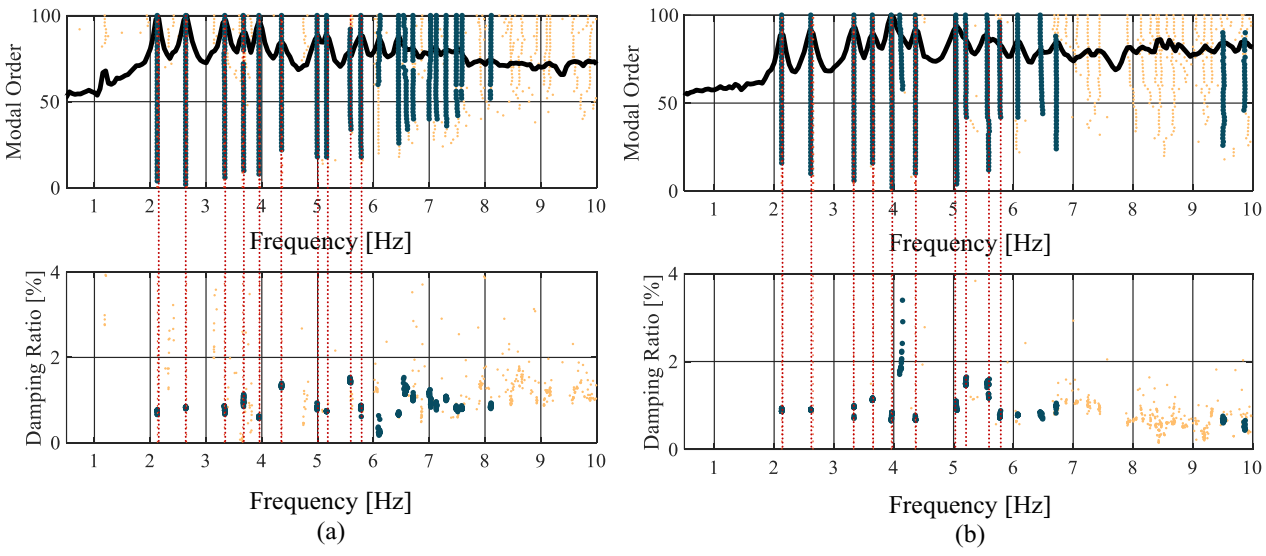

Figure 5-5: Stabilisation diagram and damping ratio frequency diagram for: (a) P1 configuration and (b) P2 configuration.

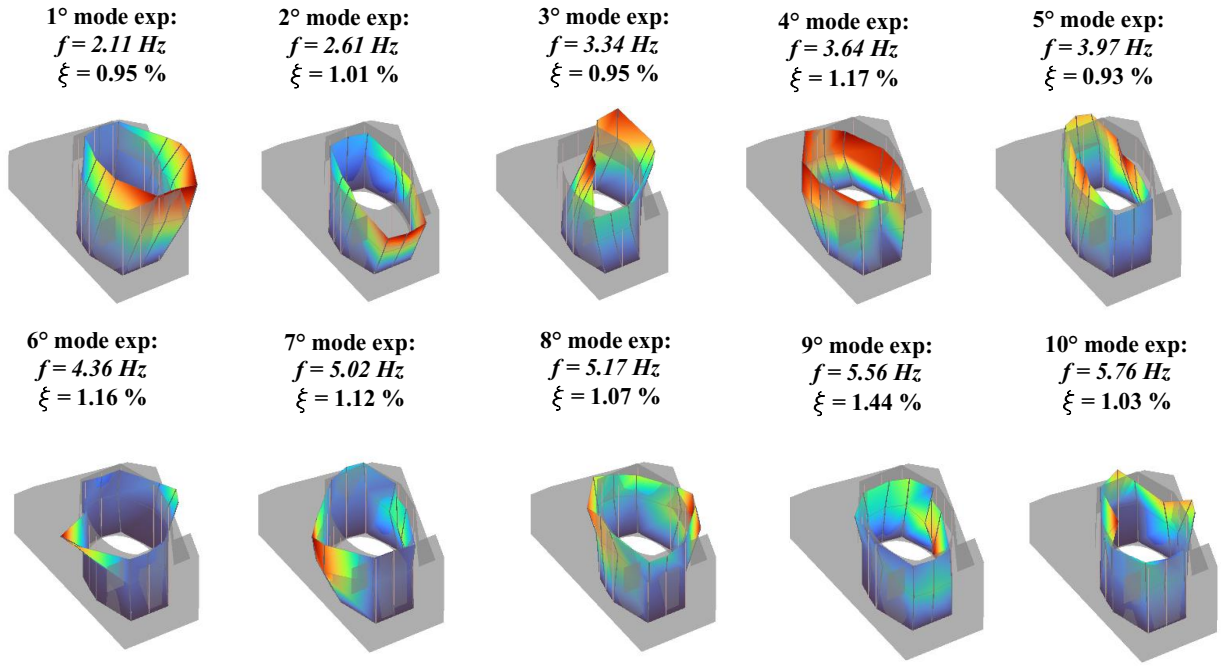

Figure 5-6: Frequencies, damping ratios and mode shapes relative to the 10 identified global modes.

Mode n	Exp. [Hz] ↓	Auto MAC									
1	2.11	1.00	0.00	0.06	0.06	0.00	0.04	0.25	0.04	0.10	0.01
2	2.61	0.00	1.00	0.00	0.00	0.02	0.02	0.02	0.01	0.20	0.01
3	3.34	0.06	0.00	1.00	0.29	0.02	0.04	0.20	0.00	0.04	0.01
4	3.64	0.06	0.00	0.29	1.00	0.00	0.00	0.07	0.05	0.06	0.00
5	3.97	0.00	0.02	0.02	0.00	1.00	0.21	0.02	0.07	0.03	0.01
6	4.36	0.04	0.02	0.04	0.00	0.21	1.00	0.08	0.04	0.01	0.05
7	5.02	0.25	0.02	0.20	0.07	0.02	0.08	1.00	0.16	0.03	0.01
8	5.17	0.04	0.01	0.00	0.05	0.07	0.04	0.16	1.00	0.13	0.01
9	5.56	0.10	0.20	0.04	0.06	0.03	0.01	0.03	0.13	1.00	0.04
10	5.76	0.01	0.01	0.01	0.00	0.01	0.05	0.01	0.01	0.04	1.00
	Exp. [Hz] →	2.11	2.61	3.34	3.64	3.97	4.36	5.02	5.17	5.56	5.76
		1	2	3	4	5	6	7	8	9	10

Figure 5-7: AutoMAC matrix relative to the 10 identified modes.

5.3. FE Modelling and model updating

5.3.1. Geometric and material survey

The geometry of the church has been surveyed, and the technical drawings are updated considering the damage the church has suffered. As can be seen from Figure 5-8, the church is characterized by a very complex interior layout, with many different volumes with different shapes distributed within the walls and creating empty spaces at different places and heights. In the axonometric view of Figure 5-8, the masonry walls are shown in transparency to emphasize the number and complexity of the corridors and interior spaces

With regard to the construction materials, the church has a regular texture brick exterior cladding, made in order to make the structure homogeneous, due to the numerous variations undergone by the building over the years. In-situ or laboratory mechanical tests on masonry have not been carried out, but a careful visual inspection has made it possible to classify the different types of masonry. A total of four different masonry typologies (M1, ..., M4) can be recognized, as illustrated in Figure 5-9. M1 masonry is composed of two outer leaves of regular-textured brickwork, which are not connected to each other, and which contain a rubble fill. This type of masonry is used to construct the perimeter walls of the façade. M2 masonry is a multi-leaf stone masonry with irregular courses and is used to build the inner walls of the façade and few walls of the church body, mainly those with high thickness. The M3 masonry is a double leaf brickwork with rubble filling and, as for M1, the connection between the different layers is almost absent. This typology is adopted for most of the walls of the church and, as a consequence, presents diffused thicknesses due to the variation of the thickness of the rubble fill. Finally, the M4 masonry is composed of two leaves: the inner one is made of masonry bricks, while the outer one of rough stone blocks with irregular courses. On the exterior side, the walls are plastered. This typology id used for the walls of the tiburium.

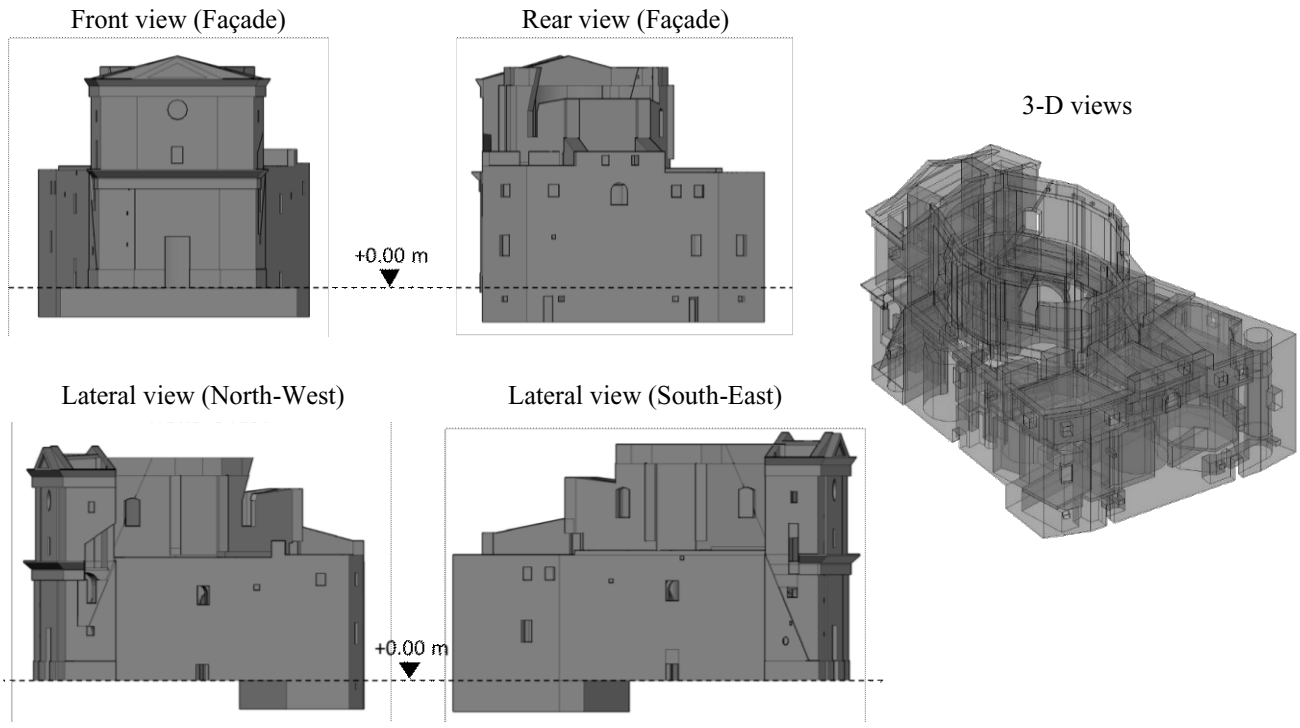

Figure 5-8: 3D geometric model of the church obtained from the survey.

Thus, the church is constituted by a very particular structural system characterized by different interacting bodies, sometimes made of poor masonry. This gives the system a very high vulnerability already exhibited after the past strong earthquakes. The parts of the church that collapses (rear part of the tiburium and lateral sides of the façade) are filled with steel latticed systems, indicated as Braced-up regions in Figure 5-9, which are considered as additional material to be added to those previously described.

Within the lateral volumes of the church and at different heights, there are many wooden floors which are localized in Figure 5-9. The pavilion roof is composed by three wooden trusses to which have been added other four steel trussed, as a result of recent restoration works, and a wooden planking with tile covering. Starting from this material survey, an initial estimate of the material mechanical characteristics has been done, and the FEM developed.

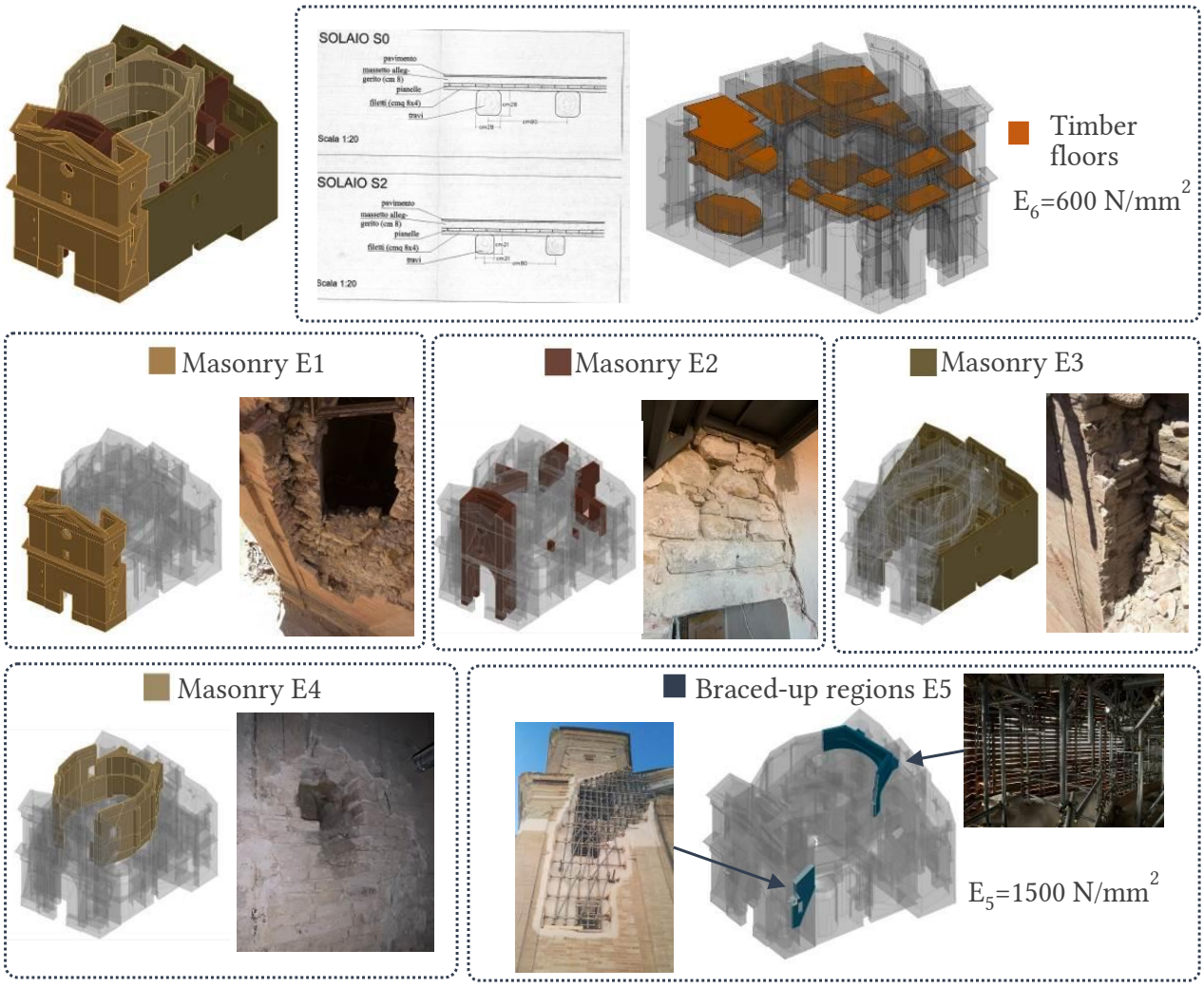

Figure 5-9: Different types of masonry recognised during the visual inspection and localization of wooden floors and repaired regions (braced-up regions).

5.3.2. Finite Element Modelling

FEM is developed with the ANSYS software, and includes the whole body of the church, modelled with tetrahedral solid elements. Furthermore, although part of the damage is simulated by changes in material properties (in particular stiffness, by varying the masonry elastic moduli), the extensive damage in the tiburium and the façade is incorporated directly into the geometric model. The numerical model is composed by five different materials based on the four masonry types and the parts that are filled with steel latticed systems, as described in detail in the previous section. The geometric model has been divided into further sections to facilitate the control of the mesh construction. The wooden floors inside the church are modelled with shell elements, namely isotropic plates, because they contribute to the development of the box-like behavior of the building, while the roof is not modelled and only its mass is taken into account, because the main part of it collapsed after the earthquakes. Moreover, the external steel securing system is modelled as well, since it is in contact with the church façade and, therefore, can contribute to the whole structural dynamic response; beam elements are adopted to model both the steel trusses and the steel cables surrounding the whole church. As far as the boundary conditions are concerned, all elements are fixed to the ground. All modelled elements are automatically meshed by the software, resulting in a FEM consisting of 538275 nodes. All construction materials are assumed homogeneous, elastic and isotropic. Some pictures of the model and an initial estimate of the elastic moduli are shown in Figure 5-10.

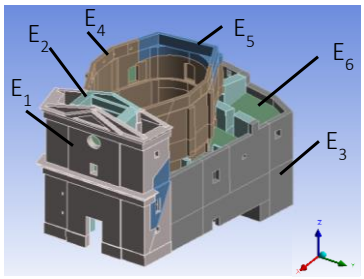

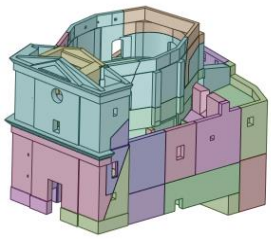

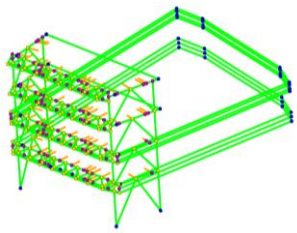

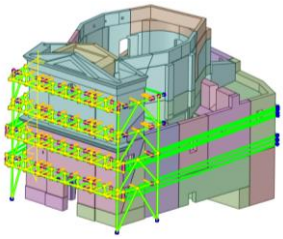

Mesh:
Sizing 0.5 m
538275 nodes
309541 tetrahedral elements

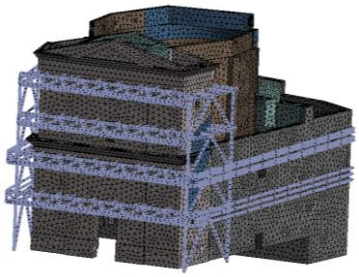

Materials:	E [N/mm2]	∂ [Kg/m3]	ν [-]
Masonry E1	1092	1937.4	0.25
Masonry E2	1230	1937.4	0.25
Masonry E3	1200	1937.4	0.25
Masonry E4	1365	1937.4	0.25
Braced up region E5	1500	1000	0.25
Timber E6	600	800	0.25
Lattice beam	210000	7850	0.3
Bracing	210000	7850	0.3
Strands	110000	7850	0.3

Figure 5-10: Pictures of the model, details of the created mesh and an initial estimate of the mechanical characteristics of the construction materials.

5.3.3. Particle swarm optimization and model updating

As discussed in chapter 3, in this work the Particle Swarm Optimization (PSO) algorithm is used to automatically update the FEM of the church. Evolutionary computing (which includes genetic algorithms) and swarm intelligence are mainly used for optimization problems, such as multi-modal and multi-objective optimization tasks. PSO technique enables an initial random population of particles to iteratively move through a hyperdimensional space to search for the optimal solution. A communication structure is also defined, assigning neighbors for each individual particle to interact with them. As mentioned above, PSO is a kind of searching process based on swarm, in which each individual, called particle, is defined as a potential solution of the optimized problem in D-dimensional search space, and it can memorize the optimal position of the swarm and that of its own, as well as the velocity. In each generation, the particles information is combined together to adjust the velocity of each dimension, which is used to compute the new position of the particle. Particles change their states constantly in the multi-dimensional search space, until they reach balance or optimal state, or beyond the calculating limits.

Several parameters can be considered in the updating procedures, as the material mechanical properties (elastic moduli, Poisson's ratio), their masses, the geometry and number of modelled elements, the boundary conditions, the presence of damage, etc. The masses of the masonries are excluded from the updating parameters since they can be calculated with good accuracy (construction typologies are known); the same can be assumed for the masses of the steel latticed systems and for the wooden floors. The base restraint stiffness is not considered as updating parameter because of the dynamics of the church mostly interests the upper part of the building; also, the Poisson's coefficient is assumed constant. The variables considered for the analysis are the masonry elastic moduli E1, E2, E3 and E4 introduced in the previous paragraph and the elastic modulus E5 of the material used in the repaired regions.

To make the optimization more efficient, PSO has been applied to the logarithm of the function already shown in equation 4.39:

$$err(\boldsymbol{E}) = \ln\left(1 + \left|\frac{f_{num}(\boldsymbol{E}) - f_{exp}}{f_{exp}}\right| + \left(1 - MAC_{num,exp.}(\boldsymbol{E})\right)\right) \text{ where: } \boldsymbol{E} = \begin{bmatrix} E_1 \\ E_2 \\ E_3 \\ E_4 \\ E_5 \end{bmatrix} \qquad (5.1)$$

where *err(**E**)* represent the objective function and returns a scalar value. The comparison is made between the experimental (*exp*) modal parameters identified though OMA, and the relevant numerical (*num*) ones obtained from FE analysis. In detail, natural frequencies and mode shapes of the 10 vibration modes are considered in the updating procedure, when the algorithm converges below an error threshold of 5%.

In practice, the APDL language (ANSYS Parametric Design Language) has been used in ANSYS Mechanical (the FEM solver) to automatically export at the end of each analysis the results in terms of frequencies and modal displacements of the DOFs involved in the comparison and relative to the target modes. The PSO algorithm is implemented in MATLAB, which automatically performs analyses in batch mode and automatically reads the results at the end of each analysis to feed them back to the main algorithm and compute the values of the objective function. It is worth noting that, at each step of the PSO updating procedure correspond fifty numerical modal analysis and, consequently, fifty estimate of the vector ***E***, since it is suggested that at least ten particles for each updating parameter are necessary for each PSO step.

Figure 5-11 shows the results of iterations performed by the algorithm and the evolution of the parameters analyzed, relative to the best solutions found at each iteration. The analyzed parameters are plotted within the Lower Bound (LB) and the Upper Bound (UB) elastic modulus chosen for the analysis. These ranges differ from the initial estimates shown in Figure 5-10 because they have been adjusted as the optimization attempts have progressed, as the initial estimates have turned out to be far from optimal values. The masonry stiffness values for the church façade and the main body turned out to be much lower than the initial estimates, which is consistent with the severe crack pattern of the church. On the other hand, the tiburium requires much higher values of the modulus of elasticity to match the experimental results. The latter aspect might be explained by the presence of the latticed structure to prevent the out of plane collapse of the tiburium walls. The material relative to braced-up regions also needs higher values of the modulus of elasticity. The material for braced-up regions also needs much higher modulus of elasticity values of around 15000 MPa. These calibrated elastic modulus values allow the dynamics of the structure to be well represented under operational conditions, i.e. with low vibration levels. As we will see in the next chapter, if the level of accelerations (earthquakes) increases, the dynamic behavior rarely remains time invariant. Nevertheless, identifying and interpreting the dynamics under operational conditions is the cornerstone for the implementation of a VB-SHM system.

The results of the modal analysis at the end of the optimization process are shown in Figure 5-11, where the numerical modes are represented together with the corresponding experimental ones. Figure 5-12 shows the MAC values between the optimized and experimental modes and a comparison in terms of frequency. As can be seen from the terms on the diagonal, a very good match has been achieved for the first 5 modes, while for modes from 6 to 10, the results are less good, but still noteworthy given the complexity of the structure.

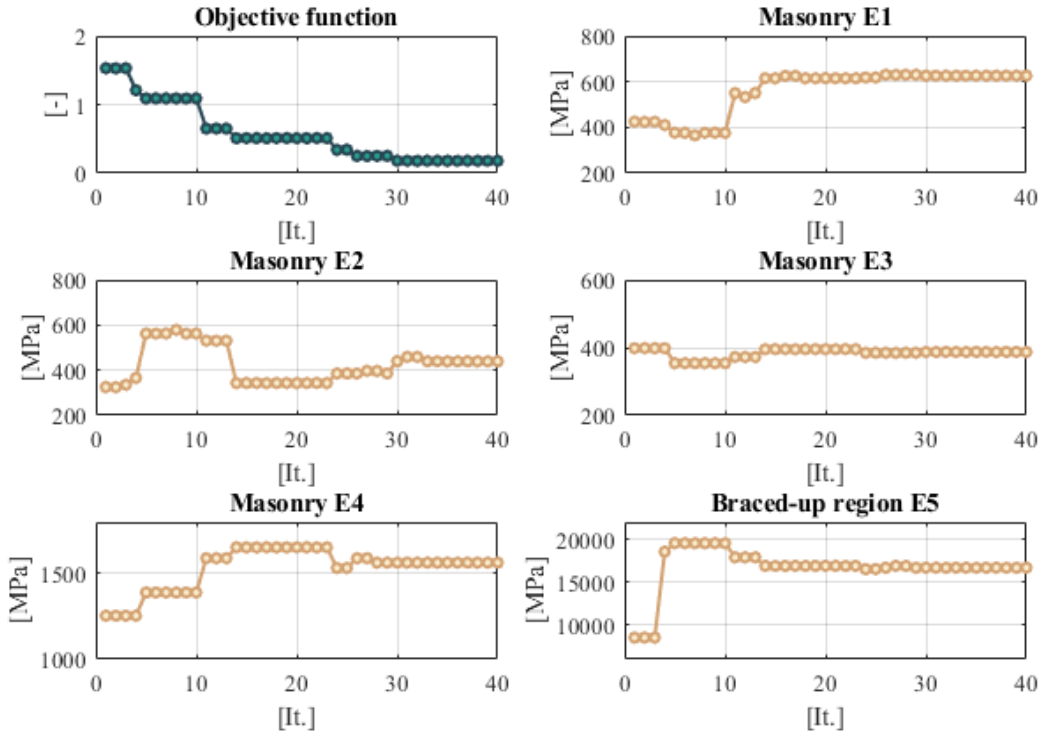

Figure 5-11: Results of the iterations performed by the algorithm and the evolution of the parameters analysed, relative to the best solutions found at each iteration.

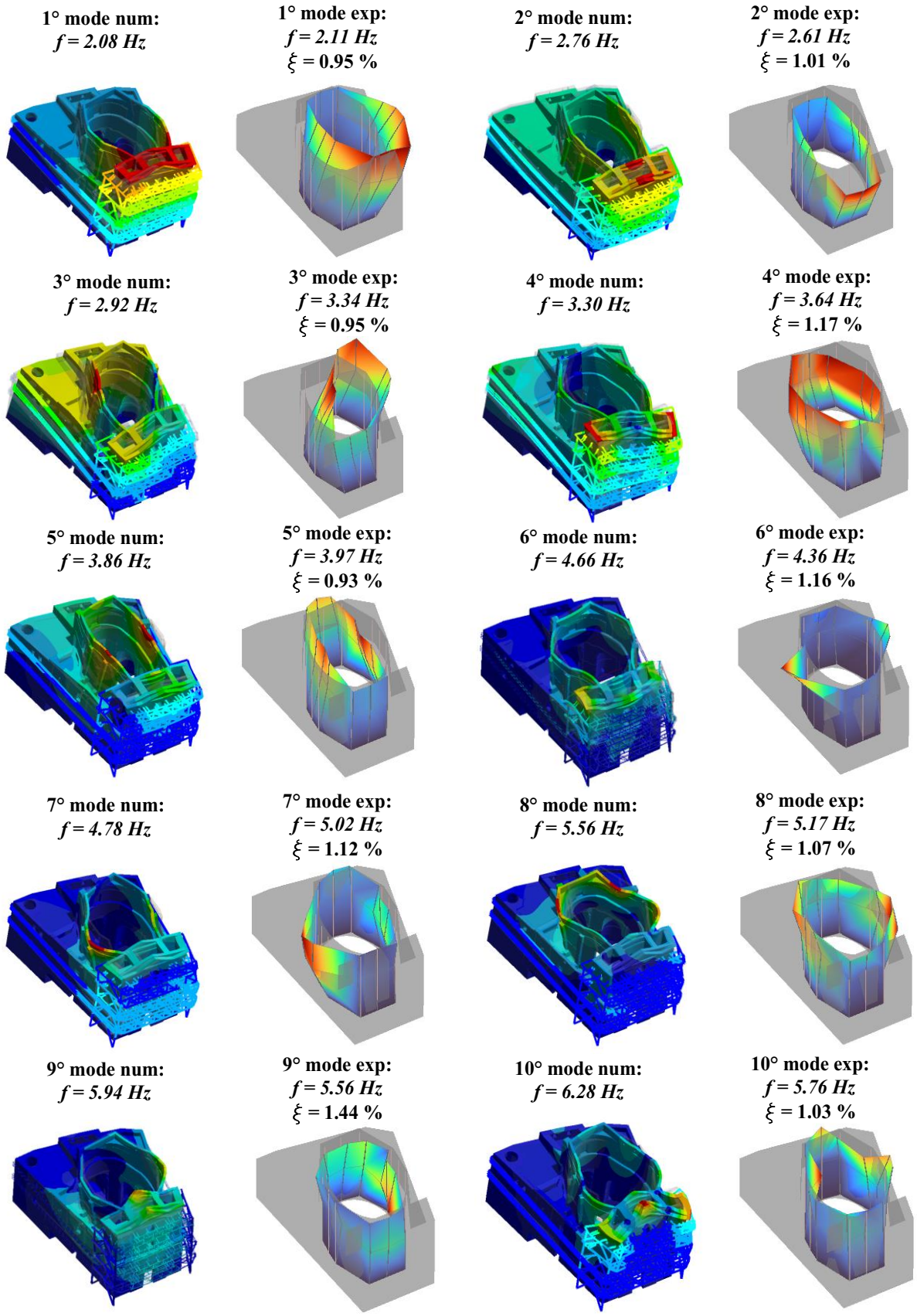

Figure 5-12: Optimazed numerical modes with the corresponding experimental ones.

Mode n ↓	Exp. [Hz] ↓										
1	2.11	0.95	0.00	0.07	0.03	0.00	0.01	0.19	0.19	0.03	0.00
2	2.61	0.00	0.86	0.08	0.01	0.03	0.20	0.02	0.00	0.08	0.04
3	3.34	0.05	0.05	0.89	0.04	0.00	0.04	0.21	0.01	0.41	0.01
4	3.64	0.06	0.02	0.45	0.77	0.03	0.00	0.02	0.00	0.04	0.00
5	3.97	0.00	0.01	0.05	0.03	0.94	0.34	0.02	0.00	0.01	0.02
6	4.36	0.07	0.02	0.11	0.00	0.21	0.51	0.18	0.02	0.04	0.00
7	5.02	0.24	0.01	0.23	0.05	0.01	0.11	0.67	0.44	0.18	0.00
8	5.17	0.05	0.03	0.01	0.08	0.06	0.07	0.28	0.47	0.07	0.00
9	5.56	0.11	0.29	0.01	0.07	0.02	0.26	0.04	0.30	0.44	0.20
10	5.76	0.00	0.01	0.00	0.00	0.01	0.01	0.01	0.02	0.17	0.42
	Model [Hz]→	2.08	2.76	2.92	3.30	3.86	4.66	4.78	5.57	5.95	6.28
	Error [%] →	1.7%	5.5%	12.6%	9.3%	2.7%	6.8%	4.9%	7.6%	7.1%	9.0%
	Mode n →	**1**	**2**	**3**	**4**	**5**	**6**	**7**	**8**	**9**	**10**

Figure 5-13: MAC matrix between numerical and experimental mode shapes.

5.4. Optimal sensors placement

OSP technique is adopted to find the best positions in which sensors should be placed to dynamically monitor the church at hand. Using OSP algorithm on the results of the modal analysis on the updated model rather than directly on the experimental results can be of great benefit, especially because, given the necessarily low number of monitored DOFs on the real structure, spatial aliasing may be encountered when choosing the optimal position.

The algorithm Effective Independence discussed in chapter 4, has been implemented in MATLAB software. The analysis has been carried out considering 10 modes of vibration so the minimum number of points where a sensor should be installed, according to the Effective Independence method, is ten. Considering only the DOFs on the on external surfaces of the model (they must be accessible for the installation of a sensor), more than 250,000 translational degrees of freedom are possible. To make the analysis faster, the points to be analyzed were randomly sampled to 25,000. After that, each iteration eliminates the position that less contributes to the system's Effective Independence, i.e., the position with the lowest ED coefficient. The iterations end when only 10 positions remain, which possess ED=1. With the aim of limiting the number of sensors as much as possible, 2 of the 10 points identified were selected manually. Figure 5-11 shows the results of the OSP analysis carried out on the updated model of the church.

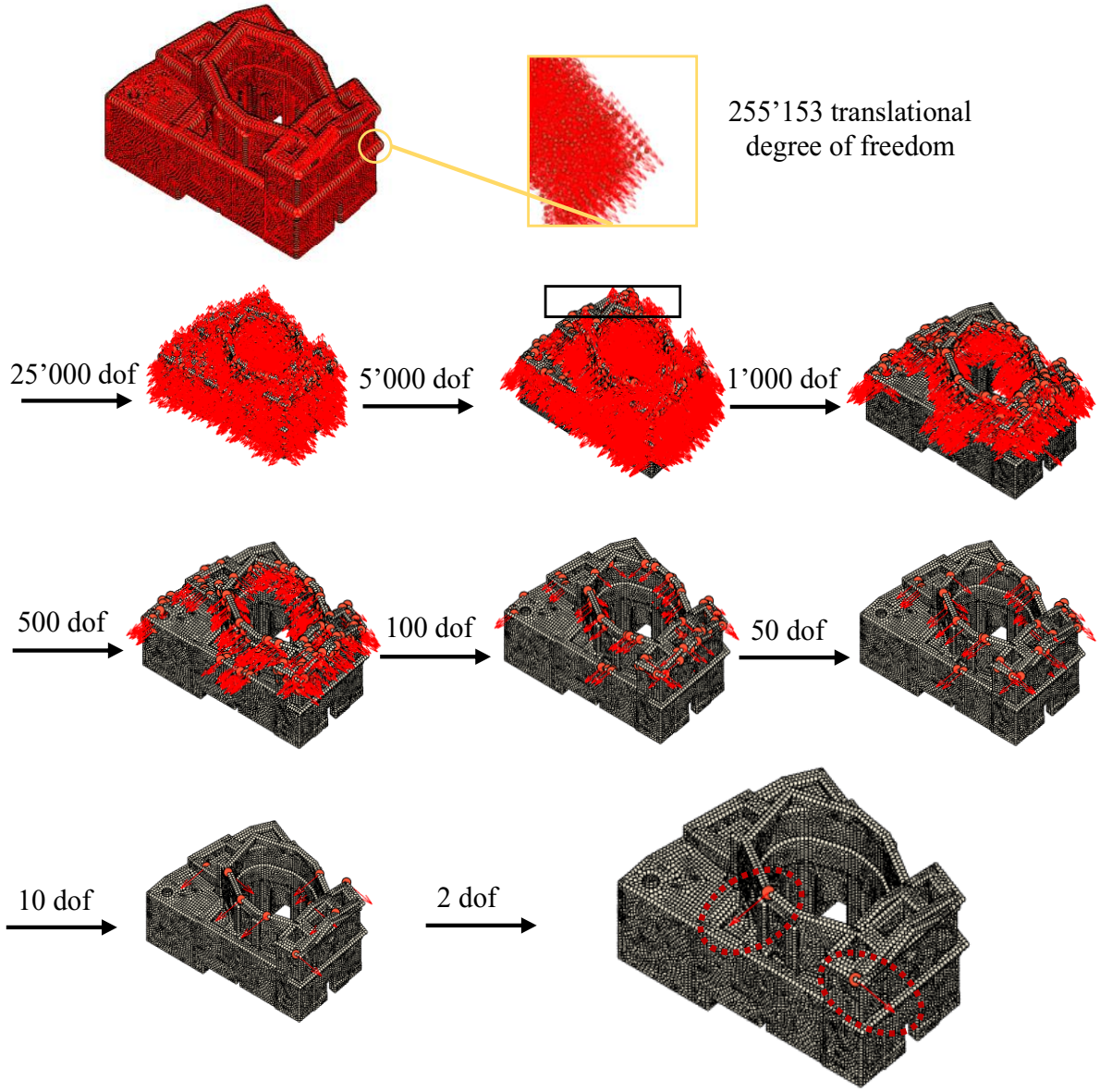

Figure 5-14: Results of the OSP analysis carried out on the updated model.

5.5. Discussion of the results

As already discussed, the design of a vibration-based structural health monitoring system requires a complete understanding of the dynamics of the structure to be monitored. Finite element modelling can substantially contribute to this preliminary phase, especially in the case of complex dynamic structures where uncertainty about material characteristics and boundary conditions may be significant. The modelling of the church of Santa Maria in Via has proved to be particularly challenging, and the intention to also calibrate the higher modes has required the use of advanced optimization techniques. In this case, the Particle Swarm Optimization algorithm has been particularly suitable. As reported in the literature search in chapter 2, the family of Swarm Intelligence is composed of several algorithms, furthermore, also the class of Genetic algorithms is becoming more and more popular in dealing with this type of problem. Among the future developments, there is certainly that of using different algorithms to evaluate their potential and compare them.

Finally, obtaining a finite element model that can accurately represent the dynamics of the structure to be monitored is particularly important for the optimal positioning of the sensors.

Dynamic identification tests are carried out with a limited number of sensors, and the identified modal shapes may suffer from spatial aliasing, especially in those cases where it is difficult to make simplifying hypotheses (e.g. presence of rigid floors). Performing a study to optimize the number and position of sensors from only the identified modal components may not be effective. On the other hand, a finite element model has many degrees of freedom and manually choosing which is the most interesting to monitor can be a non-trivial challenge. It is therefore necessary to implement algorithms for OSP and in this work EI has been used due to its easiness of interpretation and implementation. Again, this is an actual problem with the increasing adoption of artificial intelligence algorithms, and it will be interesting as a future development to study which methodology is the most effective.

6. The Varano High School in Camerino; building non-linearities in the seismic response

6.1. Presentation of the case study

The investigated case study is a RC frame building built around the year 1960 and hosting the Costanza da Varano high school in the historical town center of Camerino. The town was overall severely damaged by the Central Italy earthquake in 2016, especially by the main shocks of October, 26th and October, 30th of Richter Magnitude 5.9 and 6.1, respectively. A significant number of masonry building (e.g., the church of Santa Maria in Via; the cathedral of Santa Maria Annunziata, Palazzo Ducale) and RC buildings (e.g., the old courthouse of the town), were damaged and some partial collapses occurred.

The building, characterized by an L-shaped plan, is divided into two main blocks as shown in Figure 6-1a: block A, having 4 storeys (1 underground and 3 above ground) and plan dimensions around 25 x 19 m; and block B, having 3 storeys above ground and plan dimensions of about 13 x 27 m. Blocks are separated by a 2 cm wide joint in correspondence of the structural elements, whereas the non-structural components (screeds, floorings and infill walls) are continuous through the joints. Moreover, block A is further divided into two parts (A1 and A2) by means of another structural joint. The block A is directly founded on the sandstone rock by means of RC plinths, while block B is built over the ancient masonry ruins belonging to the S. Elisabetta Convent. All columns have square cross-sections (40 x 40 cm) and are rotated of 45° with respect to the frame plane for aesthetical reasons. Beams located at the building perimeter are linearly tapered with a cross section of about 30 x 80 cm at the beam-to-column joints and 30 x 40 cm at midspan, whereas the internal beams have uniform rectangular cross section with different dimensions depending on the beam position. It is worth noting that, due to the cross-section dimensions of structural components (columns and beams), frames tend to develop a shear-type horizontal behavior. All the beam and hollow block floors have a thickness of 24 cm. Internal partitions are constituted with light infill masonry walls, while external ones are 1.2 m high double brick walls, which leave space for large windows (Figure 6-1b).

In 2013 a seismic retrofit was carried out to improve the building seismic performance, which suffers of intrinsic vulnerabilities deriving from the structural element dimensions (e.g., strong beam, weak columns). The main blocks had structurally connected each other with thick steel plates anchored to the RC elements in correspondence of the structural joints. Then, two external steel truss towers (Figure 6-1b), called dissipative towers [112], were built, and rigidly connected with the building at the floor levels by means of steel braces anchored to the external beams.

Tower Ta is the tallest one (14.5 m) and is connected to both the block A (at the upper three floors) and the block B (at the upper two floors); tower Tb (9.3 m high) is connected only to the block B (at the upper two floors). Each tower is erected on a RC thick base plate that is centrally pinned to the foundation plate by means of a spherical support. Eight and four viscous dampers for tower Ta and Tb, respectively, are in vertical position between the base and foundation plates (one or two devices per vertex), so that the base plate rigid rotations, due to the horizontal building displacements, activate simultaneously all the devices. Articulated quadrangles are adopted to amplify the device displacements through leverage systems. Towers are founded on piles and micro-piles to transfer both compression and tension forces during earthquakes arising from the viscous forces transferred by the devices acting at the plate vertexes. More details about the seismic retrofit of the school building can be found in Balducci and Castellano [113] and in Gara et al. [60].

6.2. Dynamic monitoring system and acquired data

During the different phases of the retrofit works, AVT tests were already carried out. More precisely, ambient vibration tests (AVT) were performed before and after the seismic retrofit to identify the modal parameters characterizing the building during these two important phases. The purpose was twofold: first, the preliminary identification allowed to obtain a calibrated FEM of the structure for the design of the retrofit and, second, the investigation after the seismic retrofit allowed to verify that the modal parameters of the structure correspond to those predicted by the developed FEM, evaluating its reliability and usefulness also in a monitoring process. A more extensive description of the tests performed, and the results obtained can be found in the work of Gara et al [60]. The building suffered the Amatrice earthquake of 24 August 2016, which was strongly felt in Camerino; however, the building suffered negligible damage consisting mainly of slight cracks in internal partitions, which were immediately repaired to ensure the occupation of the building and the regular start of school in September.

6.2.1. Preliminary identification tests

After this seismic sequence, a new AVT was performed on 27 August 2016, to assess the health of the building and obtain results to be used as a benchmark for the outcomes of subsequent monitoring. The instrumentation adopted to perform the dynamic test (Figure 6-2a) consisted in low-noise uniaxial piezoelectric accelerometers with ceramic flexural ICP, model PCB 393B31, connected by means of coaxial cables to four 4-channels dynamic signal acquisition modules NI-9234 mounted on a 8-slot USB chassis NI cDAQ 9178.

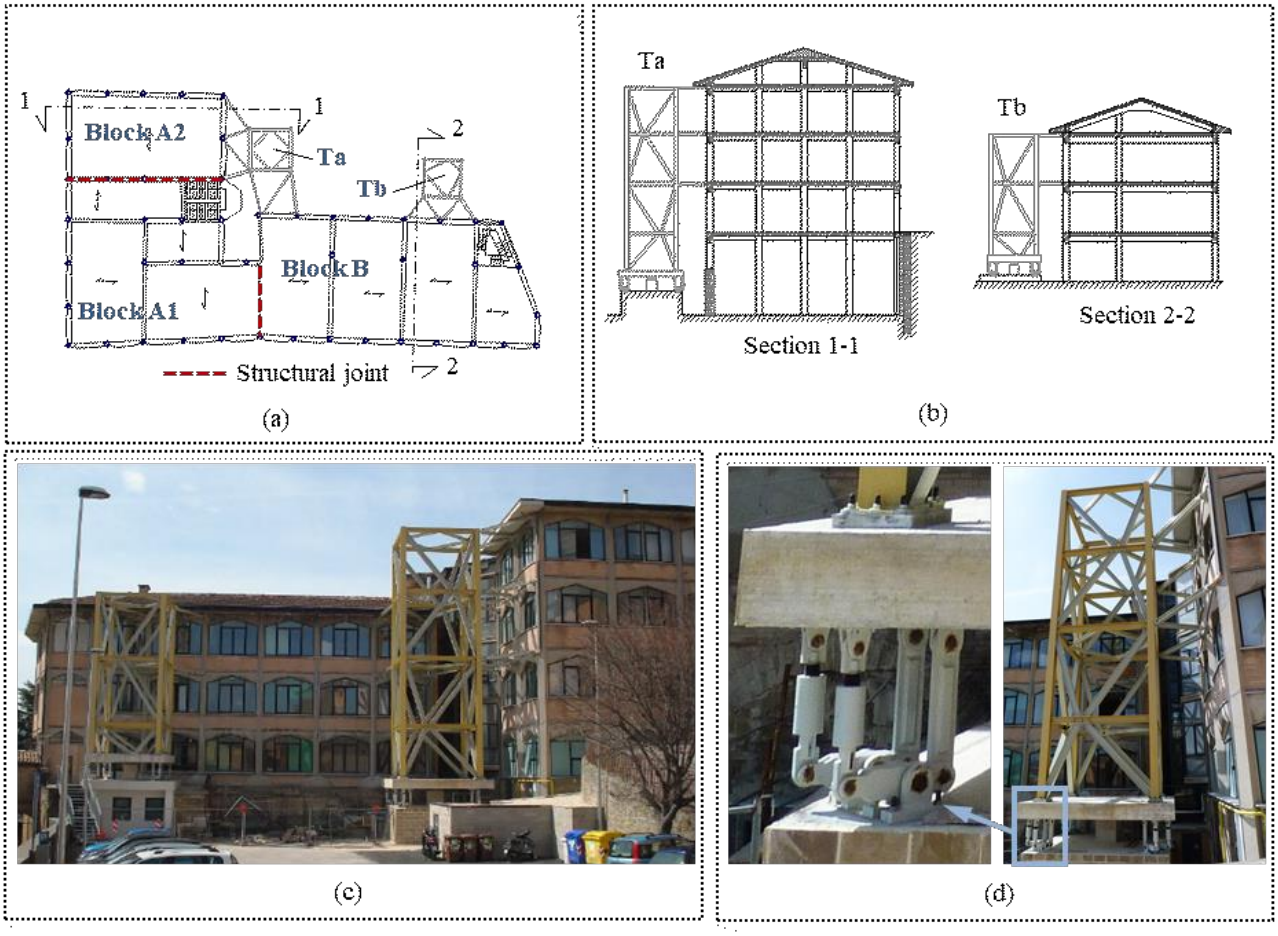

Figure 6-1: The Costanza da Varano high school: (a) plan view; (b) cross-section; (c) photo of the building; (d) photo of the Dissipative Towers with details of the dampers

A notebook equipped with dedicated software developed in the LabVIEW environment was used to acquire the signals and store the data. During the tests, 30-minute recordings were acquired and sampled at a frequency of 2048 Hz. Assuming that the floors are rigid in their plane, three accelerometers per floor were used: two measuring in the X direction and one in the Y direction (Figure 6-2b). In addition, two sensors per dissipative tower were used (Ta1 and Ta2 for the Ta tower, and Tb1 and Tb2 for the Tb tower), placed on the RC base plate and measuring in the vertical direction. The measurement configuration adopted makes it possible to investigate the dynamic behavior of the whole building by also considering the modal displacements of the tower relative to each vibration mode of the building. For the reconstruction of the mode shapes, the towers are assumed rigid, in line with the design hypotheses. The modal parameters of the building were identified through the output-only Covariance-driven Stochastic Subspace Identification (SSI-COV) technique [81]. Figure 6-3 summarizes the results of the dynamic characterization; in detail, Figure 6-3a shows the first three mode shapes, drawn based on the rigid floor hypothesis and considering the dissipative towers as non-deformable systems. The first vibration mode is a roto-translational mode in the transverse X direction with higher modal displacements near the block A; the second is mainly a rotational mode, while the third is a roto-translational mode in the longitudinal Y direction. The shapes of the modes are almost orthogonal to each other, as can be observed from the Auto-MAC matrix shown in Figures 6-3b, where the off-diagonal terms have very low values. Argand diagrams and Mode Complexity Factor (MCF) values indicating low mode complexity are also shown in Figure 6-3c.

The results of the AVT are interpreted through a refined FEM of the whole building, developed by means of commercial software (Figures 6-4a). Both beams and columns are modelled with elastic frame elements, while shell elements are used to model floors and stair slabs to account for their deformability both in-plane and out-of-plane. The old masonry walls at the base of Block B and the external and internal infill masonry walls were also modelled using shell elements. The modelling is based on the available structural drawings of the building and on in situ measurements, as well as on destructive and non-destructive tests on the structural materials; in detail, the dynamic elastic modulus of the concrete, obtained by increasing the static modulus by about 20% [114], is assumed to be 30720 MPa while the density is 2.5 t/m3.

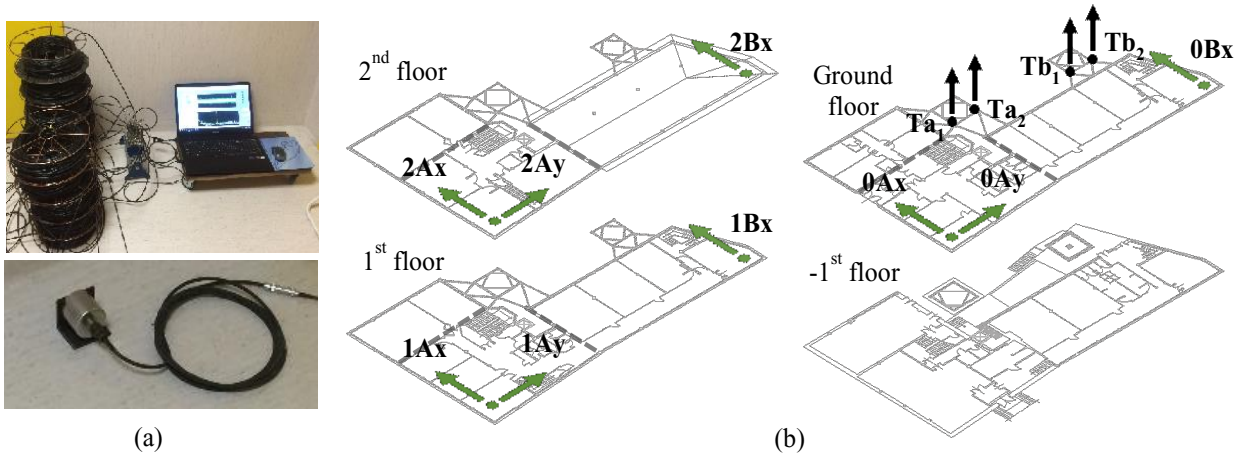

Figure 6-2: (a) Photos of the adopted instrumentation; (b) Sensor layout.

For old walls, external and internal walls, dynamic elastic moduli of 4032, 5500 and 3850 MPa, respectively, are considered, according to the indications provided by the Italian regulations (Circular 21.01.2019), depending on the type of masonry. For the previous walls, densities of 2.2, 2.0 and 1.2 t/m3 are adopted, respectively.

To simulate the localized deformability due to structural joints between building blocks sewn through steel plates, elastic connections between modelled frame elements having stiffnesses calibrated by AVT results are adopted. The base joints are fixed, and the foundations are not modelled, since the building is founded on concrete sandstone, but the contribution of the soil surrounding the ancient masonry on one side of the building is considered through springs with stiffnesses obtained assuming a subgrade reaction value of 80000 kN/m3 (medium dense sand). Further details regarding material properties, overall modelling and the model updating process can be found in Gara et al. [60]. As for the dissipative towers, the braced steel frames are modelled with beam elements, while the RC base plate is modelled with shell elements; the base plate, as well as the dissipative devices, are constrained to the ground.

An eigenvector analysis is performed to obtain the modal numerical parameters of the building, which are in very good agreement with the corresponding experimental ones (Figure 6-4b, c, d) which are determined assuming the in-plane stiffness of the floors, consistent with the available number of measurement points. It is worth noting that the good correspondence of the experimental and numerical results supports the validity of the in-plane floor stiffness assumption, which was used to derive the experimental mode shapes. This is evident by observing the MAC matrix between the numerical and experimental mode shapes (Figure 6-4d) where the MAC indices along the diagonal entries are close to 100%. The assumption of rigid behavior adopted for the reconstruction of the tower mode shapes is also validated.

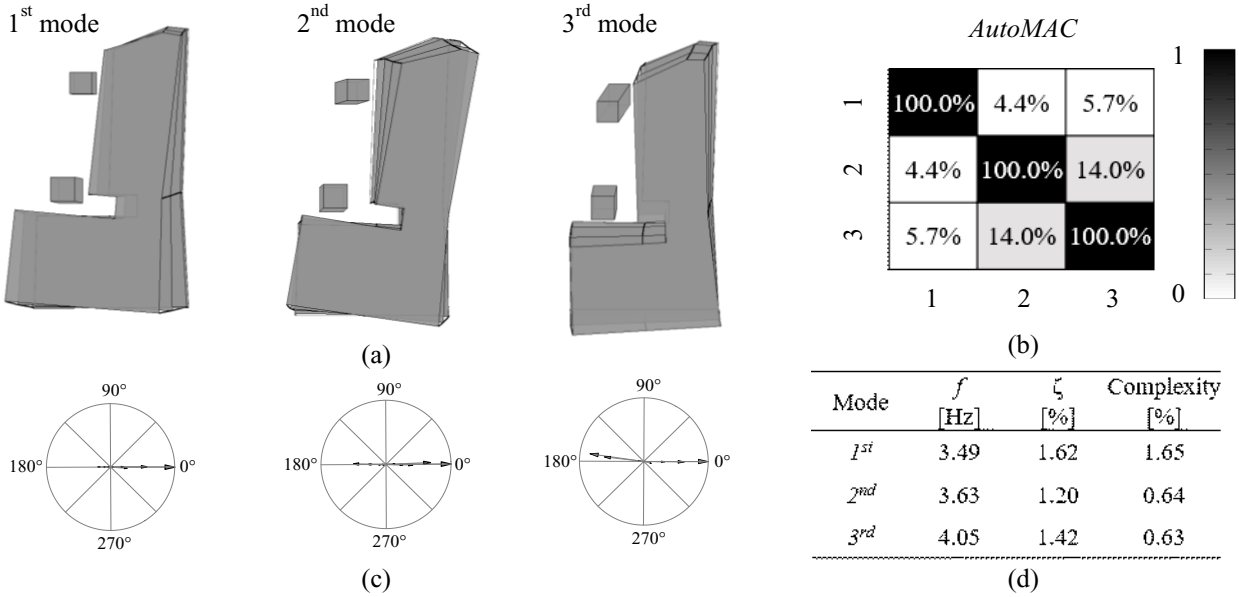

Mode	f [Hz]	ζ [%]	Complexity [%]
1st	3.49	1.62	1.65
2nd	3.63	1.20	0.64
3rd	4.05	1.42	0.63

Figure 6-3: Building experimental modal parameters from AVT of August 27th, 2016: (a) Mode shapes; (b) AutoMAC; (c) Argand diagrams; (d) Summary table of the modal parameters.

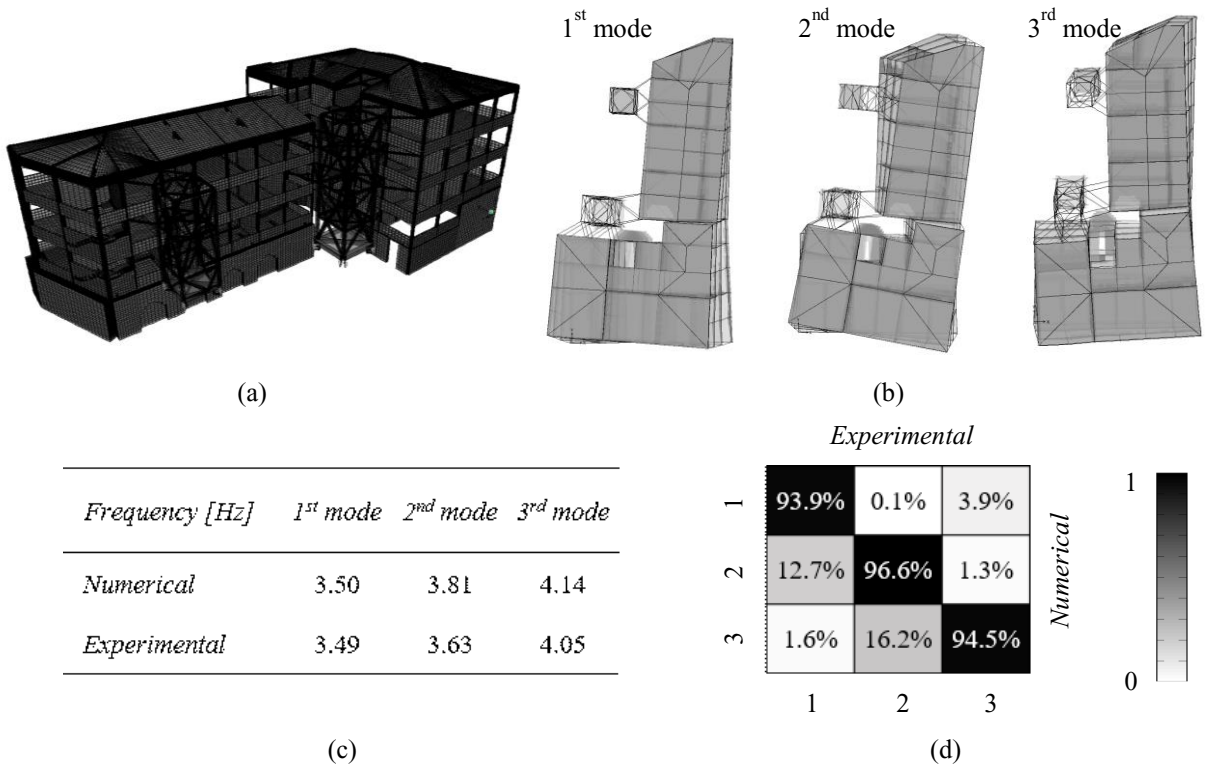

Frequency [Hz]	*1st mode*	*2nd mode*	*3rd mode*
Numerical	3.50	3.81	4.14
Experimental	3.49	3.63	4.05

Figure 6-4: Building f.e. model: (a) Global 3-D view; (b) Plan view of the mode shapes; (c) Comparison between numerical and experimental resonance frequencies; (d) MAC matrix.

6.2.2. Description of the monitoring system

Following the preliminary AVT performed on 27 August 2016, a continuous dynamic monitoring system was installed on the building and left in place for three days, with the objective of monitoring the dynamic behavior of the building during the seismic swarm following the main tremor. The monitoring system was composed of the same instrumentation adopted to perform the AVT benchmark previously described. In this case, thirteen low-noise single-axis piezoelectric accelerometers were adopted with the arrangement shown in Figure 6-5: three sensors were placed at the base floor (-1st floor) to measure the seismic input in the two orthogonal horizontal directions, six accelerometers at the 1st and 2nd floors (three for each) to measure the structural response, and four accelerometers on the tower base plates (two for each plate) to capture the tower motions. Although the signals recorded at the base of the building do not correspond to free-field seismic motion at the building location, due to kinematic and inertial effects of ground-structure interaction [115], they will be referred to as seismic input in the following for simplicity. Both the input (seismic input) and the output (building response) were recorded using a sampling frequency of 2048 Hz.

During the entire monitoring period, data were acquired continuously allowing the monitoring of both the dynamic behavior of the building subjected to environmental vibrations (i.e., between two successive seismic swarm events) and its response to seismic events. The recordings of the building's response to environmental vibrations were divided into 20-minute recordings; for each time history, an identification only output was made through the SSI-COV method, the same adopted for the AVT benchmark.

Tracking modal parameters obtained from non-earthquake data provides useful information for investigating the evolution of possible structural and non-structural damage that occurred during the earthquake sequence, as well as for investigating changes in modal properties due to environmental effects. Recordings of the building response to seismic events were isolated and used to identify the building dynamics during their occurrence, as shown below.

Many low- and medium-intensity seismic events occurred during the three days of monitoring and only those with Richter Magnitude greater than 2.6 were selected for further analysis. Table 1 reports the twenty-five seismic events considered with the occurrence data and the time, intensity (ML), depth of the hypocenter and distance of the epicenter from the investigated building; the events are ordered by decreasing intensity and the strongest one, which occurred on August 28, 2016, at 17:55, is characterized by 4.4 ML and the epicenter of about 37 km from the school. Figure 6-6 shows the epicenter positions of the seismic events and the main characteristics of the most relevant ones (first 4 events in Table 1).

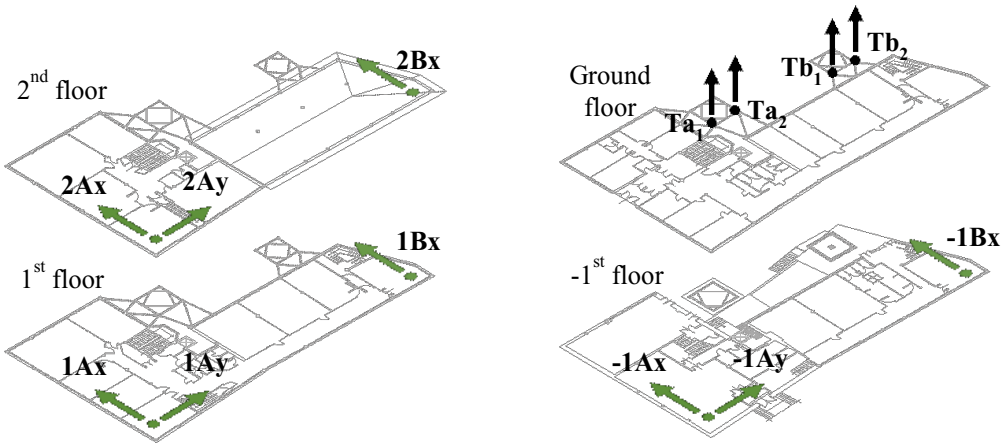

Figure 6-5: Sensor layout for the continuous dynamic monitoring system.

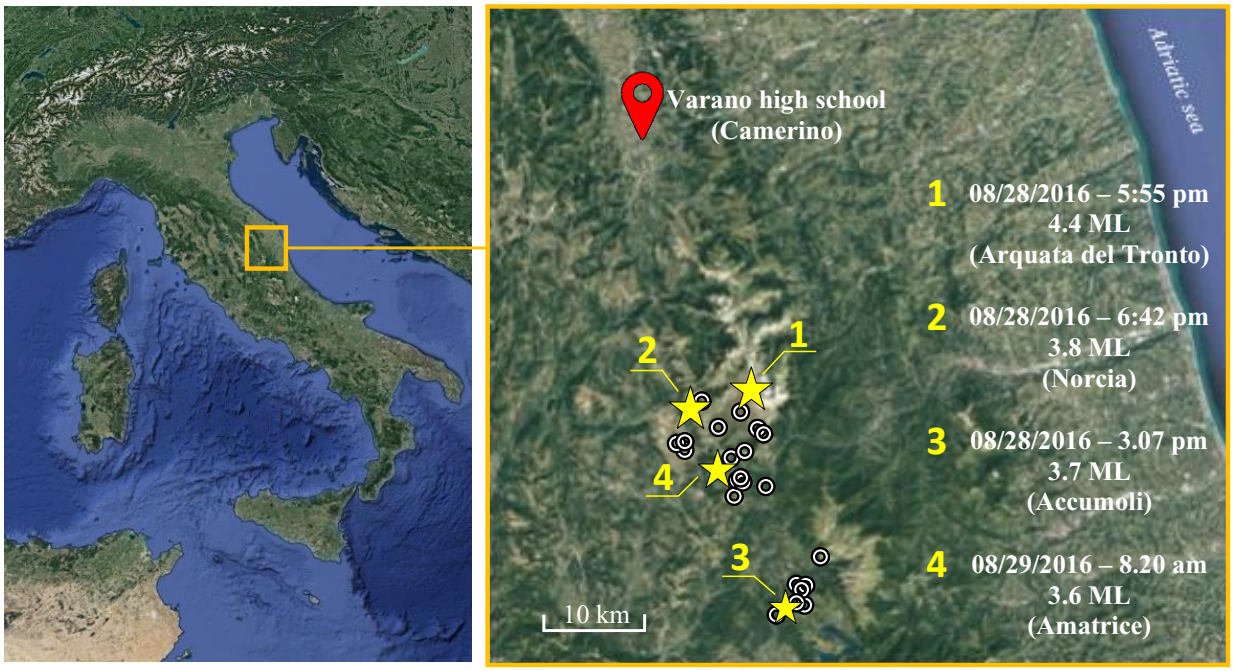

Figure 6-6: Epicenters of the considered seismic events and main features of the four strongest ones

Figure 6-7 shows the accelerations, velocities and displacements recorded by three sensors (-1Ay, 2Ay and Ta1) of the monitoring system during the most intense event (4.4 ML). It is worth noting that the seismic swarm events induced overall low accelerations, velocities, and displacements at the structure. In detail, the latter are of the order of 10^{-1} mm at the second floor and 10^{-2} mm at the base of the dissipative towers, at the level of the viscous dampers.

Table 1: Considered seismic events during the three days of monitoring.

Event n.	Intensity [ML]	Hypocentre [km]	Epicentre [km]	Date (2016)	Time	Website
1	4.4	9	36.93	Aug. 28th	5:55 pm	http://cnt.rm.ingv.it/event/7343701
2	3.8	9	35.40	Aug. 28th	6:42 pm	http://cnt.rm.ingv.it/event/7345471
3	3.7	9	61.97	Aug. 28th	3:07 pm	http://cnt.rm.ingv.it/event/7339051
4	3.6	10	43.47	Aug. 29th	8:20 am	http://cnt.rm.ingv.it/event/7370871
5	3.6	12	40.30	Aug. 28th	5:37 pm	http://cnt.rm.ingv.it/event/7343051
6	3.5	10	42.26	Aug. 29th	3:44 am	http://cnt.rm.ingv.it/event/7363391
7	3.4	11	62.03	Aug. 27th	11:31 pm	http://cnt.rm.ingv.it/event/7307161
8	3.4	11	46.88	Aug. 28th	8:37 am	http://cnt.rm.ingv.it/event/7326791
9	3.2	8	59.20	Aug. 28th	11:18 am	http://cnt.rm.ingv.it/event/7332041
10	3.1	8	45.02	Aug. 28th	10:22 pm	http://cnt.rm.ingv.it/event/7353481
11	3.1	9	62.03	Aug. 28th	7:16 am	http://cnt.rm.ingv.it/event/7323941
12	3.0	7	39.83	Aug. 28th	9:59 am	http://cnt.rm.ingv.it/event/7329641
13	3.0	10	39.42	Aug. 28th	12:25 pm	http://cnt.rm.ingv.it/event/7334431
14	2.9	8	59.75	Aug. 28th	8:13 am	http://cnt.rm.ingv.it/event/7325951
15	2.9	10	60.11	Aug. 28th	1:53 am	http://cnt.rm.ingv.it/event/7312881
16	2.8	11	46.83	Aug. 28th	6:25 pm	http://cnt.rm.ingv.it/event/7344771
17	2.8	10	57.24	Aug. 27th	11:26 pm	http://cnt.rm.ingv.it/event/7306911
18	2.8	10	37.31	Aug. 27th	7:50 pm	http://cnt.rm.ingv.it/event/7299421
19	2.8	11	41.97	Aug. 28th	4:40 am	http://cnt.rm.ingv.it/event/7318921
20	2.8	9	45.44	Aug. 29th	6:04 am	http://cnt.rm.ingv.it/event/7367651
21	2.8	10	44.94	Aug. 28th	2:44 pm	http://cnt.rm.ingv.it/event/7338361
22	2.7	9	61.41	Aug. 28th	10:00 pm	http://cnt.rm.ingv.it/event/7352691
23	2.7	10	38.31	Aug. 28th	12:44 am	http://cnt.rm.ingv.it/event/7334991
24	2.6	10	34.69	Aug. 27th	6:55 pm	http://cnt.rm.ingv.it/event/7297391
25	2.6	10	39.20	Aug. 28th	5:34 pm	http://cnt.rm.ingv.it/event/7342961

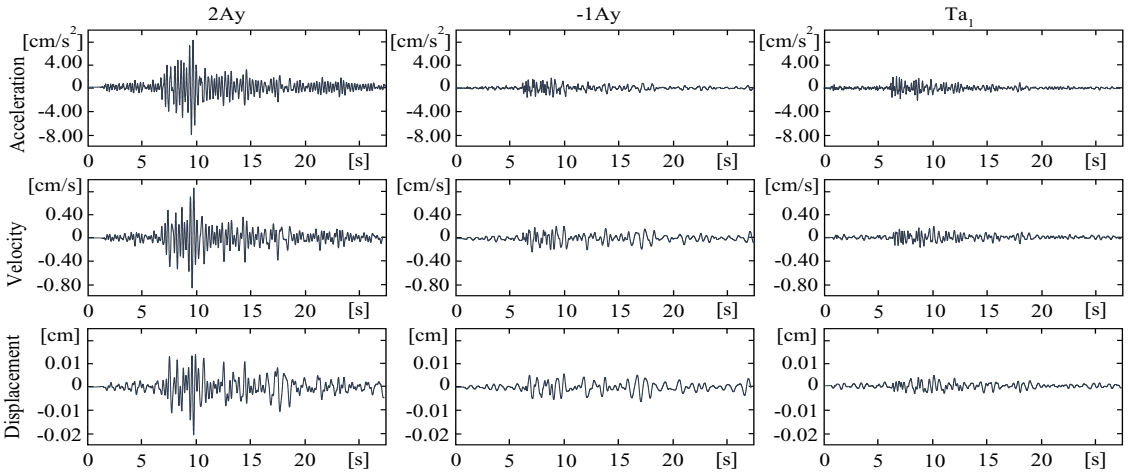

Figure 6-7: Acceleration, velocity and displacement recorded by three sensors during the 4.4 ML seismic event.

6.3. Analysis of the seismic response

As discussed in Chapter 4 through the review of the scientific literature, reinforced concrete buildings show a non-linear response to earthquakes even in the absence of damage. The same can be observed for this case study, where the non-linear behavior is evident by observing the time-frequency analyses in Figure 6-8, where the short Fourier transforms (STFT) of the signals recorded at measurement points 1Ax, 1Ay, 1Bx, 2Ax, 2Ay and 2Bx during the main seismic event (4.4 ML) are reported. As mentioned above, the main problem to be faced in the application of the dynamic identification algorithms is the non-linear nature of the building response for increasing amplitudes of the accelerations to which the structure is subjected.

6.3.1. Dynamic identification during seismic events

Figure 6-9 shows the results of the procedure introduced in Section 4.3.1 performed on the time history recorded at position 2Ay during the 4.4 ML earthquake. In detail, Figure 6-9a shows the time-frequency analysis of the signal from which the initial window lengths are determined, while Figure 6-9b shows the time histories of the accelerations (i.e., measured by the monitoring system and predicted through the identified time-invariant dynamical systems) and gives an indication of the set of windows identified with the proposed approach. A more detailed comparison between the predicted and measured time histories for each window is represented in Figure 6-9e, where it can be observed that the predicted and measured responses are almost overlapping, demonstrating the effectiveness of the proposed strategy.

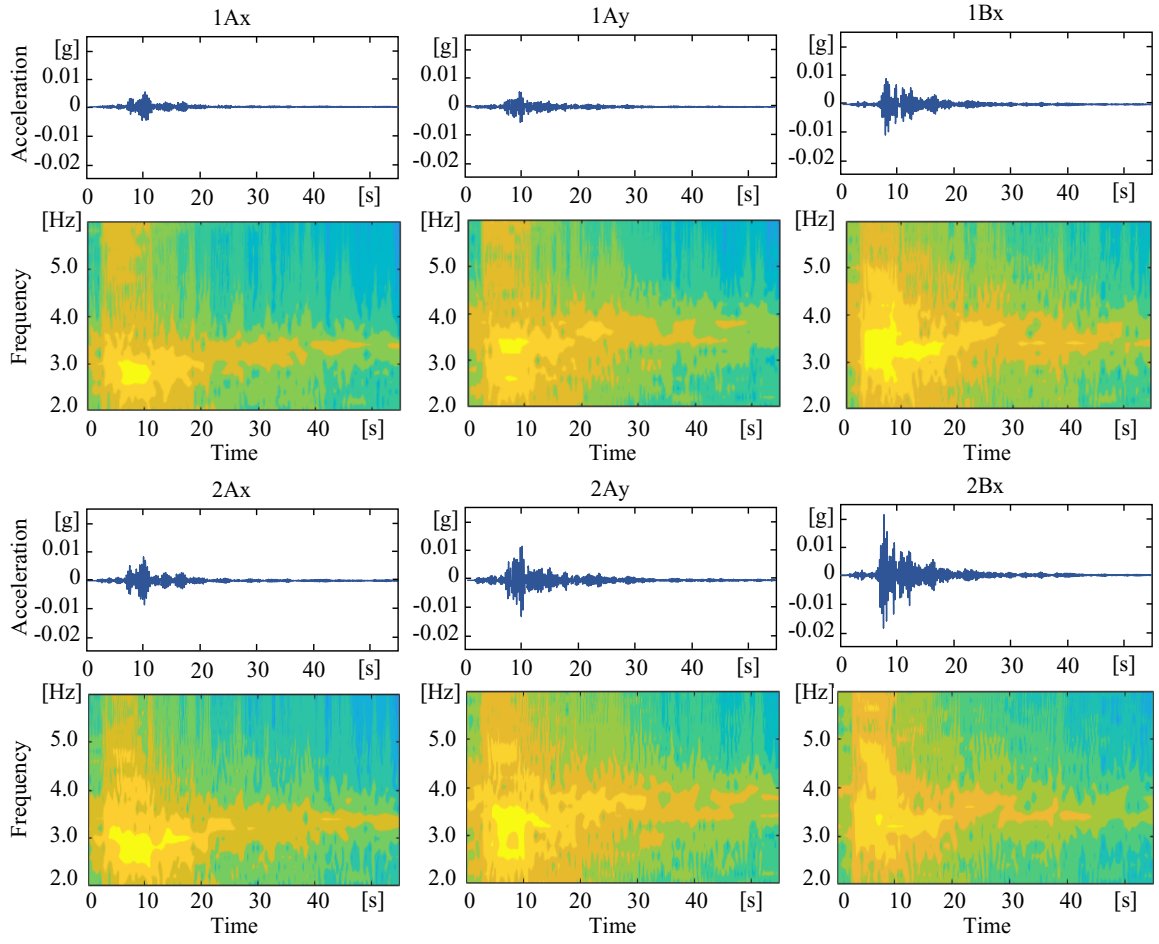

Figure 6-8: STFT for the accelerations measured at points 1Ax, 1Ay, 1Bx, 2Ax, 2Ay and 2Bx during the 4.4 ML earthquake.

Figure 6-9c shows the resonance frequencies found in each window for the first three modes of vibration. For all the modes of vibration, the values of the resonance frequencies decrease during the strong motion, where the maximum accelerations occur, and then increase again at the end of the strong motion, returning to values very close to the initial ones; for the earthquake presented and for the first mode of vibration, the value of the initial frequency is 3.51 Hz, the lowest one identified during the strong motion is 2.85 Hz and the frequency reached at the end of the signal is 3.39 Hz, very close to the initial one. Also, for the damping ratios (Figure 6-9d) a trend of increasing values at maximum accelerations and then decreasing values at the end of the earthquake, towards values close to the initial ones, is clearly visible; for the presented earthquake and the first vibration mode the initial damping ratio is 1.91%, the highest is 5.34% and the value at the end of the signal is 2.24%.

Figure 6-10 shows the first three mode shapes identified by each windowed signal, together with those identified by the OMA performed on the acceleration measurements recorded before and after the considered seismic event (i.e., the response of the building to the environmental vibrations before and after the seismic shaking). Similarly, to the frequencies and damping ratios, the mode shapes assessed before and after the seismic event are almost the same, as can be deduced by comparing the first and last rows of mode shapes (in dark grey) in Figure 6-10. In contrast, the mode shapes identified from the signals in each window through the input-output technique are drawn in light grey because the MCF values, which evolve during the shaking, indicate a non-negligible complexity of the identified modes. In any case, the absolute values of the modal displacements of the monitored points are highlighted with red lines to give an idea of the identified modal shape. The very low values of the MCF identified by the OMA procedure confirm that the modes are almost real before and after the earthquake, while the higher values obtained during the motion may be a consequence of the floor yielding in plane. Furthermore, it is interesting to note that the translational modes tend to decouple from torsional behavior, and, at the highest accelerations, the first two modes are translational while the third one is torsional. The latter phenomenon is probably due to the reduction of the contribution of non-structural elements (e.g., the infill wall) in the dynamic response of the building.

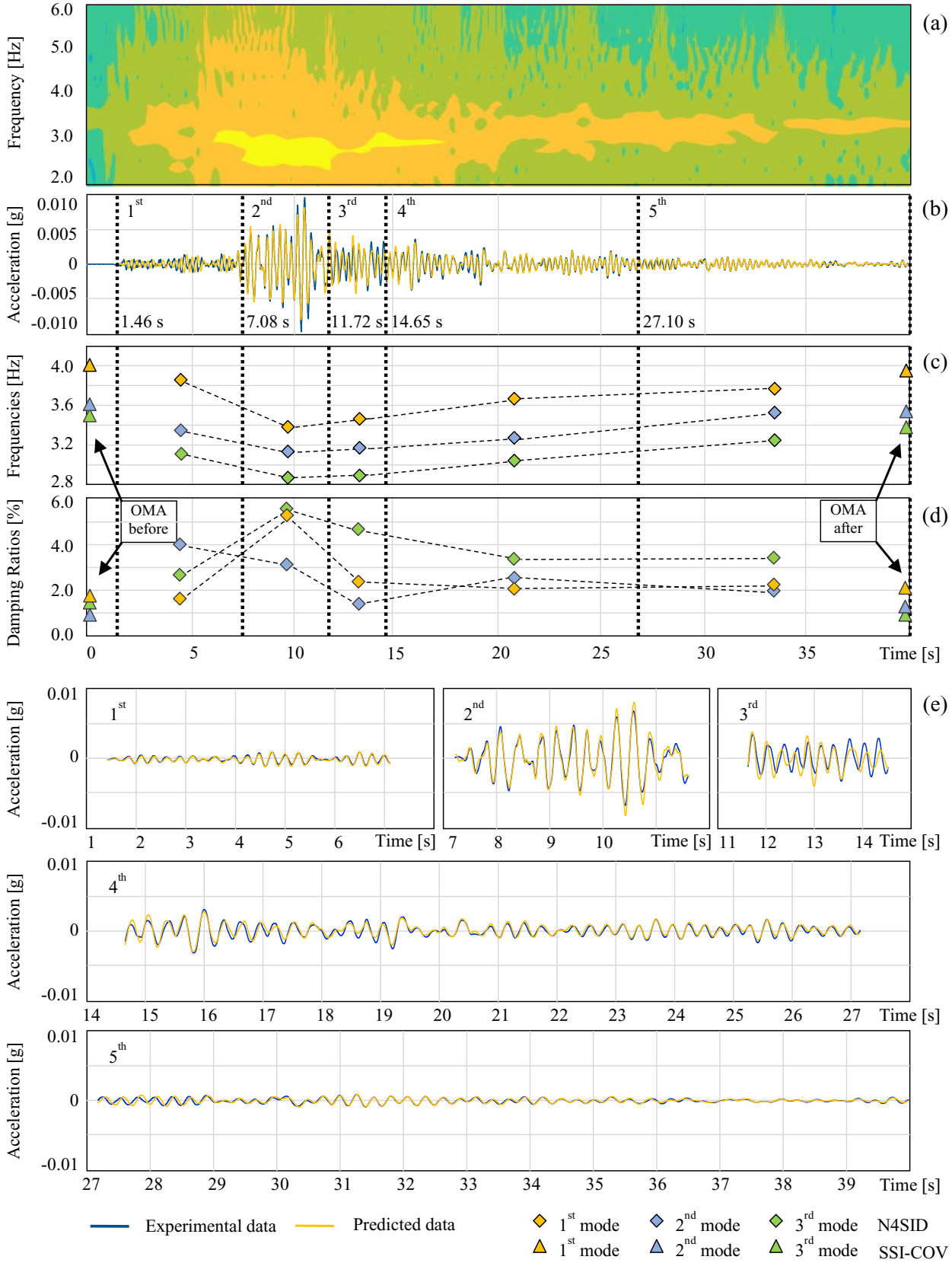

Figure 6-9: Results of the proposed methodology for 2Ay signal during the 4.4 ML earthquake: (a) STFT; (b) Measured and predicted time histories and window lengths; (c) Identified resonance frequencies; (d) Identified damping ratios; (e) Comparison between measured and predicted time histories for each window.

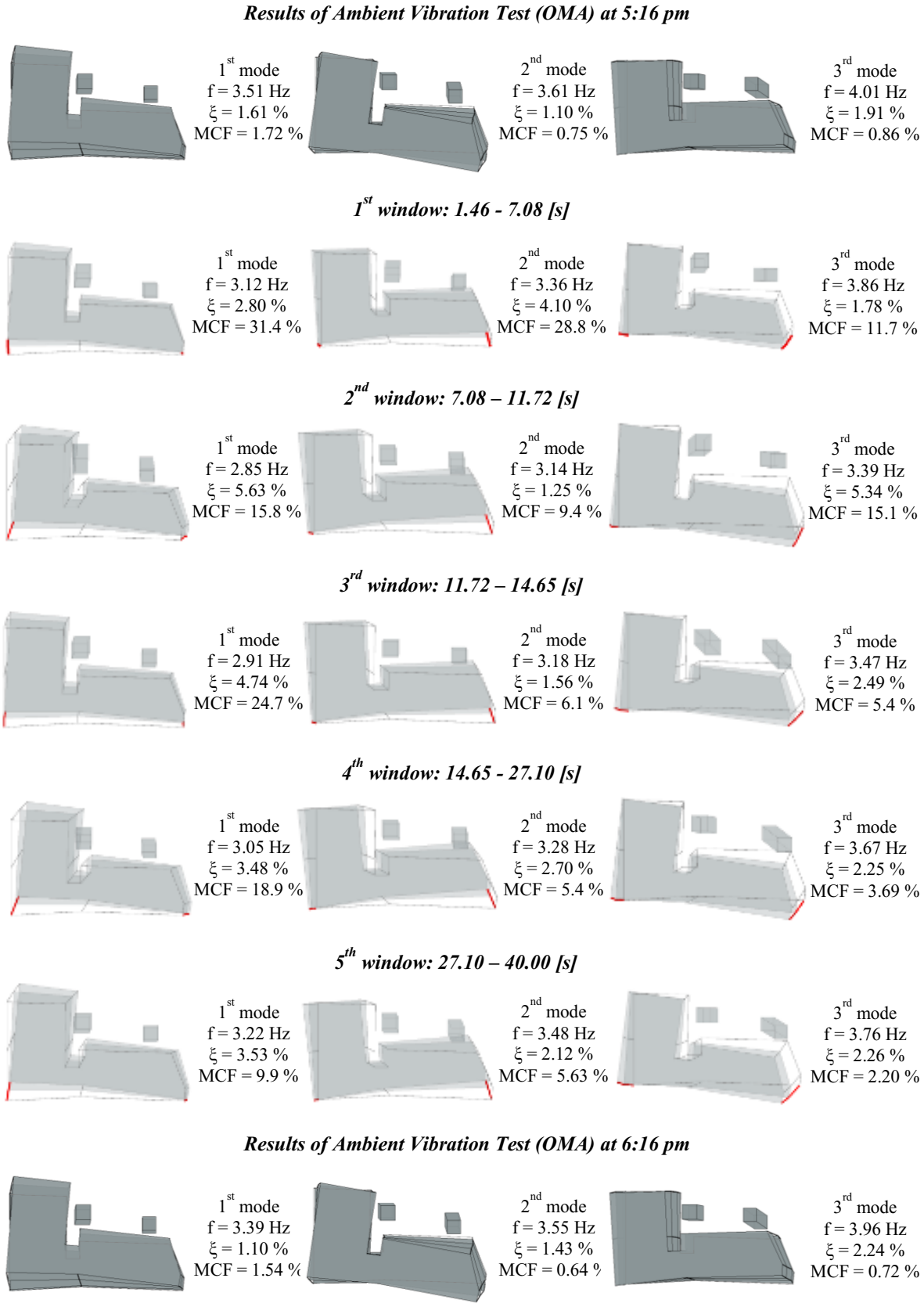

Figure 6-10: Identified mode shapes from AVTs and from the proposed methodology during the 4.4 ML earthquake.

6.3.2. Overall results

The three-day monitoring results in terms of the evolution of the building resonance frequencies are summarized in Figure 6-11. In particular, Figure 6-11a shows the results obtained from the environmental excitation data (i.e., the registrations between two successive seismic events); the resonance frequency values for the first three vibration modes of the building are identified almost every twenty minutes; the signal windows adopted for the OMA are characterized by a root mean square of the accelerations in the range 0.8-10-5 ÷ 4.4-10-5 m/s2. The value of the first frequency for each mode is very close to the one identified by the benchmark test described in the paragraph 6.2.1, since both are obtained on the same day and almost simultaneously (after the benchmark test the permanent monitoring system was immediately installed and made operational). Globally, the existence of a daily trend in the frequency data can be observed: the highest frequency values are found during the warmest hours of the day, around 13:00, while the lowest ones are found at night.

The atmospheric conditions during the monitoring days were recorded in terms of maximum and minimum temperature: the weather was sunny or partly cloudy all days, with maximum temperatures around 27°C in the middle of the day and minimum temperatures of around 16°C during the night. The observed trend is not clearly related to the seismic sequence, and the oscillations of the frequency values are due to temperature effects, with frequency values increasing as the temperature rises. We do not have a long enough monitoring period to define correlations between frequency and temperature, but the positive correlations observed are consistent with the scientific results reviewed in Chapter 2.

Eigenfrequencies identified through the proposed methodology during the twenty-five seismic events are superimposed on the data obtained from the AVTs in Figure 6-11b and plotted with circles whose diameter increases with the Peak Ground Acceleration (PGA) of the event. For each earthquake, only the frequency values obtained considering the signal window including the PGA are considered here. It can be clearly observed that the frequencies identified during the strong motion are significantly lower than the reference values and the values obtained from the OMA performed on the ambient acceleration measurements before and after the shaking. Obviously, the lowest frequency values (dashed line) are reached during the strongest earthquake (in the afternoon of 28 August). Moreover, the frequency values identified at the end of the monitoring and based on the environmental vibration data are almost the same as those obtained at the beginning of the monitoring. Therefore, it can be stated that the dynamics of the building at very low intensity actions, such as those produced by the environmental excitation, did not change after the seismic swarm observed during the monitoring days and the reduction of the frequency values during the strong movements can be attributed to non-linear phenomena of secondary importance (e.g. friction phenomena due to non-structural members, opening and re-closing of small cracks in the infill) rather than to structural or non-structural damage. In fact, when the permanent monitoring system was removed due to logistical problems related to the start of the school, the building did not show any obvious damage that could be attributed to the recorded seismic events.

To further investigate the relationships between the identified modal parameters and the characteristics of the occurred seismic events, some correlations are determined and discussed below.

In Figure 6-12a, the correlations between the modal parameters (the first three resonance frequencies and their damping ratios) identified during individual events and the PGA of the corresponding event are plotted in semi-logarithmic graphs. The data are interpolated with logarithmic functions and the corresponding coefficients of determination (R^2) are plotted. The resonant frequencies decrease as the PGA increases while the damping ratios increase as the PGA increases. Similarly, Figure 6-12b shows the correlations between the modal parameters and the maximum displacement (d_{max}), obtained from the accelerometer at the top floor, during the strong motion of the seismic events. Finally, Figure 6-12c refers to the correlations between the modal parameters and the maximum acceleration (a_{max}) measured at the top floor. It can be concluded that all selected intensity measurements are well correlated with the modal parameters, presenting very comparable correlation coefficients.

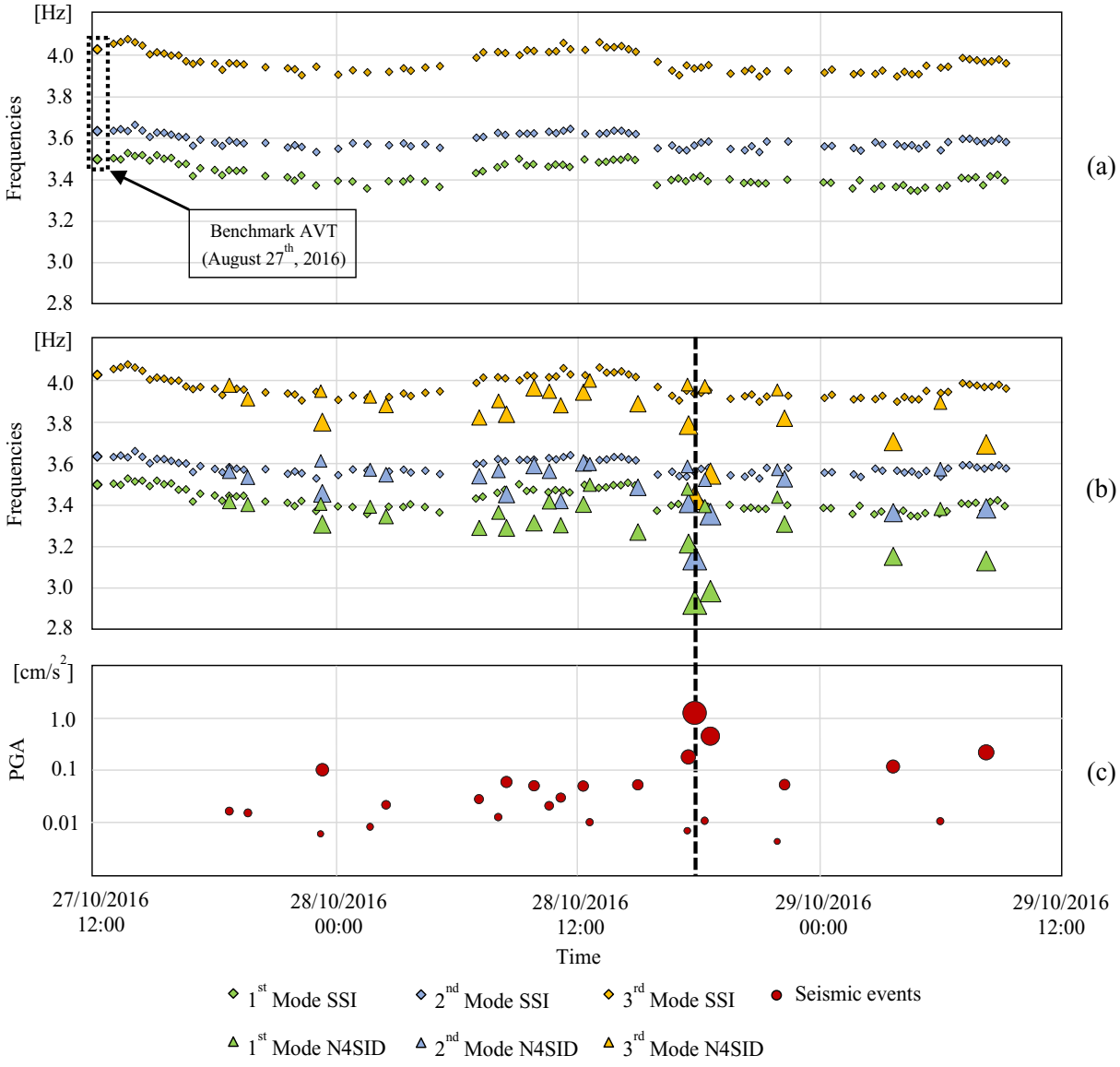

Figure 6-11: Results during the three days of monitoring: (a) Output-only identification (SSI-COV); (b) Input-output identification (N4SID) superimposed with the output-only identification; (c) PGA of seismic events.

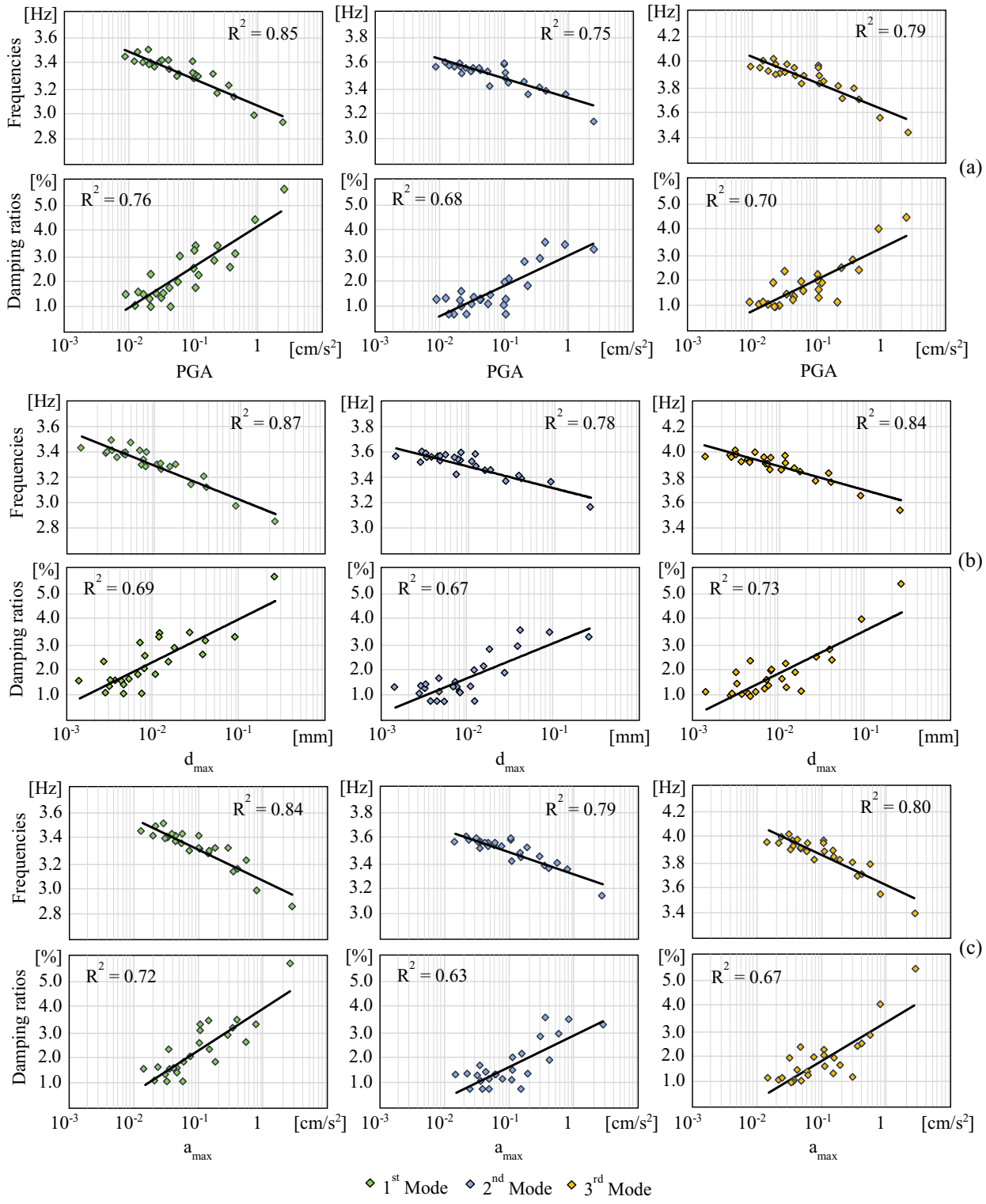

Figure 6-12: Correlations between the intensity measure of seismic events and the building modal properties: (a) Frequencies and damping ratios˚vs˚PGA; (b) Frequencies and damping ratios˚vs˚d_{max}; (c) Frequencies and damping ratios˚vs˚a_{max}.

The relationship between frequency values and relative damping ratios is fairly well interpreted through a linear trend as shown in Figure 6-13. Overall, the increase in damping ratios is consistent with the decrease in frequencies and with the interpretation given above, which attributes the reduction in resonant frequency to the development of minor non-linear phenomena, such as slight cracking and friction due to interactions between structural and non-structural members. In fact, the values of the damping ratios, which reach a maximum around 5% at the strongest events, suggest that the dissipative phenomena cannot be attributed to the dissipative system installed for the seismic retrofit of the building. This assumption is supported by the order of magnitude of the most important velocities and displacements recorded at the base of the towers, which are not considered high enough to activate the dissipative devices (as previously shown in Figure 6-7).

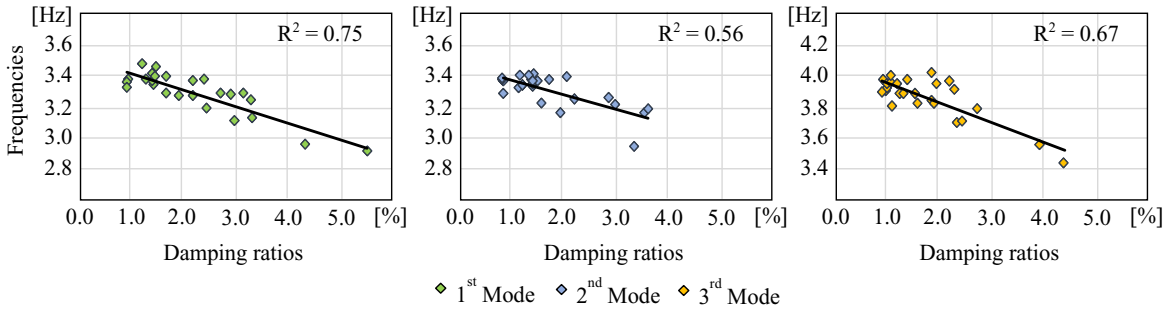

Figure 6-13: Correlations between resonance frequencies and the relative damping ratios of the building.

6.4. Discussion of the results

As already discussed in Chapter 4, with reference to a specific structural typology, the availability of simple and direct relationships between the variation of modal parameters (with respect to the intact condition), and the presumed damage levels, are of extreme importance for the practical usefulness of the data collected by monitoring systems [89]. The hypothesis of time invariant dynamic system cannot always be assumed for the building identification during the monitoring period and therefore, in case of seismic events even of low intensity, it is difficult to keep measuring the dynamic behavior through modal parameters. In this chapter, the procedure presented in Chapter 4 has been applied to the monitoring of a real case study. In particular, the procedure allows to follow the evolution of the dynamic structural properties over time, and precisely, with the increase of the accelerations. The results of this work were published in Gara et al.[116].

7. The Tower of the Faculty of Engineering in Ancona; the effects of environmental conditions

7.1. Presentation of the case study

The building object of the present chapter is located in Ancona city (Central Italy), in the campus of the Faculty of Engineering of the Università Politecnica delle Marche (Figure 7-1a). The Tower of the Faculty of Engineering is a ten-storeys building, which has the peculiarity to own floors marked with the respective heights above sea level. The building was designed and constructed between 1980 and 1983 in accordance with the standards of the time for a seismic zone. The structure, having a square floor plan, is composed by r.c. frames with 3 columns spaced 9m to each other in both the main building directions. The columns are tapered in height and therefore, depending on the floor, the maximum dimensions are between 19.2 and 18.9 meters. The interstoreys are constant throughout the height and equal to 5m. The building is flanked by a r.c. wall structure, separated by a structural joint, hosting the stairway and elevators (Figure 7-1b).

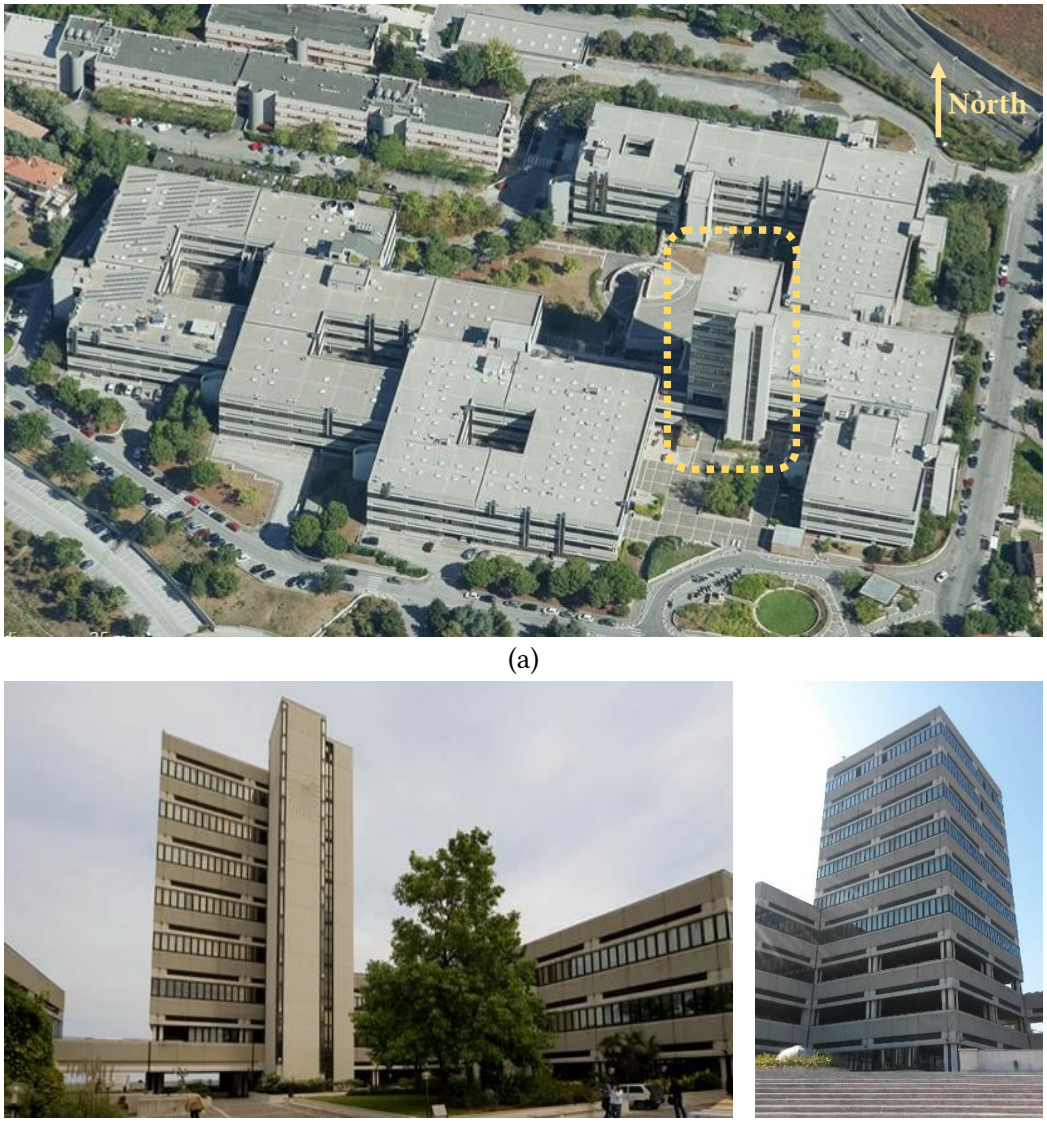

(a)

(b) (c)

Figure 7-1: View of the tower: a) aerial view from Bing Maps; b) South c) and North-West views.

With the aim of identifying the characteristics of the building, design drawings and the characteristics of the adopted construction materials were retrieved from the archives of the Department of Civil Engineering, Construction and Architecture of the Università Politecnica delle Marche.

7.1.1. The structural organization

The building is composed of a single square plan body flanked by the staircase-elevator structure, the latter separated by the main tower body by means of structural joints whose technical characteristics are not known; from the technical drawings it was only possible to recognize that the width of this joint is 5 cm.

The foundations, shown in Figure 7-2a, consists of plinths on piles, connected with tie-beams of 1m height and 0.4 m width; the columns indicated with 70, 57 and 71a in Figure 7-2a, are built on square plinths of 0. 5m on 4 piles of 1.20m diameter; columns 56b, 58a, 69b, 83 and 84a are built on 0.45 m square plinths on 4 piles of 1m diameter; column 82b is built on a triangular plinth founded on 3 piles of 1m diameter.

The columns have a square section with an indentation of 5x20 cm at the center of each side and taper in height every 2 floors, with the exception of the last three floors which have the columns divided into 4 separated columns with a 35x35 cm section and connected to each other by a 20x30 cm section rake in the middle height which extends 20 cm. The dimensions of the columns at the various floors are shown in Figure 7-3a:

The beam sections, shown in Figure 7-3c, are all 90cm wide and 65cm high and are made with a 10cm thick cupel; the bottom reinforcements are placed both in the cupel and on the other side of the beam. Both beams and columns are prefabricated, while the nodes are cast in situ.

During construction, 240 concrete samples were taken and tested at the Materials and Structures Testing Laboratory of the University. Results of experimental tests revealed that the mean cubic strength of concrete is Rck,p = 28.14 MPa for foundation piles, Rck,f = 43.91 MPa for the floors (i.e., for beams) and Rck,c = 41.62 MPa for the columns. As for reinforcements, rebars FeB44k were used.

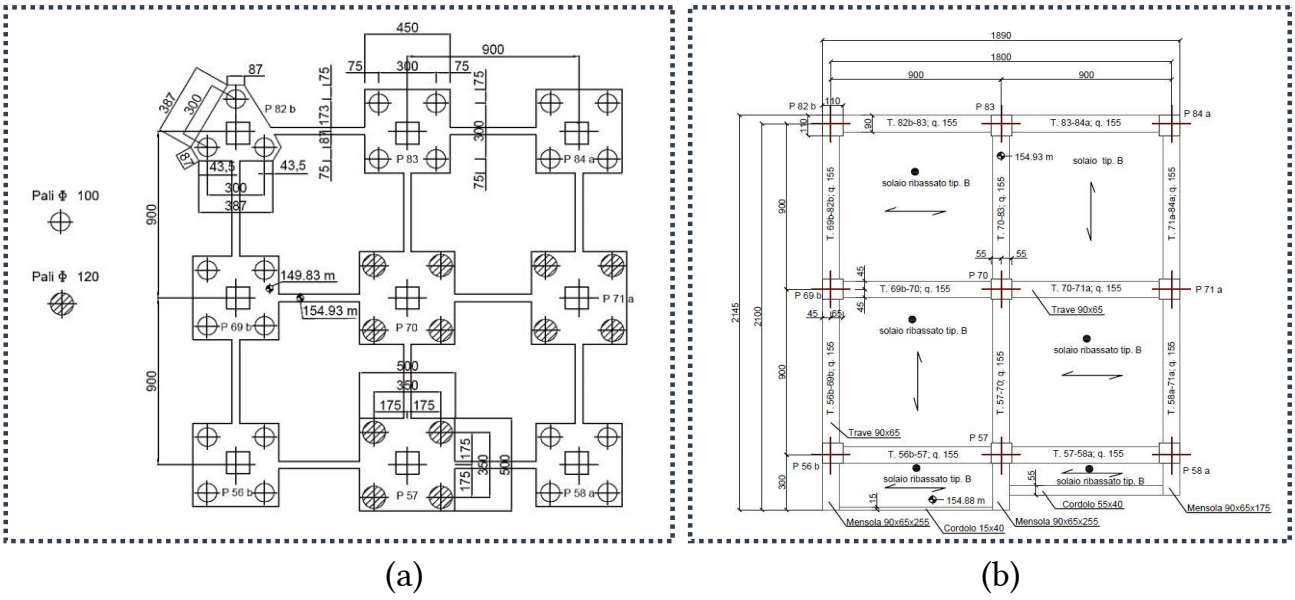

Figure 7-2: (a) Foundation layout and (b) typical plan floor.

Floor	Section
P9 - q195	4-35x35
P8 - q190	4-35x35
P7 - q185	4-35x35
P6 - q180	90x90
P5 - q175	90x90
P4 - q170	100x100
P3 - q165	100x100
P2 - q160	110x110
P1 - q155	110x110
P-1 - q150	120x120

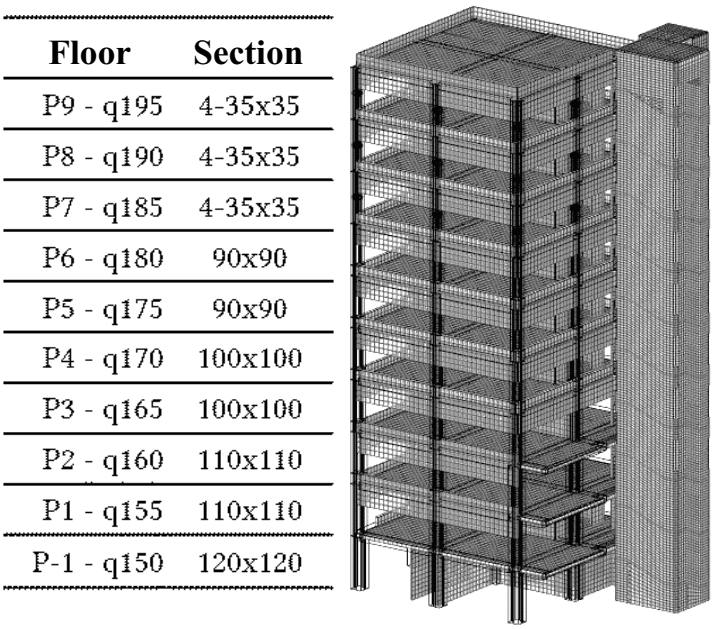

(a)

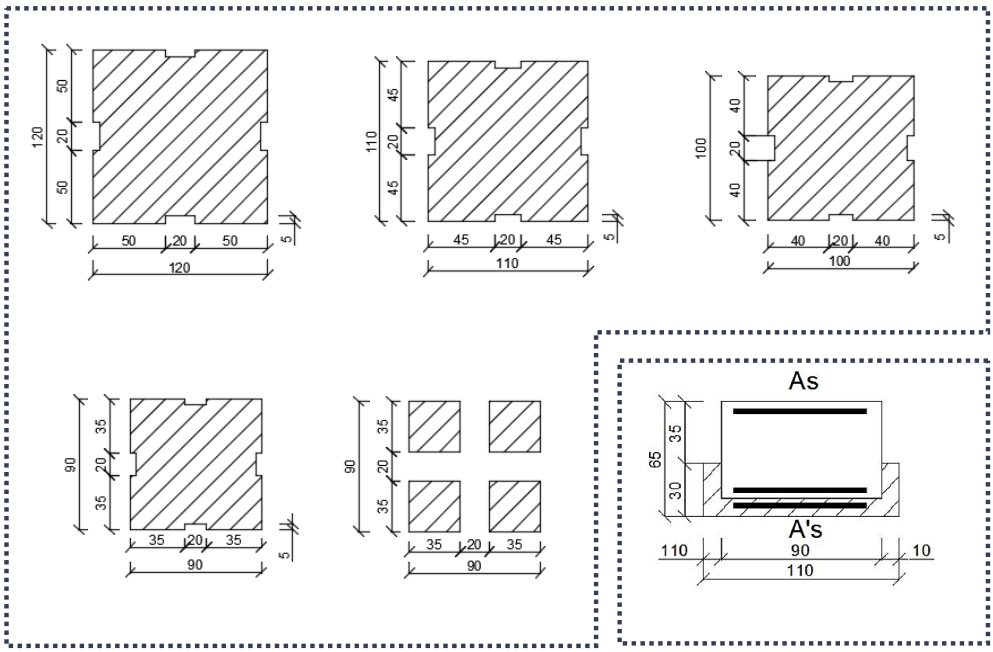

(b) (c)

Figure 7-3: (a) Schematization of column sections per floor; (b) column cross sections; (c) beam cross section.

Internal partitions are all made of light panels, while perimeter walls are realized with prefabricated r.c. panels connected to the beams and disconnected from columns. Between panels of adjacent floors, aluminum ribbon window frames are located, as can be seen from Figure 7-1b and Figure 7-1c. The prefabricated lightened concrete panels, made up of 3 m modules, are supported along their entire length on the perimeter beams to which they are bound by means of columns cast on site.

The panels are attached directly to the beam by means of steel forks placed in the casting of the beams itself. Figure 7-4c show some construction details.

The internal partitions are mostly prefabricated plastic partitions, except for the bathroom blocks, which are the same in height on all the floors except for floors at 160 and 165 levels. The bathroom blocks are made with 12 cm thick masonry infills with hollow clay bricks.

The floors are made up of a 40 cm high structural package, with a 4 cm thick prefabricated lower slab, 32 cm high joists and a 15-16 cm base with a 44.5 cm spacing, completed by a 4 cm cast in situ upper slab, while the lightening is made up of polystyrene elements.

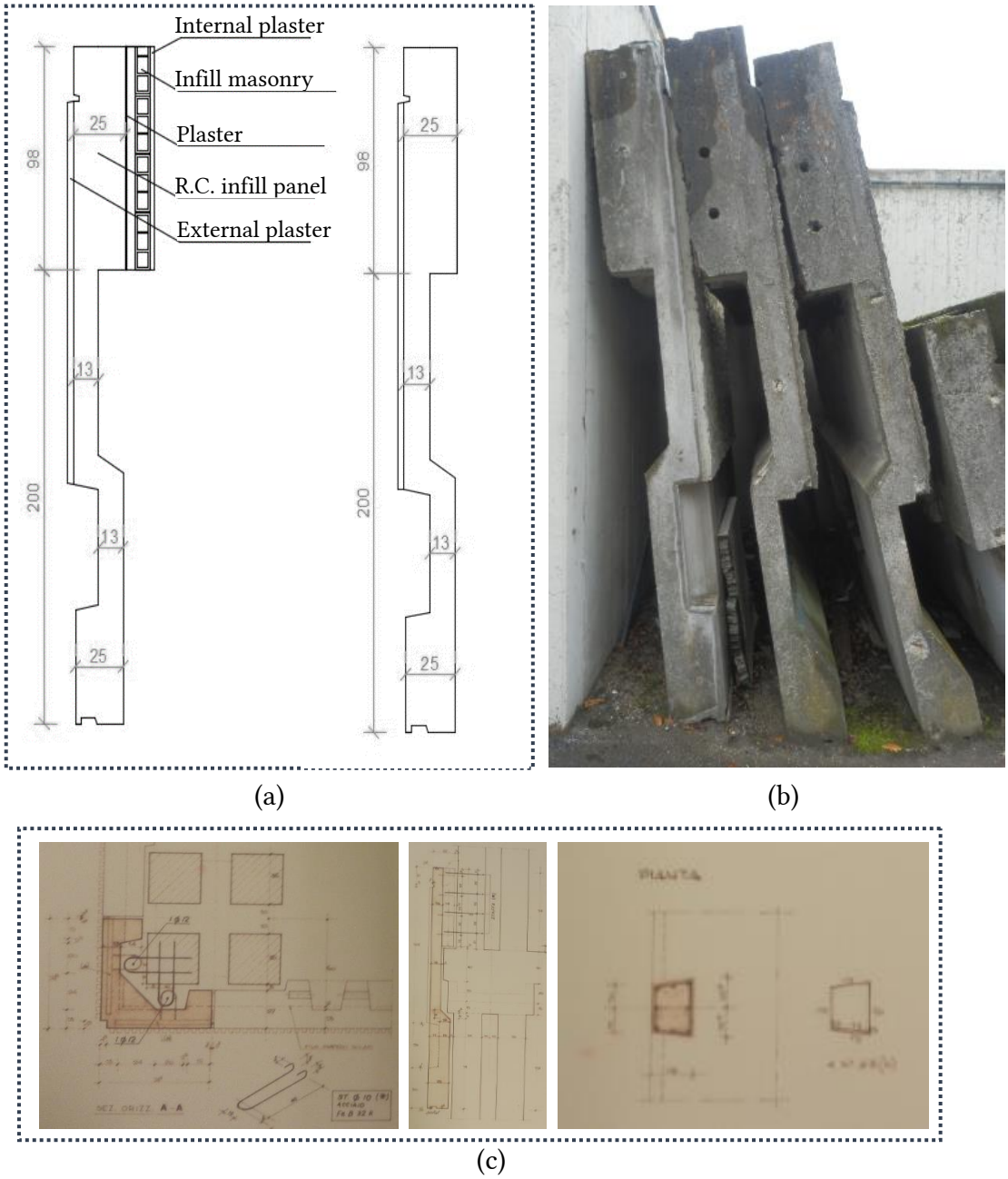

Figure 7-4: (a) External infill panel dimensions; (b) photo of prefabricated infill panels; (c) construction details of external infill panels from original design drawings.

Throughout the building three types of floors can be found: the inter-floor, which is called "normal" with a thickness of the non-structure of 12cm (Figure 7-5c); the "lowered" inter-floor with a thickness of 7cm (Figure 7-5a) in order to make the floor levels coincide in some areas of the building; the roof floor with a thickness of 12cm (Figure 7-5b).

The staircase-elevator body is 2.5 m higher than the tower to allow the access to the roof and is made of in-situ RC walls. The stairwell has 30 cm thick walls, while the walls of the elevator shaft are 20 cm thick, except for the last 2.5m which are 12 cm thick. The slab of the ramps is 15 cm thick and that of the landings 20 cm thick. The floor of the staircase is made of prefabricated slabs of the bausta 20+4 type.

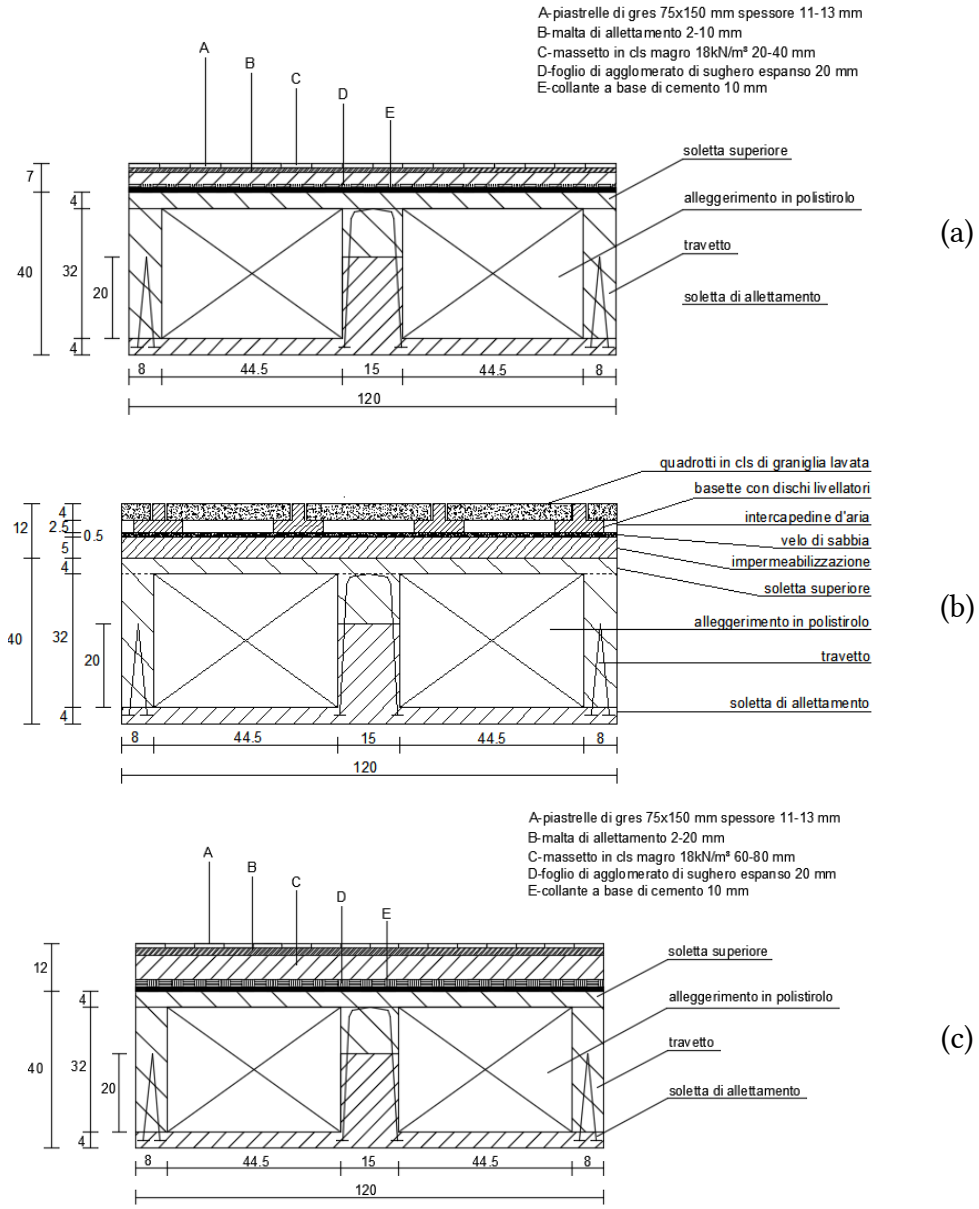

Figure 7-5: (a) Lowered intermediate floor; (b) roof floor (c); normal intermediate floor.

7.2. Monitoring system and acquired data

Over the years, several complete dynamic identifications of the tower have been carried out to calibrate a FEM and to control over time the evolution of the frequencies and mode shapes. These identifications allowed to deepen the interaction between the main body and the staircase-elevator body. In this work, results of tests carried out on September 2020 are reported. The tests carried out are vibrational tests with the aim of identifying the dynamic behaviour of the tower through the identification of the modal parameters that characterise it, i.e. the vibration eigenfrequencies, the damping ratios and the modal shapes.

7.2.1. Preliminary identification tests

The vibrations of the building were measured by Piezotronics Model 393B31 PCB accelerometers, connected to the acquisition boards with 50, 70 and 100m-long low-noise coaxial cables. Four NI-9230 acquisition boards were used. The controllers used are a CompactRIO 9045 and 2 TSN-enabled NI cDAQ-9185 chassis (4 slots) connected in series to the cRIO with Ethernet cables, Cat. 6 shielded S/FTP.

Finally, the cRIO used for the main and fixed measurement station was connected to a laptop with dedicated software. Synchronization between the main measurement station (cRIO) and the distributed measurement stations (cDAQ) is achieved using TSN (Time Sensitive Networking) technology, which provides distributed time synchronization and deterministic communication using standard Ethernet networks.

The test involved placing six accelerometers per floor, three in the stairwell and three in the tower, for each floor of the building from level 155 to the roof at elevation 200. Having defined measurement points A, B, C and D per each floor as shown in Figure 7-6, in the tower, two accelerometers were placed at measurement point A to capture accelerations in two orthogonal directions, x and y, while the third accelerometer was placed at the other end of the block in measurement point B, to better understand the building dynamics and also to capture torsional modes and any roto-translational couplings. Two accelerometers in the y-direction and one accelerometer in the x-direction, at measurement points C and D, were positioned in the stairwell in the same way.

In fact, assuming that the single floor is non-deformable, its movement in the plane is fully identified by determining two translational and one rotational component. To guarantee a correct measurement of the acceleration in the horizontal direction, sensors were mounted on metal brackets fixed to the floor with an adhesive. Since it was not possible to perform measurements simultaneously in each floor, five measurement configurations were performed, leaving the floor at elevation 195 (faculty club) as the reference level, as shown in Figure 7-6.

During the execution of tests, cables were arranged along the corridors, while the passage of the cables from one floor to another one was carried out inside the stairwell.

The signals were acquired with a dedicated software developed in LabVIEW. Scientific literature recommends making recordings of a duration of at least 1000-2000 times the first period of vibration of the structure in order to have a sufficient amount of data to represent the phenomena in a statistically adequate manner.

Therefore, considering that the first period is about 1 second (1.04-1.07 Hz), it was decided to make recordings of a duration of 30 minutes and the sampling frequency was chosen to be 2048 Hz.

As is usual in post-processing, first the signal was filtered with a low-pass filter to avoid aliasing, then the signals were resampled at 51.2 Hz to limit the amount of data, and the identification was carried out with the SSI-PC algorithm. Figure 7-7 shows results obtained in terms of PSD, a stabilization diagram superimposed on the first singular value of the CPSD matrix and a frequency-damping diagram to verify that the identified mode at that frequency actually has stable damping. This representation refers only to the results of test P1, a similar procedure was carried out for all other tests and then results were scaled using the PoSER (Post Separate Estimation Re-scaling) technique.

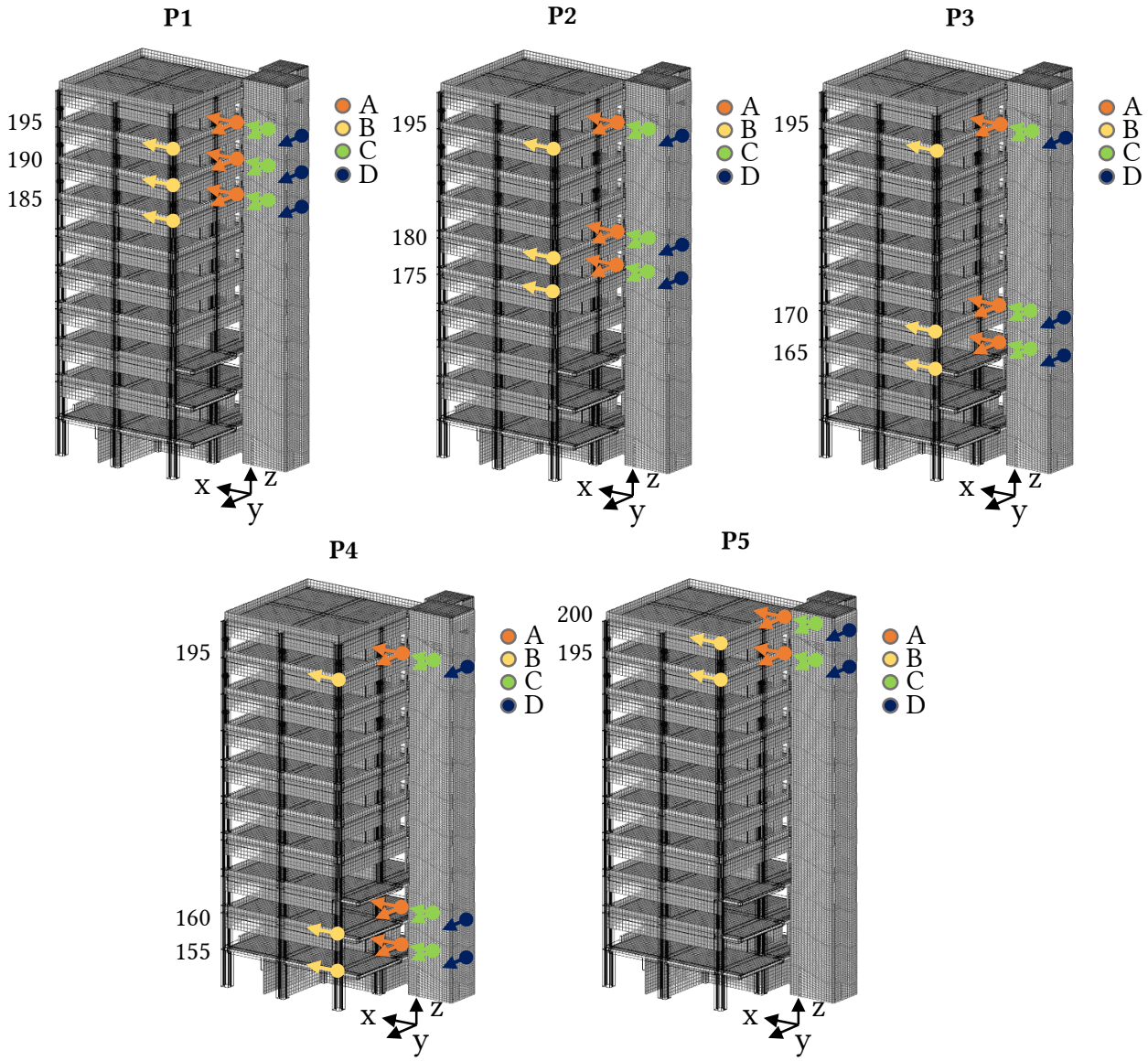

Figure 7-6: layout of the sensors for the 5 AVTs.

Figure 7-8 shows the identification results in terms of frequencies, damping ratios and modal shapes of the first three modes. The higher modes are not shown as they need to be further investigated. The interactions at the joints level with the adjacent buildings at lower floors make identification at higher frequencies particularly complex.

From the analysis of the results, it can be seen that the first three modes of vibration are evidenced by the first three peaks of the PSDs for all tests and are stable in terms of both frequency and damping. The first mode results to be translational with torsional coupling, the second mode is translational in y-x, and the third mode is purely torsional. The first mode is translational-torsional coupled because the r.c. frame of the tower is less rigid therefore, the first pivots on the second.

Figure 7-8 also shows the Modal Complexity Factor (MCF) values and it can be seen that these values are very low, indicating that the modes are real, and the modal components are almost perfectly phased.

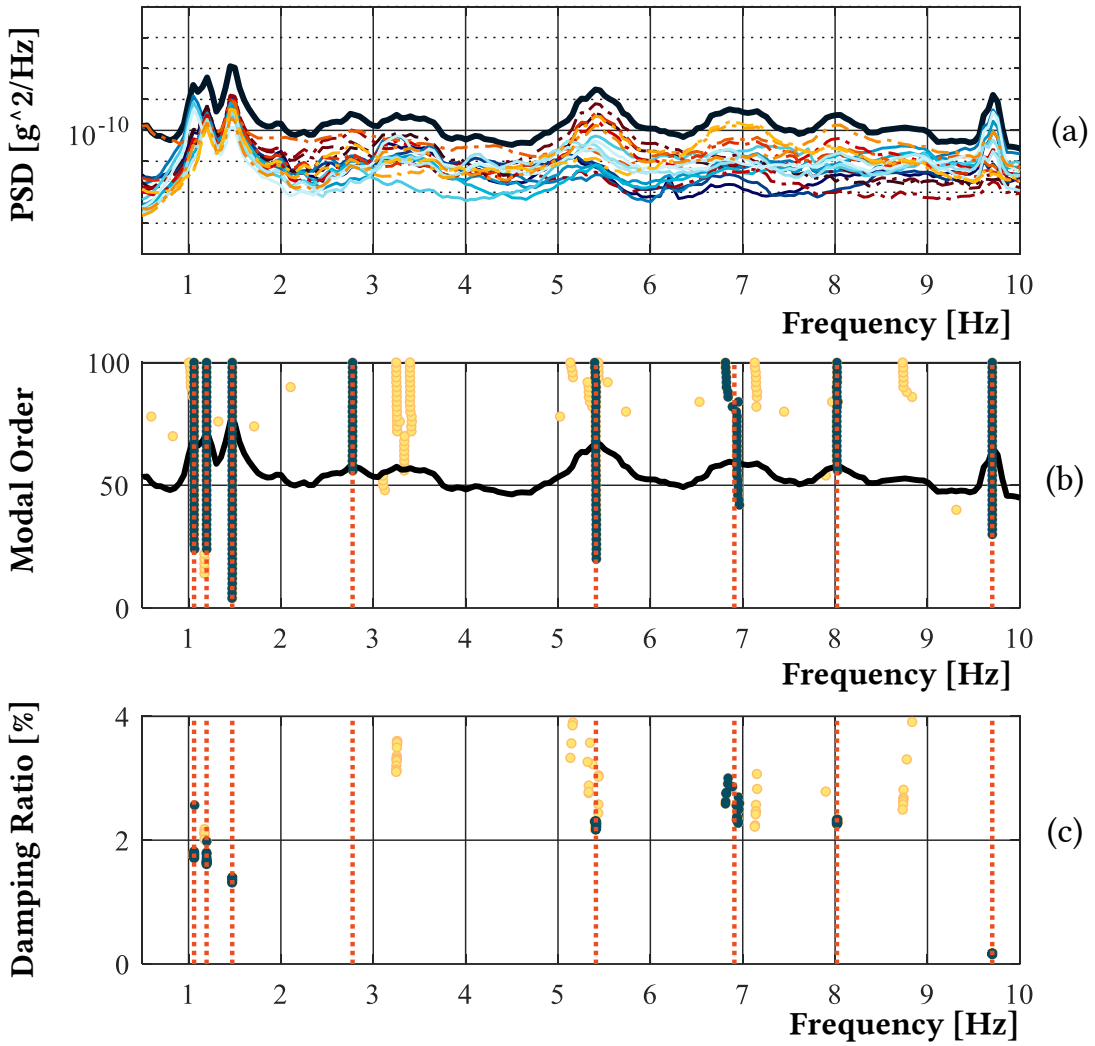

Figure 7-7: (a) PSD and first singular value of the CPSD matrix; (b) stabilization diagram; (c) frequency-damping diagram.

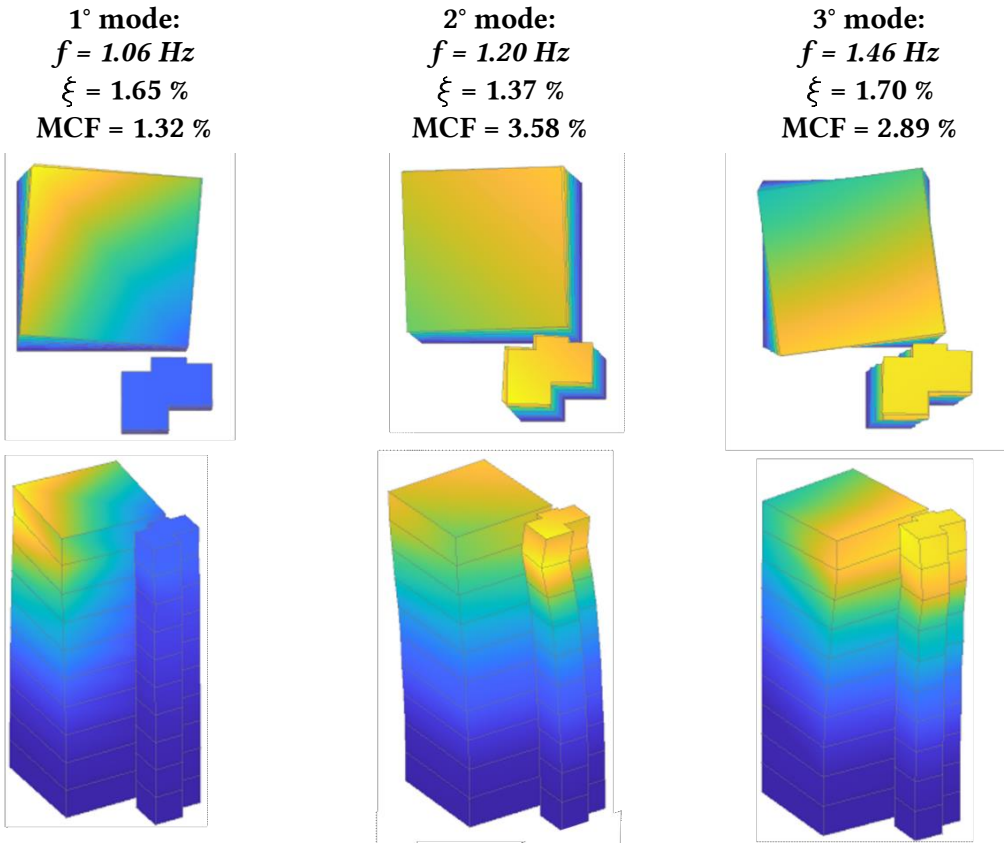

Figure 7-8: Dynamic identification results in terms of modal parameters of the first three modes of vibration

7.2.2. Description of the monitoring system

In 2017 a continuous monitoring system was mounted on the tower to monitor the evolution of its modal parameters and to measure its structural response to possible earthquakes. Measurement points A and B, already shown in Figure 7-6, are positioned as far as possible to each other, and on the same vertical alignment for all elevations. This allows the dynamics of the building to be better represented and the torsional modes to be monitored correctly. The system is fully wired and consists of model 393B31 PCB accelerometers, a c-DAQ 9178 data acquisition unit and a computer. With the help of recordings made by two meteorological stations close to the Engineering Faculty (namely, weather station Q2 and Brecce Bianche, BB), temperature and wind speed are recorded during each acquisition.

In June 2018, the monitoring system was integrated with a Davis Vantage pro2 wireless weather station used to collect recordings on environmental features exactly on the tower, mainly indoor and outdoor temperature, and wind, in order to more accurately control the variation of modal parameters of the structure with environmental changes.

The computer had been equipped with an acquisition software, developed in the LabVIEW environment, which manages and saves the recordings every ten minutes. The analogue signal has been sampled at fs = 2048 Hz and resampled at fs = 51.2 Hz before saving. To avoid signal aliasing, all frequency components in the analogue signal that are above the Nyquist frequency are removed through a low-pass filter. In addition, the automatic modal parameter identification algorithm already presented in Chapter 3 has been implemented.

Since April 2021, the monitoring system has been extended with the use of three additional accelerometers PCB-393B31 placed on the top floor of the stairwell in order to monitor the mutual influence of the two buildings due to the structural joint between them. The three accelerometers were placed at the same locations that were used for the identification shown in Figure 7-6. In addition, two T-type thermocouples (i.e., a temperature sensor) were installed to monitor the temperature of the fixtures (one facing east and one facing south) and one K-type thermocouple in the acquisition module, the latter to check for any temperature effect in the acquisition hardware operation. Finally, the monitoring system was also equipped with a Gemini-2 triaxial velocimeter positioned at foundation level. This is a high-performance 3D geophone with a resonant frequency of 2 Hz and a sensitivity of 2 V/cm·s-1, which has the task of measuring the seismic input. Figure 7-9 shows a schematic diagram of the actual monitoring system.

The Compaq-RIO saves twenty-minute signal recordings with a sampling rate of 1024 Hz and sends them via FTP to a computer within the department used as a server, and the weather station was connected to the University network with the help of an Ethernet data-logger, so that it can be read, configured and saved on the same computer where the recordings are stored.

The implemented architecture has been presented in chapter 3. The automatic identification is performed through the SSI-PC algorithm by calculating the solution with a model order that increases each time by 2 up to 100. Stable solutions have been found with the criteria of clustering which has been already described. The stabilization diagram is further cleaned of spurious modes by adding the stability condition on the damping in terms of variance. In this way, only solutions with stable damping (variance less than 5%) are retained, i.e., solutions that have physical significance in terms of damping.

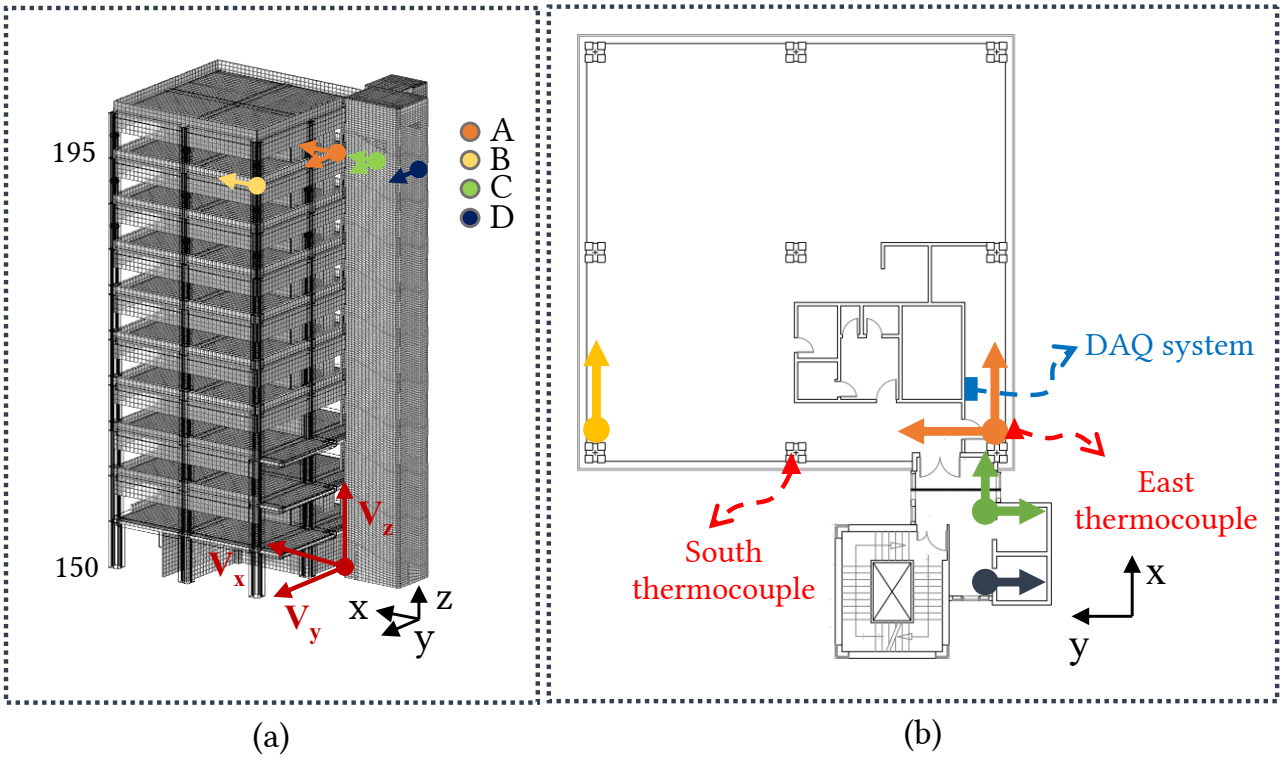

Figure 7-9: Actual layout of the monitoring system.

Figure 7-10 shows the overall results obtained from 2017 to date. Data for the months of 2020 are missing because the monitoring continuity could not be guaranteed in those months due to the lock down due to Covid-19 pandemic, and the not yet fully developed Chapter 3 framework.

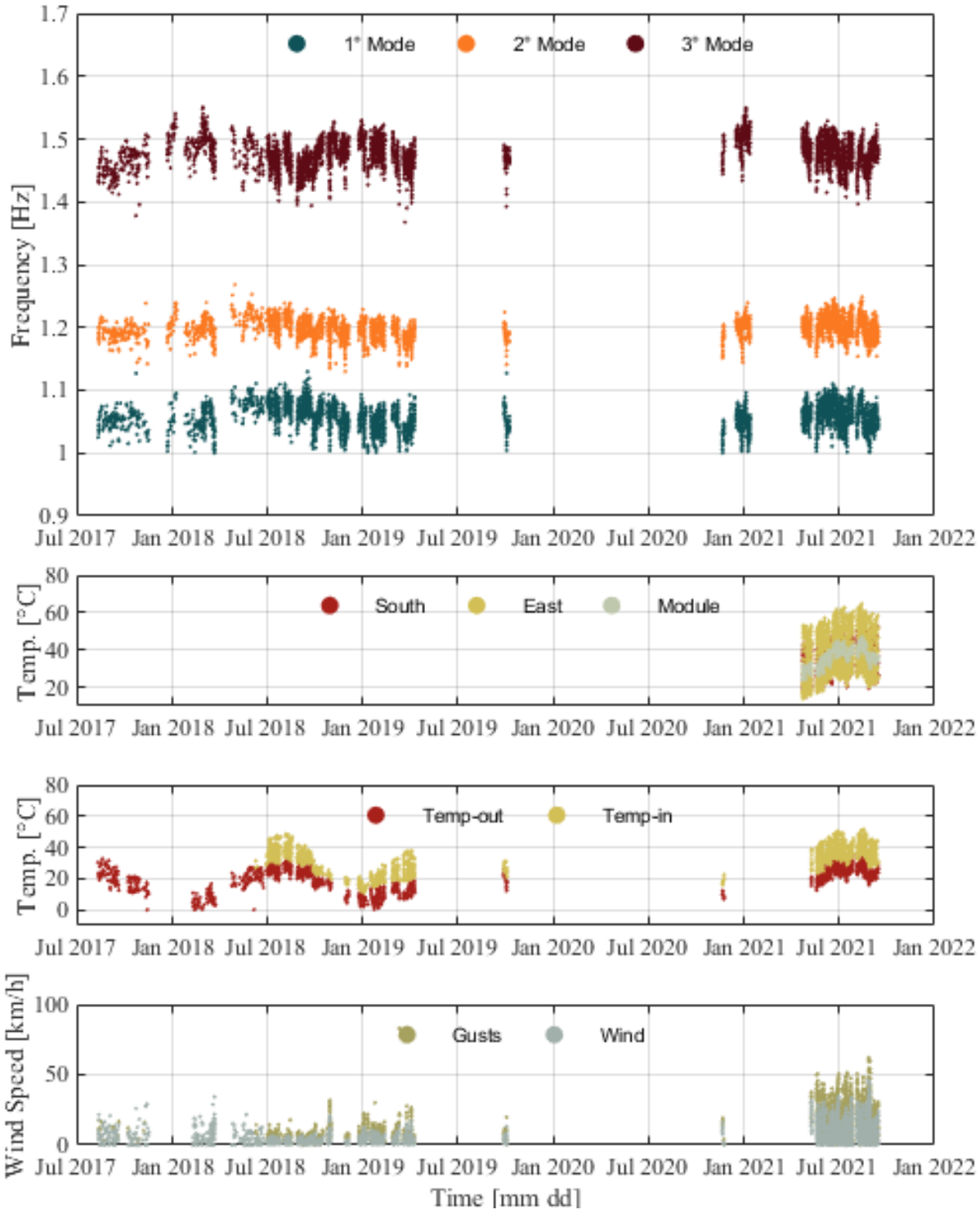

Figure 7-10: Global results from 2017 until now.

7.2.3. Monitoring results

In this section, the correlations of all data acquired during the monitoring with the simultaneous values of environmental parameters are shown.

To start with, Figure 7-11a shows the frequency values for the first three vibration modes vs the corresponding external temperature values while, in Figure 7-11b, vs the internal temperature. It can be seen that, as the external temperature increases, the frequencies of the first and second modes clearly increase, while in the third mode this trend is not perfectly linear since for lower temperatures it seems to have a downward trend, while for higher temperatures it increases. The situation is almost similar with respect to indoor temperature.

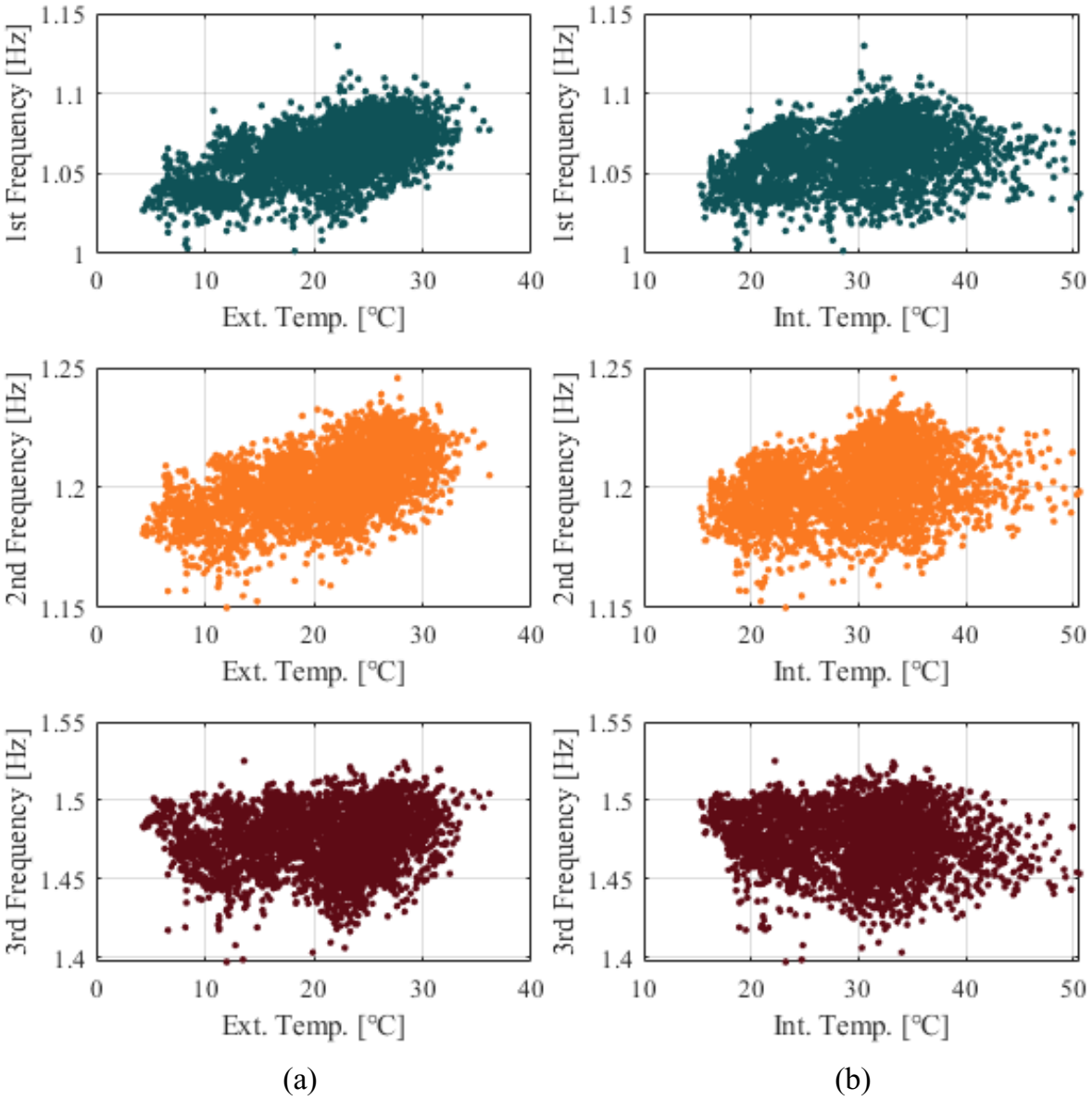

Figure 7-11: Correlations between frequencies and (a) external temperature, (b) internal temperature.

Figure 7-12a shows the correlations with the relative damping ratios; overall, a decrease in the damping ratio is observed for an increase in eigen-frequency, consistent with an increase in "apparent" stiffness and a reduction in dissipative contributions (e.g., material damping effects, friction between structural and non-structural elements, small non-linear effects). The relationship between frequencies and damping ratios shown can be better interpreted by observing the variation of the modal parameters with respect to the Root Mean Square (RMS) of the recorded acceleration signals (Figure 7-12b), suitably filtered with a band-pass filter (in the range 0.5 - 3.0 Hz) in order to eliminate the contributions not related to the investigated modes.

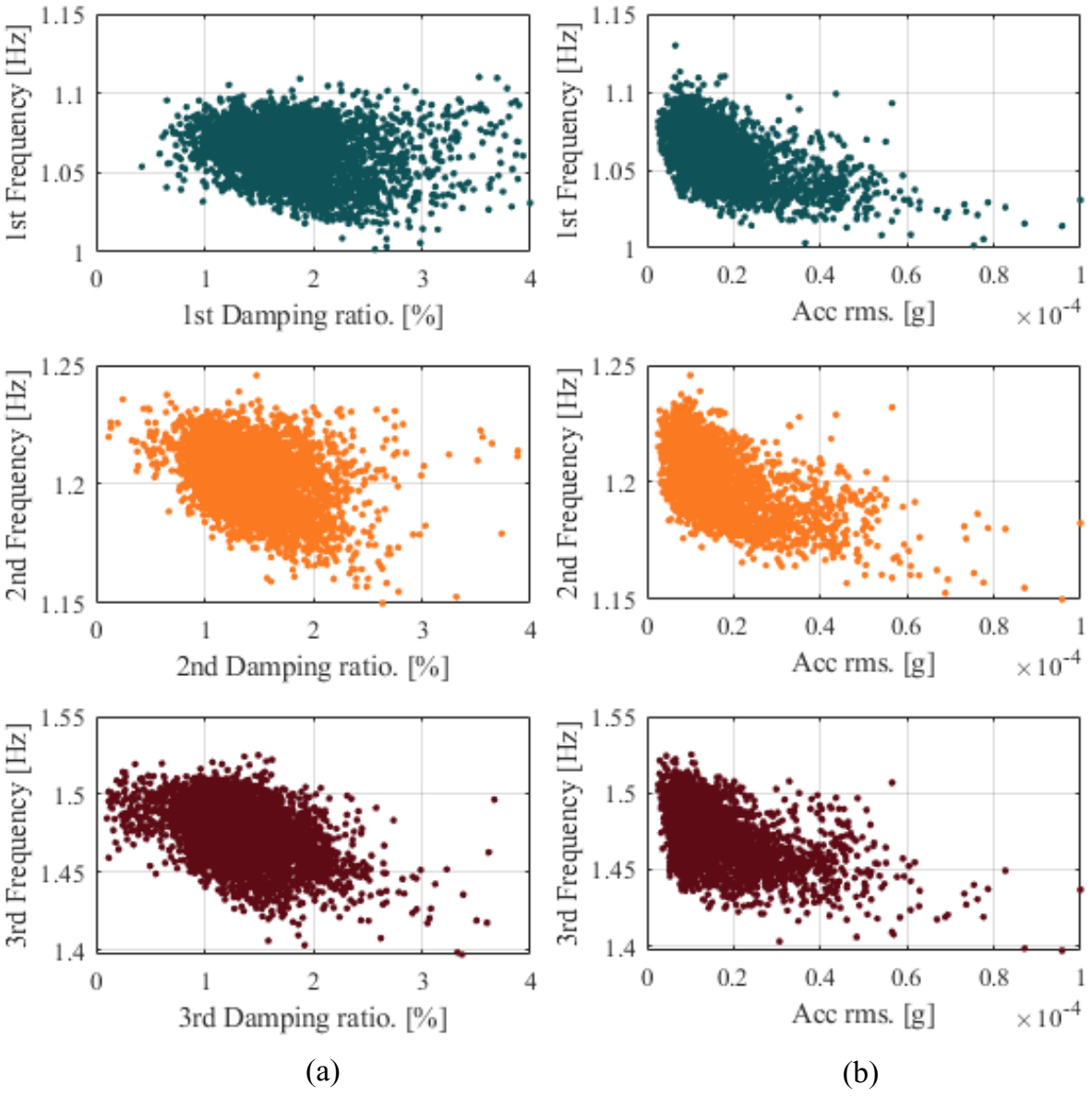

Figure 7-12: Correlation between frequencies and: (a) corresponding damping ratios; (b) root mean square of the time history from which modal parameters have been identified.

7.3. Data cleansing by unsupervised learning

As already addressed in chapters 2 and 3, one of the main obstacles to the implementation of a SHM system for in-service structures is the environmental and operational variation of the structure properties. Indeed, these changes can often hide more subtle structural changes caused by damage. Often the so-called damage-sensitive features used in damage detection techniques are also sensitive to changes in the environmental and operational conditions of the facilities. It is intuitive that temperature can change the material stiffness properties of a structure, and the temporal variation of temperature must also be noted, as many structures have daily and seasonal temperature variations. Furthermore, it is also intuitive that the energy input from the wind-induced vibration, besides to increasing the oscillations of the structure, causes frictions between the non-structural components and the structure, affecting the dynamic response of the structure due to non-linear effects. In order to create a statistical model capable of capturing possible changes in the dynamics of the structure due to damage or modification, it is necessary to cleanse the data, in particular frequencies, from possible correlations with environmental factors.

In this section, this problem is handled through an "unsupervised" approach. In the first part, data cleaning is addressed through Principal Component Analysis. In the last part, an artificial neural network will be implemented to deal with the monitoring data.

At this point, it is useful to introduce the Gaussian Mixture Model, which allows us to synthesise the information related to the three monitored frequencies by defining a statistical model composed of three averages, one for each variable, and a 3 x 3 covariance matrix, where the element (i,j) is the variance between variable i and variable j, capable of representing the variation of the first three frequencies.

If we consider the three frequencies separately, each of them can be represented by a Gaussian distribution, but if we want to condense them into a single distribution, the Gaussian distribution can no longer be used to correctly represent the variable. In order to fit the data with a single distribution, what we do is a linear combination of several Gaussian distributions (in this case three) and this combination generates the Gaussian Mixture Model. Then by using a sufficient number of Gaussians and adjusting their averages and covariances and using the right coefficients in the linear combination we can approximate any probability distribution. Consider a superposition of k Gaussians:

$$p(x) = \sum_{k=1}^{K} \pi_k \, N(x|\mu_k, \sum_k) \tag{7.1}$$

each Gaussian probability density $N(x|\mu_k, \sum_k)$ is called a component and has its mean μ_k and variance Σ_k. The parameter π_k is called the combination coefficient and is between 0 and 1, and the sum of all coefficients used must make 1. The first step is to identify the parameters of each Gaussian (mean and variance), but, in general, this is not straightforward because we do not know a priori which data make up one component of the distribution and which the other components, so the problem is governed by three parameters:

$$\pi = \{\pi_1, \ldots, \pi_K\} \tag{7.2a}$$

$$\mu = \{\mu_1, \ldots, \mu_K\} \tag{7.2b}$$

$$\sum = \{\Sigma_1, \ldots, \Sigma_K\} \tag{7.2c}$$

One way to find the values of these parameters is to maximize the logarithm of the likelihood function so as to have a distribution that best fits the data.

$$ln\, p\,(X|\pi,\mu,\Sigma) = \sum_{n=1}^{N} ln\, p\,(x_n) = \sum_{n=1}^{N} ln\left\{\sum_{k=1}^{K} \pi_k N(x_n|\mu_k,\Sigma_k)\right\} \qquad 7.3$$

where $X = \{x_1,\ldots,x_N\}$ and N is the total number of observations. Due to the presence of the sum over k within the logarithm, the equation does not have a closed-form analytical solution, so it is necessary to use iterative numerical techniques. To obtain the solution, we use what in statistics is called the EM-expectation maximization algorithm, which is an iterative method to find the maximum likelihood function in cases where the model depends on unobserved variables. The EM algorithm consists of two steps, in the first step the model parameters (mean, variance and combination coefficients) are chosen and the probability of each observation x_n to belong to component k is calculated, using these probabilities as weights in the second step the algorithm calculates the model parameters and evaluates the logarithm of the likelihood function, if the result converges with the estimate of the function calculated with the hypothesized parameters I have found the solution, otherwise the probability that observation x_n belongs to component k is recalculated from the new model parameters and we go on for iterations until we reach convergence.

7.3.1. Principal Component Analysis

In this section, results of principal component analysis (PCA) on the monitoring data with the aim remove the influence of environmental factors on the eigenfrequencies of vibration are reported. PCA linearly transforms the original set of autocorrelated variables into a smaller set of uncorrelated variables that can describe most of the information in the original data set.

The algorithm applied to the dataset of frequencies and environmental parameters is described in Chapter 4. Figure 7-13 shows the raw modal parameter data overlaid by the data cleansed through PCA.

As can also be seen from the Gaussian mixture model shown in Figure 7-14, after cleansing operation, the data show smaller oscillations around the mean and the associated covariance matrix components decrease. However, obtained residuals show an obvious bias and, while it is possible to partially clean the seasonal fluctuations, this type of analysis fails to clean the daily fluctuations.

Finally, the analysis of residuals between the original dataset and the statistical model shown in Figure 7-15 does not suggest a significant change in structural dynamics.

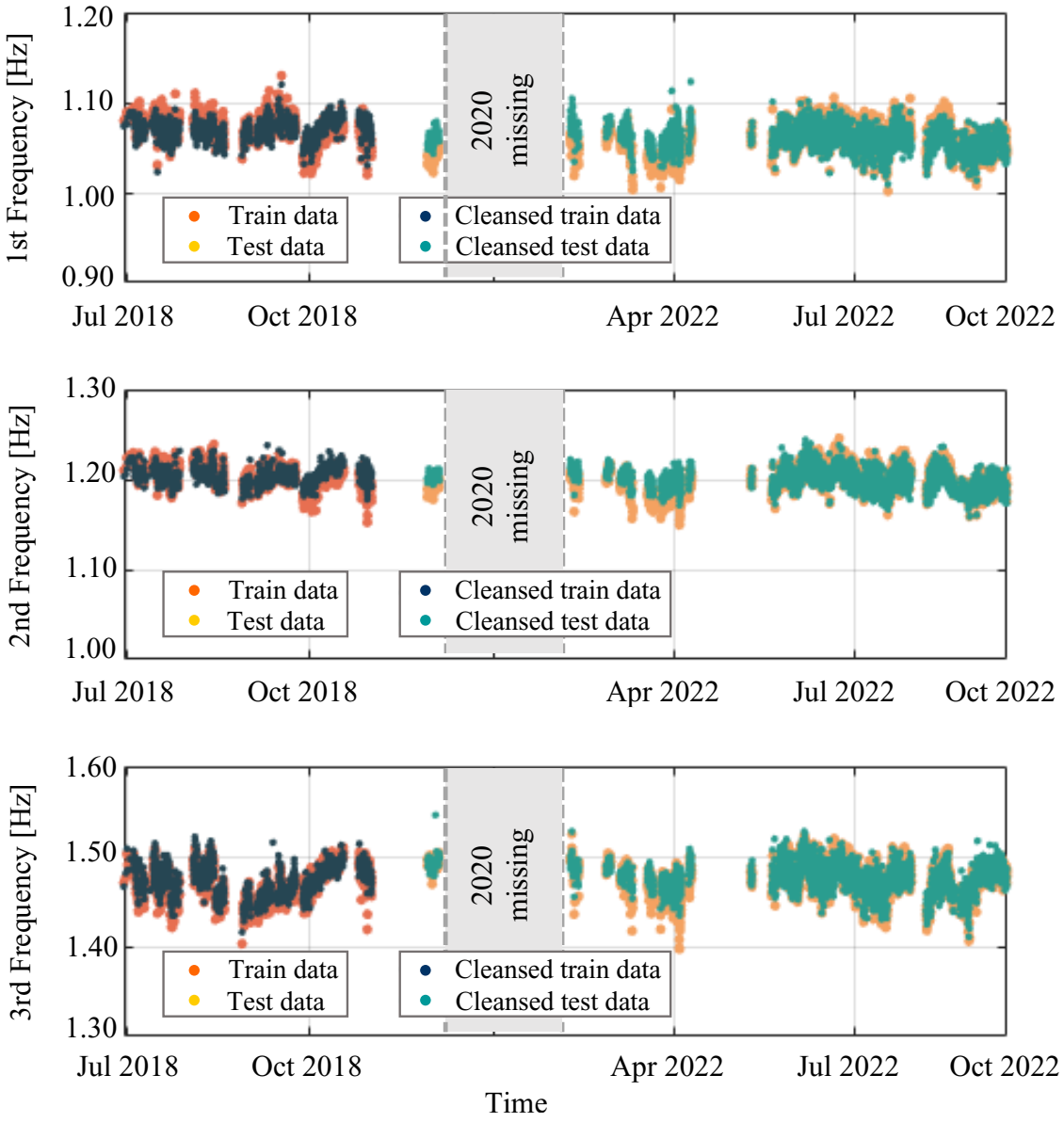

Figure 7-13: Original dataset superimposed on data predicted by statistical model via PCA.

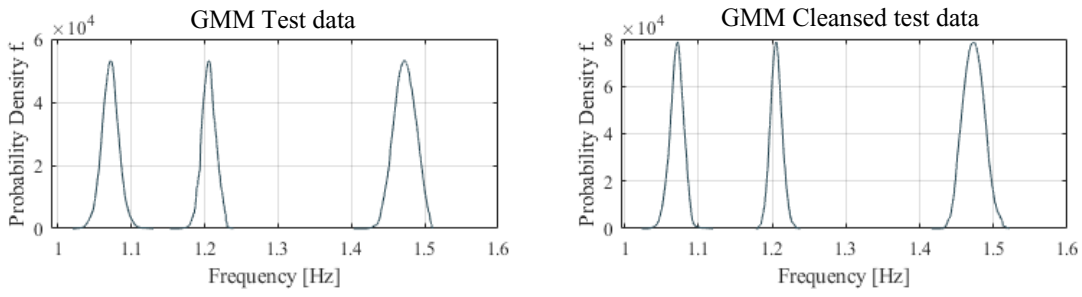

$$\Sigma = 1.00E{+}05 \begin{vmatrix} 19.62 & 14.51 & 9.05 \\ 14.51 & 13.77 & 11.42 \\ 9.05 & 11.42 & 35.34 \end{vmatrix} \qquad \Sigma = 1.00E{+}05 \begin{vmatrix} 11.39 & 7.09 & 9.49 \\ 7.09 & 8.12 & 10.78 \\ 9.49 & 10.78 & 29.59 \end{vmatrix}$$

Figure 7-14: Gaussian Mixture Model of the original dataset and the cleansed data via PCA.

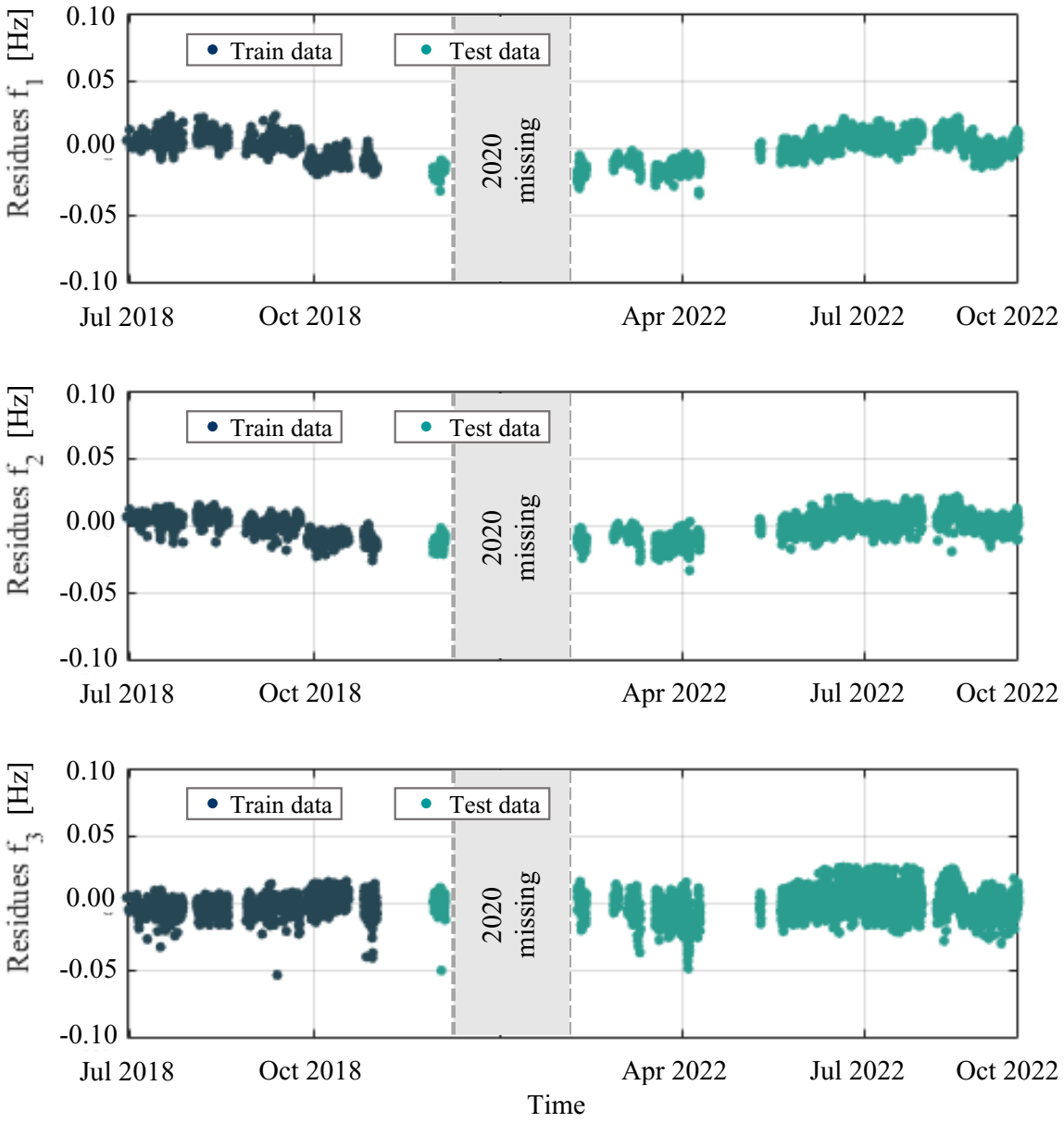

Figure 7-15: Residues between the original frequency dataset and the values predicted by the statistical model obtained from PCA.

7.3.2. Nonlinear autoregressive neural network with external input (NARX)

The exposed dependence of the building on environmental parameters proved to be very complicated from a phenomenological point of view, exhibiting a non-linear behavior. In order to effectively clean the daily and seasonal variations of data, an artificial neural network described in Chapter 4 has been implemented. Figure 7-16 shows the adopted neural network implemented with the aid of machine learning toolbox provided by MATLAB. Output y(t) contain the time history of eigenfrequencies relative to the first three modes of vibration while, predictor x(t), contains the relative environmental parameters, i.e., external temperature, internal temperature, wind velocity and the root mean square of the acceleration measurements. The neural network has been trained on data from the same period used in the previous chapter with principal component analysis. Similarly to the previous section, Figure 7-17 shows the cleansed data overlaid on the original data. It is important to note, when analyzing the training period, that the components of the covariance matrix of the GMM in Figure 7-18 relative to the neural network-purified data are much smaller

than those of the principal component analysis. Furthermore, the training period residues are unbiased and homoscedastic.

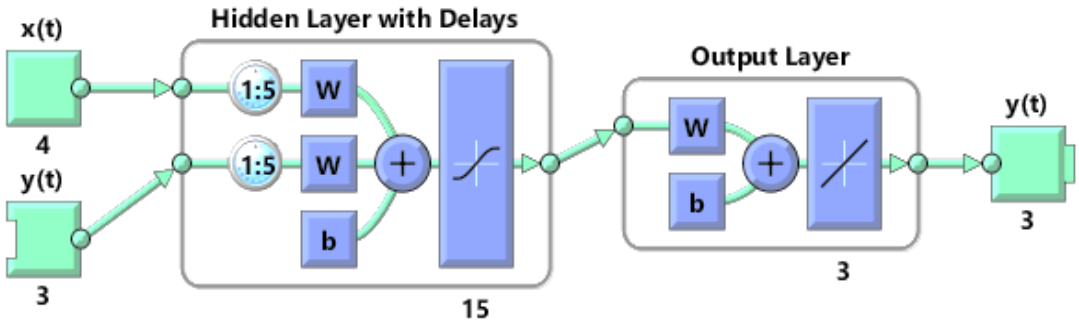

Figure 7-16: Neural network adopted for the data normalization.

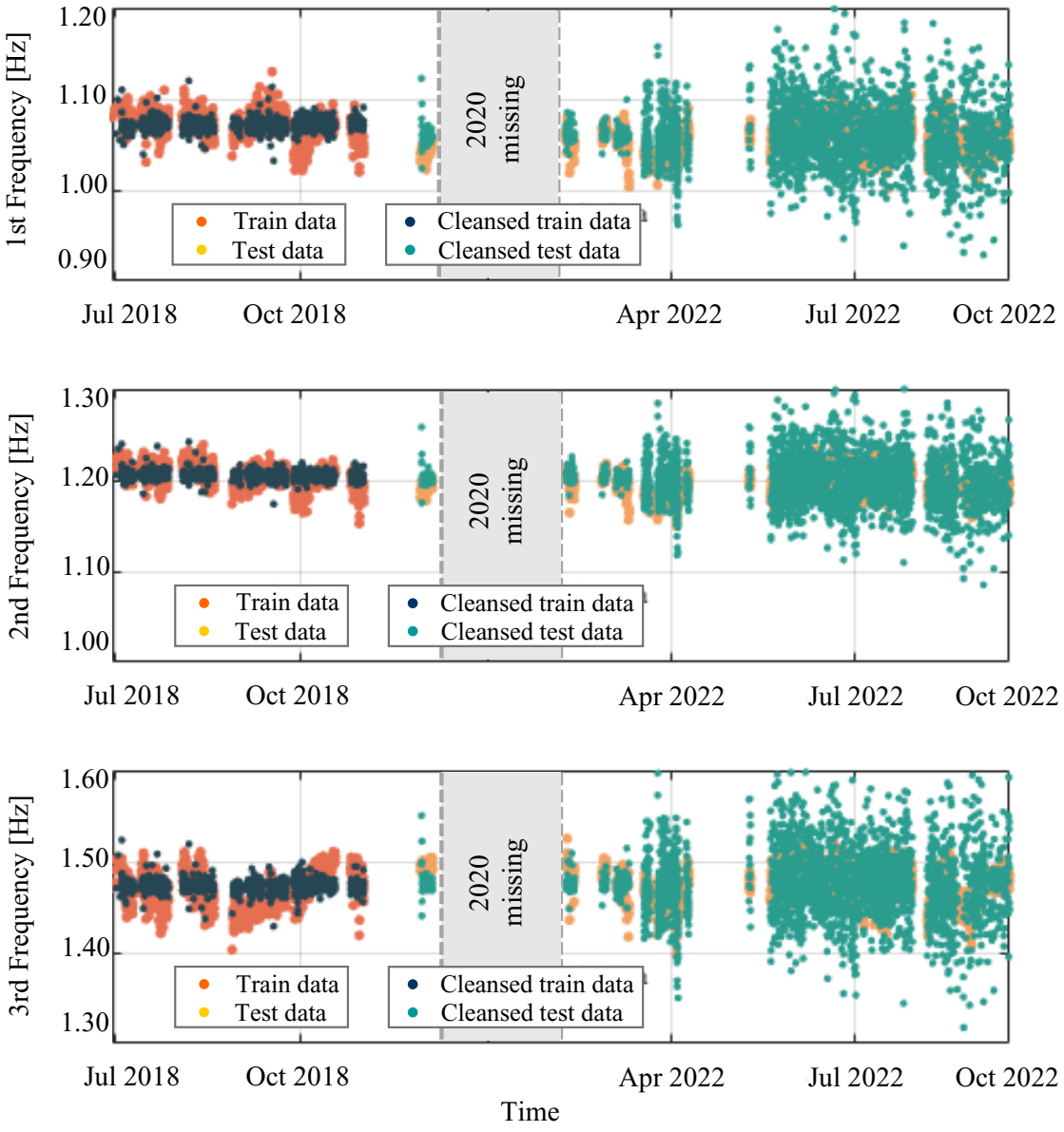

Figure 7-17: Original dataset superimposed on data predicted by statistical model via NARX.

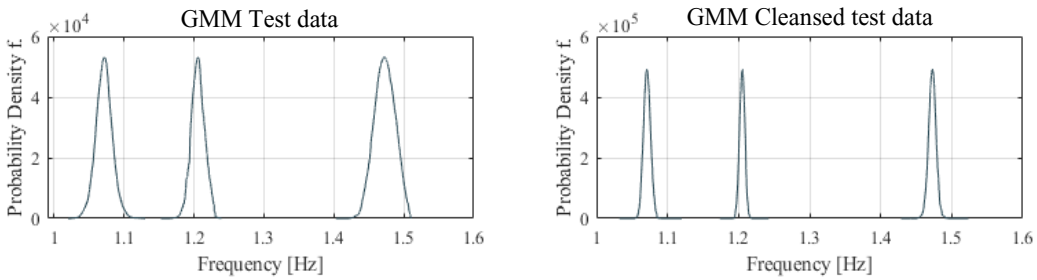

$$\Sigma = 1.00E{+}05 \begin{vmatrix} 19.62 & 14.51 & 9.05 \\ 14.51 & 13.77 & 11.42 \\ 9.05 & 11.42 & 35.34 \end{vmatrix} \qquad \Sigma = 1.00E{+}05 \begin{vmatrix} 3.71 & 1.50 & 1.55 \\ 1.50 & 2.15 & 1.64 \\ 1.55 & 1.64 & 4.23 \end{vmatrix}$$

Figure 7-17: Gaussian Mixture Model of the original dataset and the cleansed data via NARX.

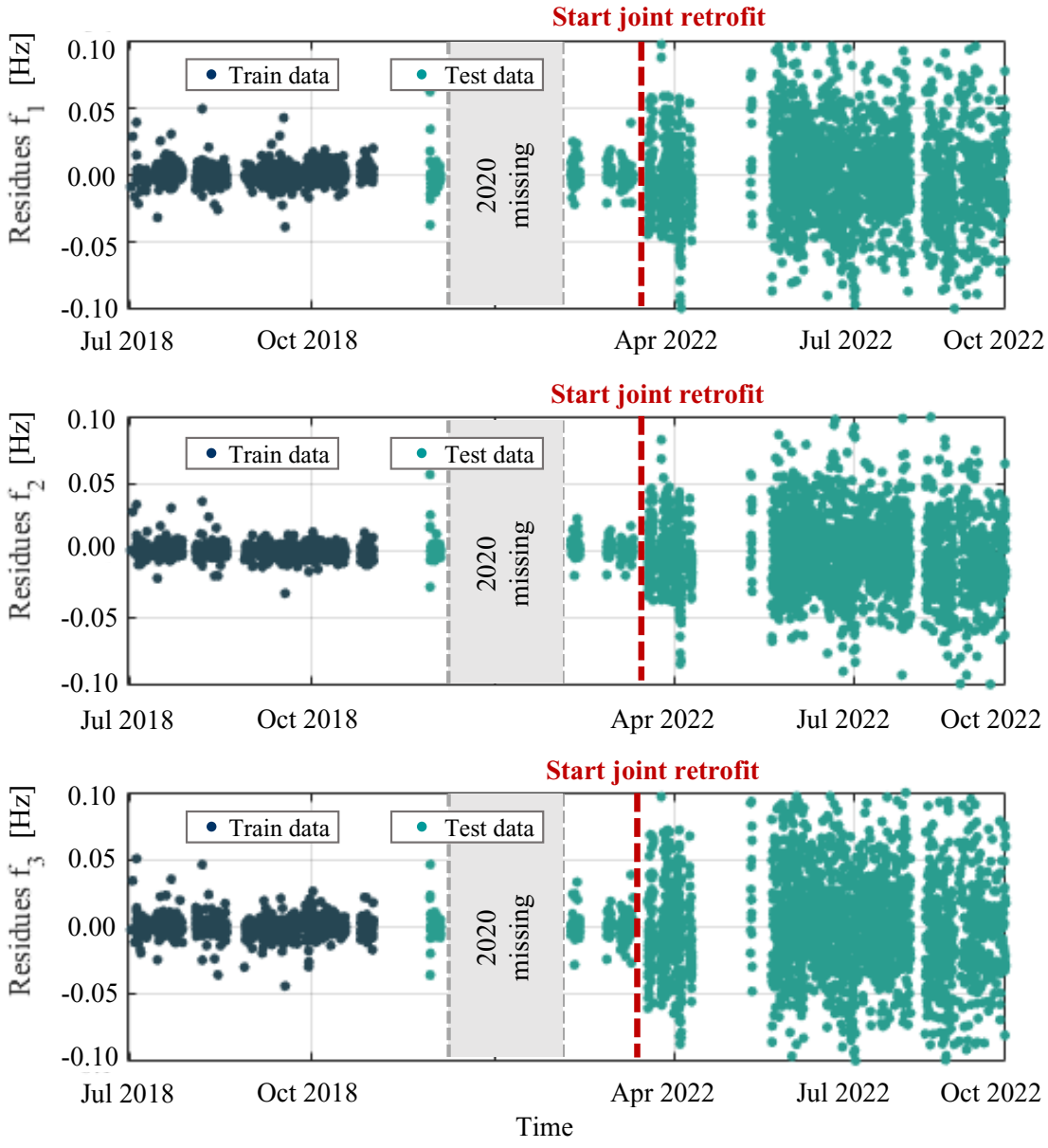

Figure 7-19: Residues between the original frequency dataset and the values predicted by the statistical model obtained from NARX.

A very interesting aspect should be noted in the analysis of the residues obtained between the original data and the statistical model found from the NARX algorithm shown in Figure 7-19. As it can be seen by increase in residue dispersion, starting from March 2021, the neural network predicts results of the monitoring system with increasing uncertainty. This indicates a change in the dynamic behavior of the tower and the main reason is the retrofit work carried out on the structural joints, which started in March 2021. Figure 7-20 shows some photos of the work done on all the structural joints separating the tower from the adjacent buildings. A slight variation in dynamics may be due to a different interaction of the tower with the adjacent buildings, in particular with the stairwell-elevator body, especially because, as shown in Figure 7-20, joints were completely filled with debris.

Figure 7-20: Some photos of the retrofit works carried out on the tower structural joints.

7.4. Discussion of the results

As discussed, the characteristics of a structure that are most sensitive to damage used in damage detection techniques are also the characteristics that are most sensitive to changes in the environmental and operational conditions of structures. As shown in the literature review, the

influence of temperature on the vibration frequencies of a structure is extensively studied in recent years and it is known that temperature can have important effects on the modal parameters of structures. In some cases, the frequency variation induced by temperature variation may be greater than those caused by damage.

These effects are due not only to the dependence of material stiffness on temperature, but also to the interaction between structural and non-structural elements. In addition, seasonal fluctuations can be different from daily fluctuations. All this leads to a high complexity of the problem, and it is not always possible to remove the effect of these phenomena by using simple linear regressions.

Furthermore, especially in the case of buildings, understanding the interaction between structural and non-structural elements may require a very advanced level of engineering analysis that can lead to unsustainable timing and economic resources.

In this context, the use of machine learning techniques may be critical in order to correctly remove the effects of temperature and promptly and effectively assess changes in structural dynamics. In particular, in this work it was decided to implement an artificial neural network for the analysis of data. The validity of this approach has been demonstrated by analyzing data from three years of monitoring the tower, during which it has been possible to detect the changes in eigenfrequencies induced by the modest retrofit work carried out on the structural joints. In this case, the retrofit works carried out on the tower contributes to increasing the structural safety of the building and the slight variation in structural dynamics is not a cause for concern. However, it is important to note that, if there had been a variation of the same magnitude due to the occurrence of structural damage or material degradation, without an effective data cleansing strategy, the variation would not have been detected by the VB-SHM system.

8. Conclusions

In recent years, there has been an increasing interest in structural health monitoring. This was also seen in Italy where, on the one hand, the awareness of an aged asset of structures and infrastructures, and on the other hand, the recent catastrophic events such as the collapse of the Polcevera viaduct in 2018, have produced a growing concern about the health state of civil structures present on the national territory. Moreover, Italy has several regions prone to seismic risk. The availability of VB-SHM systems spread all over the country would allow not only a deeper understanding of the monitored structures and their vulnerability, but also a more accurate estimation of the seismic hazard, thanks to a larger amount of earthquake records. As already discussed in several parts throughout this thesis, developing a VB-SHM system is not an easy task due to the high multi-disciplinary nature of the topic. The design and development of effective and replicable monitoring systems on a large scale requires the interaction of different specialists and considerable costs for installation and implementation.

The aim of this thesis has been to analyze the bases of VB-SHM systems, discussing every single step, and putting together a framework relatively easy to replicate and effective in tracking the structural condition over time. In particular, problems still under investigation in the dynamic monitoring field have been approached, attempting to provide a practical and effective solution.

A strategy for the initial definition of the design of a monitoring system has been presented, covering the preliminary identification, the automatic Model Updating using Particle Swarm Optimization algorithms, and the Optimal Sensor Placement through the Effective Independence method. The importance of this phase has been highlighted through the application to the design of the monitoring system of the Church of Santa Maria in Via. Indeed, this is a very complicated case study in terms of geometry and heterogeneity of materials, and the employed strategy made it possible to efficiently define the optimal position for the sensors.

After that, implementation of hardware and software for dynamic monitoring has been presented and a procedure for automatic Operational Modal Analysis via cluster analysis on solutions obtained from parametric identification techniques has been provided.

Finally, practical tools for data processing have been provided, addressing how to deal with non-linearities in the seismic response of structures and the importance of environmental condition effects on modal parameters. A relevant result has been the correct identification of the impact of the retrofit works on the structural joints of the Ancona Engineering Faculty tower, highlighting the importance of dealing appropriately with the effects of environmental conditions.

As already discussed in chapter 2, VB-SHM frameworks can be divided into 4 levels. Determination of the occurrence of the damage (level 1), determination of the geometric position of the damage (level 2), quantification of the severity of the damage (level 3), and prediction of the remaining useful life and decision-making (level 4). The most sophisticated level (Level 4) can predict the remaining life of the structure and make autonomous decisions from the results of damage diagnosis. The framework developed in this work stops at level 1, but its replicability characteristics and effectiveness may promote the spread of dynamic monitoring, allowing more and more data to be collected, and consequently, support VB-SHM research with the aim of developing increasingly advanced and intelligent frameworks.

REFERENCES

[1] Rainieri, C., and Giovanni Fabbrocino. 2014. Operational Modal Analysis of Civil Engineering Structures, An Introduction and a Guide for Applications. https://doi.org/10.1007/978-1-4939-0767-0.

[2] Ewins. D. J. 2009. Modal Testing: Theory, Practice and Application, 2nd Edition. ISBN: 978-0-863-80218-8.

[3] Farrar, Charles, and Keith Worden. 2013. Structural Health Monitoring A Machine Learning Perspective. Structural Health Monitoring: A Machine Learning Perspective. https://doi.org/10.1002/9781118443118.

[4] Carden, E. Peter, and Paul Fanning. "Vibration Based Condition Monitoring: A Review." Structural Health Monitoring, vol. 3, no. 4, Dec. 2004, pp. 355–377, doi:10.1177/1475921704047500.

[5] Farrar C.R., Worden K. (2010) An Introduction to Structural Health Monitoring. In: Deraemaeker A., Worden K. (eds) New Trends in Vibration Based Structural Health Monitoring. CISM Courses and Lectures, vol 520. Springer, Vienna. https://doi.org/10.1007/978-3-7091-0399-9_1.

[6] Rytter, A. Vibration Based Inspection of Civil Engineering Structure; Department of Building Technology and Structure Engineering, Aalborg University: Aalborg, Denmark, 1993.

[7] Dettmann, K.U.; Soeffker, D. Adaptive modeling of reliability properties for control and supervision purposes. Int. J. Appl. Math. Comput. Sci. 2011, 21, 479–486.

[8] Doebling, Scott & Farrar, Charles and Prime, Michael. (1998). A Summary Review of Vibration-Based Damage Identification Methods. The Shock and Vibration Digest. 30. 91-105. 10.1177/058310249803000201.

[9] Sohn, H, Farrar, C R, Hemez, F M, and Czarnecki, J J. 2002. "A Review of Structural Health Review of Structural Health Monitoring Literature 1996-2001.". United States. https://www.osti.gov/servlets/purl/976152.

[10] Yan, Y. J., Cheng, L., Wu, Z. Y., and Yam, L. H., "Development in vibration-based structural damage detection technique", Mechanical Systems and Signal Processing, vol. 21, no. 5, pp. 2198–2211, 2007. doi:10.1016/j.ymssp.2006.10.002.

[11] Wang, Liang and Chan, Tommy H.T. (2009) Review of vibration-based damage detection and condition assessment of bridge structures using structural health monitoring. In: The Second Infrastructure Theme Postgraduate Conference: Rethinking Sustainable Development: Planning, Engineering, Design and Managing Urban Infrastructure, 26 March 2009, Queensland University.

[12] Moughty, J.J.; Casas, J.R. Vibration Based Damage Detection Techniques for Small to Medium Span Bridges: A Review and Case Study. In Proceedings of the 8th European Workshop on Structural Health Monitoring (EWSHM 2016), Bilbao, Spain, 5–8 July 2016.

[13] Kong, Xuan, Chun-Sheng Cai, and Jiexuan Hu. 2017. "The State-of-the-Art on Framework of Vibration-Based Structural Damage Identification for Decision Making." Applied Sciences 7 (5). https://doi.org/10.3390/app7050497.

[14] Saisi, Antonella, Carmelo Gentile, and Marco Guidobaldi. 2015. "Post-Earthquake Continuous Dynamic Monitoring of the Gabbia Tower in Mantua, Italy." Construction and Building Materials 81 (April): 101–12. https://doi.org/10.1016/j.conbuildmat.2015.02.010.

[15] Giordano, Pier Francesco, Filippo Ubertini, Nicola Cavalagli, Alban Kita, and Maria Masciotta. 2020. "Four Years of Structural Health Monitoring of the San Pietro Bell Tower in Perugia, Italy: Two Years before the Earthquake versus Two Years After." International Journal of Masonry Research and Innovation 5 (December): 445–67. https://doi.org/10.1504/IJMRI.2020.111797.

[16] Cabboi, Alessandro, Filipe Magalhães, Carmelo Gentile, and Alvaro Cunha. 2017. "Automated Modal Identification and Tracking: Application to an Iron Arch Bridge." Structural Control and Health Monitoring 24 (February): 2017. https://doi.org/10.1002/stc.1854.

[17] Li, Binbin, Dongsheng Li, Xuefeng Zhao, and Jinping Ou. (2012). "Optimal sensor placement in health monitoring of suspension bridge". Science China Technological Sciences 55 (luglio). https://doi.org/10.1007/s11431-012-4815-8.

[18] Meo, M., and G. Zumpano. (2005). “On the optimal sensor placement techniques for a bridge structure”. Engineering Structures 27 (10): 1488–97. https://doi.org/10.1016/j.engstruct.2005.03.015.

[19] Kammer, Daniel. (1991). Sensor Placement for On-Orbit Modal Identification and Correlation of Large Space Structures. Journal of Guidance, Control, and Dynamics. 14. 251 - 259. 10.2514/3.20635.

[20] Heo, G., M.L. Wang, and D. Satpathi. (1997). “Optimal transducer placement for health monitoring of long span bridge”. Soil Dynamics and Earthquake Engineering 16 (7): 495–502. https://doi.org/10.1016/S0267-7261(97)00010-9.

[21] Guo, H Y, L Zhang, L L Zhang, and J X Zhou. (2004). “Optimal placement of sensors for structural health monitoring using improved genetic algorithms”. Smart Materials and Structures 13 (3): 528–34. https://doi.org/10.1088/0964-1726/13/3/011.

[22] Flynn, Eric B., and Michael D. Todd. (2010). “A Bayesian approach to optimal sensor placement for structural health monitoring with application to active sensing”. Mechanical Systems and Signal Processing 24 (4): 891–903. https://doi.org/10.1016/j.ymssp.2009.09.003.

[23] Worden, K, and A.P Burrows. (2001). “Optimal Sensor Placement for Fault Detection.” Engineering Structures 23 (8): 885–901. https://doi.org/10.1016/S0141-0296(00)00118-8.

[24] Jiang, Yaoguang, Dongsheng Li, and Gangbing Song. (2017). “On the physical significance of the Effective Independence method for sensor placement”. Journal of Physics: Conference Series 842: 012030. https://doi.org/10.1088/1742-6596/842/1/012030.

[25] Jin, Chenhao, Shinae Jang, Xiaorong Sun, Jingcheng Li, and Richard Christenson. 2016. “Damage Detection of a Highway Bridge under Severe Temperature Changes Using Extended Kalman Filter Trained Neural Network.” Journal of Civil Structural Health Monitoring 6 (July): 545–60. https://doi.org/10.1007/s13349-016-0173-8.

[26] Xia, Yong, Bo Chen, Shun Weng, Yi-Qing Ni, and You-Lin Xu. 2012. “Temperature Effect on Vibration Properties of Civil Structures: A Literature Review and Case Studies.” Journal of Civil Structural Health Monitoring 2 (May). https://doi.org/10.1007/s13349-011-0015-7.

[27] Jung, Jin-Woo, Dae-Joong Moon, Ji-Won Jung, Sang-Kon Ro, and Ji-Hyun Park. 2015. “A Correlation Analysis Regarding the Temperature Effect for a Suspension Bridge.” In , 99–106. https://doi.org/10.1007/978-3-319-15248-6_11.

[28] Cross, E.J., K.Y. Koo, J.M.W. Brownjohn, and K. Worden. 2013. “Long-Term Monitoring and Data Analysis of the Tamar Bridge.” Mechanical Systems and Signal Processing 35 (1): 16–34. https://doi.org/10.1016/j.ymssp.2012.08.026.

[29] Kim, Y., M. Cho, S. Shin, and J.-C. Park. 2013. “Health Monitoring of a Cable-Stayed Bridge Considering the Temperature Change.” In .

[30] Cornwell, Phillip, Charles Farrar, and S.W. Doebling. 2008. “Environmental Variability Of Modal Properties.” Experimental Techniques 23 (January): 45–48. https://doi.org/10.1111/j.1747-1567.1999.tb01320.x.

[31] Zolghadri, Navid. 2015. “Effects of Temperature on Bridge Dynamic Properties.” PhD dissertation.

[32] Li, Jingcheng. 2014. “Structural Health Monitoring of an In-Service Highway Bridge with Uncertainties,” PhD dissertation.

[33] Peeters, Bart, and Guido De Roeck. 2001. “One-Year Monitoring of the Z24-Bridge: Environmental Effects versus Damage Events.” Earthquake Engineering & Structural Dynamics - EARTHQUAKE ENG STRUC DYNAM 30 (February): 149–71. https://doi.org/10.1002/1096-9845(200102)30:23.0.CO;2-Z.

[34] Clinton, John, S. Bradford, Thomas Heaton, and Javier Favela. 2006. “The Observed Wander of the Natural Frequencies in a Structure.” Bulletin of the Seismological Society of America 96 (March): 237–57.

[35] Mikael, Ali, Philippe Gueguen, Pierre-Yves Bard, Philippe Roux, and Mickael Langlais. 2013. “The Analysis of Long-Term Frequency and Damping Wandering in Buildings Using the Random Decrement Technique.” Bulletin of the Seismological Society of America 103 (March). https://doi.org/10.1785/0120120048.

[36] Marco Regni, Davide Arezzo, Sandro Carbonari, Fabrizio Gara, Daniele Zonta, "Effect of Environmental Conditions on the Modal Response of a 10-Story Reinforced Concrete Tower", Shock and Vibration, vol. 2018, Article ID 9476146, 16 pages, 2018. https://doi.org/10.1155/2018/9476146.

[37] Ramos, L.F., L. Marques, P.B. Lourenço, G. De Roeck, A. Campos-Costa, and J. Roque. 2010. "Monitoring Historical Masonry Structures with Operational Modal Analysis: Two Case Studies." Special Issue: Operational Modal Analysis 24 (5): 1291–1305. https://doi.org/10.1016/j.ymssp.2010.01.011.

[38] Rainieri, C., Danilo Gargaro, and Giovanni Fabbrocino. 2015. "Statistical Tools for the Characterization of Environmental and Operational Factors in Vibration-Based SHM." Conference Proceedings of the Society for Experimental Mechanics Series 7 (January): 175–84. https://doi.org/10.1007/978-3-319-15230-1_16.

[39] Reynders E, Wursten G, De Roeck G. Output-only structural health monitoring in changing environmental conditions by means of nonlinear system identification. Structural Health Monitoring. 2014;13(1):82-93. https://doi.org/10.1177/1475921713502836.

[40] Avendaño-Valencia, Luis David, and Eleni N. Chatzi. 2020. "Multivariate GP-VAR Models for Robust Structural Identification under Operational Variability." Probabilistic Engineering Mechanics 60 (April): 103035. https://doi.org/10.1016/j.probengmech.2020.103035.

[41] Mishra, Mayank. 2020. «Machine learning techniques for structural health monitoring of heritage buildings: A state-of-the-art review and case studies». Journal of Cultural Heritage 47 (October). https://doi.org/10.1016/j.culher.2020.09.005.

[42] K. S. M. H. Ibrahim, Y. F. Huang, A. N. Ahmed, C. H. Koo, and A. El-Shafie (2022). A review of the hybrid artificial intelligence and optimization modelling of hydrological streamflow forecasting. Alexandria Engineering Journal, vol. 61, no. 1, pp. 279–303, https://doi.org/10.1016/j.aej.2021.04.100.

[43] Xu, Yan, and James Brownjohn. 2018. "Review of Machine-Vision Based Methodologies for Displacement Measurement in Civil Structures." Journal of Civil Structural Health Monitoring 8 (January). https://doi.org/10.1007/s13349-017-0261-4.

[44] Salehi, Hadi, and Rigoberto Burgueño. 2018. "Emerging Artificial Intelligence Methods in Structural Engineering." Engineering Structures 171 (September): 170–89. https://doi.org/10.1016/j.engstruct.2018.05.084.

[45] Mishra Mayank, Barman Swarup K., Maity Damodar, and Maiti Dipak Kumar. 2020. "Performance Studies of 10 Metaheuristic Techniques in Determination of Damages for Large-Scale Spatial Trusses from Changes in Vibration Responses." Journal of Computing in Civil Engineering 34 (2): 04019052. https://doi.org/10.1061/(ASCE)CP.1943-5487.0000872.

[46] Das, Swagato, P. Saha, and S. K. Patro. 2016. "Vibration-Based Damage Detection Techniques Used for Health Monitoring of Structures: A Review." Journal of Civil Structural Health Monitoring 6 (3): 477–507. https://doi.org/10.1007/s13349-016-0168-5.

[47] Barontini, Alberto, Maria-Giovanna Masciotta, Luís F. Ramos, Paulo Amado-Mendes, and Paulo B. Lourenço. 2017. "An Overview on Nature-Inspired Optimization Algorithms for Structural Health Monitoring of Historical Buildings." X International Conference on Structural Dynamics, EURODYN 2017 199 (January): 3320–25. https://doi.org/10.1016/j.proeng.2017.09.439.

[48] Falcone, Roberto, Carmine Lima, and Enzo Martinelli. 2020. "Soft Computing Techniques in Structural and Earthquake Engineering: A Literature Review." Engineering Structures 207 (March): 110269. https://doi.org/10.1016/j.engstruct.2020.110269.

[49] Wu, Rih-Teng, and Mohammad Reza Jahanshahi. 2020. "Data Fusion Approaches for Structural Health Monitoring and System Identification: Past, Present, and Future." Structural Health Monitoring 19 (2): 552–86. https://doi.org/10.1177/1475921718798769.

[50] Rainieri, C., and G. Fabbrocino. 2010. "Automated Output-Only Dynamic Identification of Civil Engineering Structures." Mechanical Systems and Signal Processing 24 (3): 678–95. https://doi.org/10.1016/j.ymssp.2009.10.003.

[51] Rainieri, C., Giovanni Fabbrocino, and Edoardo Cosenza. 2011. “Near Real-Time Tracking of Dynamic Properties for Standalone Structural Health Monitoring Systems.” Mechanical Systems and Signal Processing 25 (November): 3010–26. https://doi.org/10.1016/j.ymssp.2011.04.010.

[52] Hasan, Muhammad Danial Bin Abu, Zair Asrar Bin Ahmad, Mohd Salman Leong, Lim Meng Hee, and M. Haffizzi Md Idris. 2019. “Cluster Analysis for Automated Operational Modal Analysis: A Review.” MATEC Web of Conferences.

[53] Magalhaes, Filipe. 2010. “Operational Modal Analysis for Testing and Monitoring of Bridges and Special Structures.” PhD thesis.

[54] JF. Hair, RE. Anderson, RL. Tatham. 1998. WC Black, Multivariate data analysis.

[55] P. Verboven, P. Guillaume, B. Cauberghe, E. Parloo, S. Vanlanduit, Proceedings of the IMACXXI Conference and Exposition on Structural Dynamics, 3–6 (2003)

[56] Pappa, Richard S., George H. James, and David C. Zimmerman. 1998. “Autonomous Modal Identification of the Space Shuttle Tail Rudder.” Journal of Spacecraft and Rockets 35 (2): 163–69. https://doi.org/10.2514/2.3324.

[57] Goethals, I., B. Vanluyten, and B. De Moor. "Reliable spurious mode rejection using self learning algorithms." The Shock and Vibration Digest 38, no. 3 (2006): 260. Gale Academic OneFile (accessed February 18, 2022).

[58] Magalhães, Filipe, Álvaro Cunha, and Elsa Caetano. 2009. “Online Automatic Identification of the Modal Parameters of a Long Span Arch Bridge.” Mechanical Systems and Signal Processing 23 (2): 316–29. https://doi.org/10.1016/j.ymssp.2008.05.003.

[59] Zhang, Q., Tou Pin Chang, and Cc Chang. 2001. “Finite-Element Model Updating for the Kap Shui Mun Cable-Stayed Bridge.” Journal of Bridge Engineering - J BRIDGE ENG 6 (August). https://doi.org/10.1061/(ASCE)1084-0702(2001)6:4(285).

[60] Gara, Fabrizio, Sandro Carbonari, Davide Roia, Alessandro Balducci, and Luigino Dezi. 2021. “Seismic Retrofit Assessment of a School Building through Operational Modal Analysis and f.e. Modeling.” Journal of Structural Engineering 147 (January). https://doi.org/10.1061/(ASCE)ST.1943-541X.0002865.

[61] Bayraktar, Alemdar, Barış Sevim, Ahmet Altunişik, and Temel Türker. 2008. “Analytical and Operational Modal Analyses of Turkish Style Reinforced Concrete Minarets for Structural Identification.” Experimental Techniques 33 (October): 65–75. https://doi.org/10.1111/j.1747-1567.2008.00400.x.

[62] Wu, J.R., and Q.S. Li. 2004. “Finite Element Model Updating for a High-Rise Structure Based on Ambient Vibration Measurements.” Engineering Structures 26 (7): 979–90. https://doi.org/10.1016/j.engstruct.2004.03.002.

[63] Bayraktar, Alemdar, Ahmet Altunişik, Barış Sevim, and Temel Türker. 2009. “Modal Testing, Finite-Element Model Updating, and Dynamic Analysis of an Arch Type Steel Footbridge.” Journal of Performance of Constructed Facilities - J PERFORM CONSTR FACIL 23 (April). https://doi.org/10.1061/(ASCE)0887-3828(2009)23:2(81).

[64] Roca, Pere, Miguel Cervera, Giuseppe Gariup, and Luca Pela’. 2010. “Structural Analysis of Masonry Historical Constructions. Classical and Advanced Approaches.” Archives of Computational Methods in Engineering 17 (3): 299–325. https://doi.org/10.1007/s11831-010-9046-1.

[65] Castellazzi, Giovanni, Antonio Maria D’Altri, Stefano de Miranda, and Francesco Ubertini. 2017. “An Innovative Numerical Modeling Strategy for the Structural Analysis of Historical Monumental Buildings.” Engineering Structures 132 (February): 229–48. https://doi.org/10.1016/j.engstruct.2016.11.032.

[66] Ramos, Luís, Murat Alaboz, Rafael Aguilar, and Paulo Lourenco. 2011. “Dynamic Identification and FE Updating of S. Torcato Church, Portugal.” In *Conference Proceedings of the Society for Experimental Mechanics Series*, 4:71–80. https://doi.org/10.1007/978-1-4419-9831-6_9.

[67] Torres, Wilson, José Luis Almazán, Cristián Sandoval, and Rubén Boroschek. 2017. “Operational Modal Analysis and FE Model Updating of the Metropolitan Cathedral of Santiago, Chile.” Engineering Structures 143 (July): 169–88. https://doi.org/10.1016/j.engstruct.2017.04.008.

[68] Sabbatini, Valerio, Carlo Baggio, and Silvia Santini. 2019. “Model updating of a masonry historical church based on operational modal analysis: the case study of San Filippo Neri in Macerata.” https://doi.org/10.7712/120119.7186.18559.

[69] Blum, Christian, and Xiaodong Li. 2008. “Swarm Intelligence in Optimization.” In Swarm Intelligence: Introduction and Applications, 43–85. https://doi.org/10.1007/978-3-540-74089-6_2.

[70] Beni G, Wang J. 1989. “Swarm intelligence.” In Proceedings of the Seventh Annual Meeting of the Robotics Society of Japan. RSJ Press; p. 425–8

[71] Falcone, Roberto, Carmine Lima, and Enzo Martinelli. 2020. “Soft Computing Techniques in Structural and Earthquake Engineering: A Literature Review.” Engineering Structures 207 (March): 110269. https://doi.org/10.1016/j.engstruct.2020.110269.

[72] J. Kennedy and R. Eberhart. 1995. “Particle Swarm Optimization.” In Proceedings of ICNN’95 - International Conference on Neural Networks, 4:1942–48 vol.4. https://doi.org/10.1109/ICNN.1995.488968.

[73] Karaboga, Dervis, and Bahriye Basturk. 2007. “A Powerful and Efficient Algorithm for Numerical Function Optimization: Artificial Bee Colony (ABC) Algorithm.” Journal of Global Optimization 39 (3): 459–71. https://doi.org/10.1007/s10898-007-9149-x.

[74] Yang, Xin-She. 2008. Nature-Inspired Metaheuristic Algorithms. Luniver Press.

[75] Fister, Iztok, Iztok Fister, Xin-She Yang, and Janez Brest. 2013. “A Comprehensive Review of Firefly Algorithms.” Swarm and Evolutionary Computation 13 (December): 34–46. https://doi.org/10.1016/j.swevo.2013.06.001.

[76] Geem, Zong Woo. 2010. Recent Advances In Harmony Search Algorithm. Vol. 270. https://doi.org/10.1007/978-3-642-04317-8.

[77] Dorigo, Marco, Thomas Stützle, Tu Darmstadt, and Intellectics Group. 2001. “The Ant Colony Optimization Metaheuristic: Algorithms, Applications, and Advances,” March.

[78] Tran-Ngoc, H., S. Khatir, G. De Roeck, T. Bui-Tien, L. Nguyen-Ngoc, and M. Abdel Wahab. 2018. “Model Updating for Nam O Bridge Using Particle Swarm Optimization Algorithm and Genetic Algorithm.” Sensors 18 (12). https://doi.org/10.3390/s18124131.

[79] Saada, Mohamed M., Mustafa H. Arafa, and Ashraf O. Nassef. 2013. “Finite Element Model Updating Approach to Damage Identification in Beams Using Particle Swarm Optimization.” Engineering Optimization 45 (6): 677–96. https://doi.org/10.1080/0305215X.2012.704026.

[80] Engineer’s Guide to the Digitization of Analog Signals. White paper from National Instruments https://download.ni.com/evaluation/daq/NI_Engineers_Guide_to_Digitization.pdf

[81] Van Overschee, Peter, and Bart De Moor. 1996. “Subspace Identification for Linear Systems. Theory, Implementation, Applications. Incl. 1 Disk.” In Springer Science & Business Media, xiv:xiv + 254. https://doi.org/10.1007/978-1-4613-0465-4.

[82] Brincker R, Andersen P. Understanding Stochastic Subspace Identification. In Conference Proceedings : IMAC-XXIV : A Conference & Exposition on Structural Dynamics. Society for Experimental Mechanics. 2006

[83] Peeters, Bart. 2000. “System Identification and Damage Detection in Civil Engineering,” PhD dissertation.

[84] Udwadia, Firdaus, and J.A. Garba. 1985. “Optimal Sensor Location for Structural Identification JPL.” JPL Proceedings of the Workshop on Identification and Control of Flexible Space Structures 247–261 (May).

[85] Ceravolo, Rosario, Emiliano Matta, Antonino Quattrone, and Luca Zanotti Fragonara. 2017. “Amplitude Dependence of Equivalent Modal Parameters in Monitored Buildings during Earthquake Swarms.” Earthquake Engineering & Structural Dynamics 46 (March). https://doi.org/10.1002/eqe.2910.

[86] Calvi, G., Rui Pinho, and Helen Crowley. 2006. “State-of-the-Knowledge on the Period Elongation of RC Buildings during Strong Ground Shaking,” ECEES First European Conference on Earthquake Engineering and Seismology, Geneva, Switzerland, 3-8 September 2006, Paper n.1535.

[87] Ditommaso, Rocco, Marco Mucciarelli, and Felice Ponzo. 2012. “Analysis of Non-Stationary Structural Systems by Using a Band-Variable Filter.” Bulletin of Earthquake Engineering, June. https://doi.org/10.1007/s10518-012-9338-y.

[88] Ghahari, Farid, Fariba Abazarsa, Mohammad Ali Ghannad, and Ertugrul Taciroglu. 2013. “Response-only Modal Identification of Structures Using Strong Motion Data.” Earthquake Engineering & Structural Dynamics 42 (July). https://doi.org/10.1002/eqe.2268.

[89] Hu, Rongpan, and You-Lin Xu. 2019. SHM-Based Seismic Performance Assessment of High-Rise Buildings under Long-Period Ground Motion. Journal of Structural Engineering. Vol. 145. https://doi.org/10.1061/(ASCE)ST.1943-541X.0002323.

[90] O’Reilly, Gerard, Daniele Perrone, Matt Fox, Ricardo Monteiro, Andre Filiatrault, Igor Lanese, and Alberto Pavese. 2019. “System Identification and Seismic Assessment Modeling Implications for Italian School Buildings.” Journal of Performance of Constructed Facilities 33 (February). https://doi.org/10.1061/(ASCE)CF.1943-5509.0001237.

[91] Verhaegen, Michel. 1994. “Identification of the Deterministic Part of MIMO State Space Models given in Innovations Form from Input-Output Data.” Special Issue on Statistical Signal Processing and Control 30 (1): 61–74. https://doi.org/10.1016/0005-1098(94)90229-1.

[92] Skolnik, Derek, Ying Lei, Eunjong Yu, and John Wallace. 2006. “Identification, Model Updating, and Response Prediction of an Instrumented 15Story Steel-Frame Building.” Earthquake Spectra - EARTHQ SPECTRA 22 (August). https://doi.org/10.1193/1.2219487.

[93] Miguel Ángel García-Illescas, David Murià-Vila, Luis Alvarez-Icaza, "Monitoring and Identification of Vibration Frequencies on a Portion of México City Metro Line 12", Advances in Civil Engineering , vol. 2019, Article ID 4128320, 13 pages, 2019. https://doi.org/10.1155/2019/4128320.

[94] Boroschek, Rubén. 2013. “Structural Health Monitoring Performance During the 2010 Gigantic Chile Earthquake.” In , 197–216. https://doi.org/10.1007/978-94-007-5182-8_8.

[95] Chiuso, Alessandro, and Giorgio Picci. 2005. “PREDICTION ERROR VS SUBSPACE METHODS IN CLOSED LOOP IDENTIFICATION.” 16th IFAC World Congress 38 (1): 506–11. https://doi.org/10.3182/20050703-6-CZ-1902.00085.

[96] A. D. R. Tamariz, C. P. Bottura, and G. Barreto. 2005. “Iterative MOESP Type Algorithm for Discrete Time Variant System Identification.” In Proceedings of the 2005 IEEE International Symposium on, Mediterrean Conference on Control and Automation Intelligent Control, 2005., 399–404. https://doi.org/10.1109/.2005.1467048.

[97] Robles, Alexander, and Mateus Giesbrecht. 2018. N4SID-VAR Method for Multivariable Discrete Linear Time-Variant System Identification. https://doi.org/10.5220/0006907505020509.

[98] Loh, Chin-Hsiung, and Jun-Da Chen. 2017. “Tracking Modal Parameters from Building Seismic Response Data Using Recursive Subspace Identification Algorithm.” Earthquake Engineering & Structural Dynamics 46 (13): 2163–83. https://doi.org/10.1002/eqe.2900.

[99] Kavrakov, Igor, Ahsan Kareem, and Guido Morgenthal. 2020. “Comparison Metrics for Time-Histories: Application to Bridge Aerodynamics.” Journal of Engineering Mechanics 146 (June): 04020093. https://doi.org/10.1061/(ASCE)EM.1943-7889.0001811.

[100] Huynh, Thanh-Canh, Ngoc-Loi Dang, and Jeong-Tae Kim. 2018. “PCA-Based Filtering of Temperature Effect on Impedance Monitoring in Prestressed Tendon Anchorage.” SMART STRUCTURES AND SYSTEMS 22 (July). https://doi.org/10.12989/sss.2018.22.1.057.

[101] Tibaduiza, D.A., Mujica, L.E. & Rodellar, J. 2011. “Structural health monitoring based on principal component analysis: damage detection, localization and classification”, in Pozo, F. & Zapateiro, M. (eds), Advances in Dynamics, Control, Monitoring and Applications, pp. 8-17, Universitat Politècnica de Catalunya, Departament de Matemàtica Aplicada III (MA3), ISBN 978-84-7653-539-4

[102] Tharwat, Alaa. 2016. “Principal Component Analysis - a Tutorial.” International Journal of Applied Pattern Recognition 3 (January): 197. https://doi.org/10.1504/IJAPR.2016.079733.

[103] Markova, M. 2019. Foreign Exchange Rate Forecasting by Artificial Neural Networks. AIP Conference Proceedings. Vol. 2164. https://doi.org/10.1063/1.5130812.

[104] Baum, Eric B., and David Haussler. 1989. "What Size Net Gives Valid Generalization?" Neural Computation 1 (1): 151–60. https://doi.org/10.1162/neco.1989.1.1.151.

[105] Masters, Timothy, ed. 1993. "Practical Neural Network Recipies in C++", iv. San Francisco (CA): Morgan Kaufmann. https://doi.org/10.1016/B978-0-08-051433-8.50002-1.

[106] Bailey, David L., and Donna Thompson. 1990. "Developing Neural-Network Applications." AI Expert 5 (9): 34–41.

[107] Katz, J. O. 1992. "Developing neural network forecasters for trading." Technical Analysis of Stocks and Commodities 8, 58–70.

[108] Ersoy, O. 1990. "Neural Network Tutorial." Hawaii International Conference on System Sciences.

[109] Klimasauskas, C. C. "Applying Neural Networks," in Trippi, Robert R., and Efraim Turban. 1992. "Neural Networks in Finance and Investing: Using Artificial Intelligence to Improve Real World Performance". USA: McGraw-Hill, Inc.

[110] Haykin, Simon. 1998. Neural Networks: A Comprehensive Foundation. 2nd ed. USA: Prentice Hall PTR.

[111] Beagle, M., Hagan, M., and Demuth, H. "Neural Network Toolbox: User's Guide." The MathWorks, Inc., Natick, MA, 2016.

[112] Balducci, A., 2005. "Dissipative Towers". Application n. EP20100747238, PCT n. WO2010EP62748

[113] Balducci, A., and Castellano, M. G. (2015). "Adeguamento sismico del liceo Varano di Camerino mediante sistema a torri dissipative." Progettazione Sismica, no. 01: 69–91. https://doi.org/10.7414/PS.6.1.69-91.

[114] Lydon, F.D., and R.V. Balendran. 1986. "Some Observations on Elastic Properties of Plain Concrete." Cement and Concrete Research 16 (3): 314–24. https://doi.org/10.1016/0008-8846(86)90106-7.

[115] Capatti, Maria Chiara, Giuseppe Tropeano, Michele Morici, Sandro Carbonari, Francesca Dezi, Graziano Leoni, and Francesco Silvestri. 2017. "Implications of Non-Synchronous Excitation Induced by Nonlinear Site Amplification and of Soil-Structure Interaction on the Seismic Response of Multi-Span Bridges Founded on Piles." Bulletin of Earthquake Engineering 15 (November): 1–33. https://doi.org/10.1007/s10518-017-0165-z.

[116] Gara Fabrizio, Arezzo Davide, Nicoletti Vanni, and Carbonari Sandro. 2021. "Monitoring the Modal Properties of an RC School Building during the 2016 Central Italy Seismic Swarm." Journal of Structural Engineering 147 (7): 05021002. https://doi.org/10.1061/(ASCE)ST.1943-541X.0003025.

Ringraziamenti

Ho incontrato l'argomento delle misure dinamiche e del monitoraggio strutturale con la mia tesi di laurea magistrale, la quale mi ha lasciato con molte domande aperte. Queste domande sono state una delle motivazioni principali che mi hanno spinto a intraprendere il percorso, a tratti faticoso e stressante, di un dottorato di ricerca. Arrivo alla fine di questo percorso con molte risposte e con la speranza che queste, seppur limitate, siano utili ad altri. Arrivo anche con la consapevolezza di aver appena intaccato la superficie di un problema vasto, ma con in tasca qualche strumento in più e parecchia esperienza che confido mi aiuteranno per le sfide future.

Per tutto questo devo ringraziare il mio tutor, il Prof Fabrizio Gara, che mi ha concesso fiducia, mezzi e libertà di azione non indifferenti e, immagino, non comuni. Voglio anche ringraziare il Prof Sandro Carbonari. Ogni confronto con lui è stato occasione di riflessione e crescita.

Non posso non ringraziare l'Ing Vanni Nicoletti, non solo per l'attenta rilettura di questa tesi e le correzioni del mio pessimo inglese, ma anche per l'amicizia nata in questi quattro anni di collaborazione.

Una nota di merito ai ragazzi che ho avuto il piacere e l'onore di seguire nel loro lavoro di tesi presso il nostro dipartimento, ormai tutti ingegneri. Simone, Francesca, Hedi, Paolo, Leonardo, spero che il mio supporto vi sia stato utile perché, in cambio, ho preso un pezzetto del vostro valido lavoro. Ringrazio in particolar modo Simone, diventato ormai un collaboratore e un amico.

Infine, ringrazio la mia compagna Aloisa. Non esagero se dico che probabilmente senza di lei non sarei arrivato fin qui. Condividere la vita con lei è continua fonte di motivazione e ispirazione.